Structure et dynamique des membranes photosynthétique relevé par diffusion de neutrons

Gergely Nagy

PRES « Université de Grenoble »

Ecole Doctorale de Physique

Eötvös Loránd University

Doctoral School in Physics

Ph.D. thesis

Gergely NAGY

To obtain the title of

Docteur de l'Université de Grenoble

Discipline of the Doctoral (PhD) Degree of Eötvös Loránd University

Structure and Dynamics of Photosynthetic Membranes as Revealed by Neutron Scattering

Composition of the jury:

Prof. Dr. Marie-Claire Bellissent-Funel	Reviewer
Dr. Thomas Hauß	Reviewer
Dr. Frank Gabel	Member of the jury
Dr. Peter Timmins	Member of the jury
Dr. Giuseppe Zaccai	Member of the jury
Prof. Dr. Judith Peters	Supervisor
Dr. László Rosta	Supervisor
Dr. Győző Garab	Supervisor

Thesis prepared at the Institut Laue-Langevin, Grenoble

and at the Research Institute for Solid State Physics and Optics, Budapest

Contents

Acknowledgements

First of all I wish like to thank my supervisors Prof. Judith Peters, Dr. Győző Garab, Dr. László Rosta and Dr. Peter Timmins for their continuous support during my doctoral studies, for their help in all the aspects of this work, starting from the choice of the various interesting thesis topics, the planning of the experiments, the discussion about the problematic points of the data treatment or the following biologically relevant interpretation of the results and finally in the presentation of our results in this thesis and in our articles. Their help was also indispensable in finding the opportunities to work, study and perform experiments in various different research laboratories and universities. I also would like to thank Dr. Győző Garab for his friendly guidance in many not only science related questions during these past few years.

I wish to say special thanks to Prof. Dorthe Posselt for her help in most of our SANS experiments and for the helpful discussions especially about the thorough data treatment methods and to Prof. Jörg Pieper for his introduction about application of neutron scattering for dynamical studies.

I would like to thank to the staff of the Institut Laue-Langevin (Grenoble) for creating an inspiring work environment, especially to Dr. Philip Callow, Dr. Francesca Natali, Dr. Lionel Porcar, and Peter Cross for helping us in configuring the experiments, to Dr. Charles Dewhurst, Dr. Bruno Demé, Dr. Péter Falus, Dr. Béla Faragó, Dr. Menyhért Kocsis and Dr. Marcus Trapp for advice on data treatment and interpretation and to Dr. Isabelle Grillo for her support in the sample preparations.

I would like to thank Prof. Ferenc Mezei for giving me the opportunity to join his “The Structure and Dynamics of Lamellar, Self-assembling Molecular Devices” project. I also want to thank the other scientists in the Research Institute for Solid State Physics and Optics, György Káli, Dr. Márton Markó, Dr. Eszter Rétfalvi, Dr. Noémi Székely and Renáta Ünnep for introducing me to different neutron scattering techniques.

I always received warm hospitality during my visits to the Biological Research Center. First of all I would like to say thanks to Dr. László Kovács for participating in almost all of our experiments, performing and teaching me the sample preparations and presenting the biology of photosynthesis. I also wish to thank Dr. Petar Lambrev, Dr. Yuliya Miloslavina, Dr. Bettina Ughy, Dr. Zsuzsanna Várkonyi and Dr. Ottó Zsiros for

their help in the preparation or execution of different experiments and to Ágnes Rédai for helping me to obtain the necessary articles. I wish to thank Dr. Milán Szabó for the CD measurements and helpful discussions and Dr. Sashka B. Krumova for the DSC and CD measurements.

I would like to thank the Institut Laue Langevin, the Research Institute for Solid State Physics and Optics and the French Government for their financial support.

I want to thank my friends and colleagues Dániel Rémai, Rudolf Paksa, Razmig Démirdjian, Dr. Mansour Tawk, Péter Reischig, Pawinee Boonyasopon, Jessica Valle Orero, Dr. Michael Baker, Dr. Stuart Fisher and Peggy Heunemann for making my PhD studies memorable.

And last but not least I wish to thank to my sister, parents and grandparents for setting an example, for inspiring and helping me to overcome the difficulties and offering the best advices when I needed, and to my girlfriend Brigi for her support and patience during the time I prepared this thesis.

Abbreviations

BBY	photosystem II membrane fragments
CD	circular dichroism
Chl	chlorophyll
DCMU	(3-(3,4-dichlorophenyl)-1,1-dimethylurea)
DGDG	digalactosyl-diacylglycerol
DMPC	1,2-dimyristoyl-*sn*-glycero-3-phosphocholine
DQH_2	duroquinol (tetramethyl-*p*-hydroquinone)
DSC	differential scanning calorimetry
EINS	elastic incoherent neutron scattering
EM	electron microscopy
FCP	fucoxanthin-chlorophyll a/c protein
LHCII	main light harvesting complex of PSII
MGDG	monogalactosyl-diacylglycerol
NPQ	non-photochemical quenching
OEC	oxygen evolving complex
PBS	phycobilisome
PG	phosphatidylglycerol
PMS	N-methyl phenazonium methosulphate
Psi	polymer and salt induced
PSI	photosystem I
PSII	photosystem II
RD	repeat distance
r.h.	relative humidity
Q	scattering vector
SANS	small-angle neutron scattering
SD	sample-to-detector distance
SLD	scattering length density
SQDG	sulfoquinovosyl-diacylglycerol
TRIS	tris-(hydroxymethyl)aminomethane

1. General Introduction

The present thesis is prepared for submission in order to obtain the Ph.D. degree at the Physics for the Life Sciences doctoral program of the Ecole Doctorale de Physique of the PRES «Université de Grenoble» (Grenoble, France) and at the Statistical Physics, Biological Physics and Physics of Quantum Systems doctoral program of the Doctoral School in Physics of the Eötvös Loránd University of Sciences (Budapest, Hungary).

The thesis was carried out at the Institut Laue-Langevin (Grenoble, France) under the joint supervision of Prof. Judith Peters and Dr. Peter Timmins and at the Research Institute for Solid State Physics and Optics (Budapest, Hungary) under the joint supervision of Dr. Győző Garab and Dr. László Rosta.

One of the most important scientific challenges of our time is to find answers and solutions for the various questions and problems about the rapidly increasing energy consumption of humanity. The present predominance of fossil fuels in the global energy production cannot be maintained in the long term, due to the rapid decrease of the easily exploitable resources and potentially catastrophic consequences of increasing atmospheric carbon dioxide concentration. As a consequence, scientific studies on the utilization of renewable resources, their transformation to environmentally friendly, easily storable and transportable energy sources are gaining more and more importance.

Solar energy has an exceptional role among these resources, taking into account that every hour sufficient light reaches the Earth's surface to meet the world's annual energy needs (Harnessing solar energy for the production of clean fuel (2008) Science Policy Briefing of the European Science Foundation). In the Biosphere, solar energy conversion to chemical energy is performed by photosynthetic organisms. Photosynthesis serves as the energy input for the current terrestrial life and it regulates the carbon dioxide and oxygen concentration in the atmosphere. Modified photosynthetic organisms or solar energy converting artificial devices inspired by photosynthesis may make a significant contribution to industrial energy production. Photosynthesis, in its natural form, however, is far from being understood. This statement is especially true for different regulatory mechanisms, which allow the photosynthetic apparatus to accommodate to various environmental conditions.

Thylakoid membranes are the most abundant membranes on earth and possess a central role in photosynthesis by giving place to its light reactions. In the present thesis we investigate structural parameters of the thylakoid membranes, isolated from higher plants and in different algal and cyanobacterial cells, with small-angle neutron scattering, and the dynamics of isolated thylakoid membrane fragments with elastic incoherent neutron scattering. In the planning of our experiments one of our main goals was, by capitalizing on the non-invasive nature of neutron scattering techniques, to investigate the samples as close to the *in vivo* conditions as possible. The results presented, in addition to providing clear evidence for the occurrence of small but well discernible membrane reorganizations in thylakoid membranes during photosynthesis, and for a transition in BBY membranes at physiological temperatures, also show possible applications of neutron scattering for the investigation of *in vivo* biological samples.

This thesis consists of nine chapters. After this general introduction about the motivation of the work, some important aspects of neutrons, production of neutrons and theoretical background of thermal neutron scattering is presented in Chapter 2, along with a short introduction of the two types of neutron scattering instruments used in our experiments. In Chapter 3 a short overview of photosynthesis is given with a brief presentation of the light reactions and the participating protein complexes, and with more detailed discussion about structure of the thylakoid membrane which accommodates these complexes.

Afterwards the sample preparation protocols, composition analysis of some of the investigated samples, description of the applied experimental techniques is presented in Chapter 4, along with brief description of the different methods and calculations used in the interpretation of the experimental data.

Structural investigations of thylakoid membranes isolated from spinach leaves with small-angle neutron scattering are presented in Chapters 5 and 6. We start the discussion with the identification of the two characteristic peaks present in the radially averaged scattering curves through results presented in the literature and our experimental data. Afterwards we investigate the influence of different environmental parameters, such as osmolarity, ionic strength and phosphorylation on the structure of stroma and granum

thylakoids. In Chapter 6 we present our results which reveal structural reorganizations of the stroma thylakoids during photosynthesis, with a time resolution of several seconds. We show that the changes are most pronounced when the PSI cyclic electron transport is operating and that they are driven by the transmembrane ΔpH generated during photosynthesis.

In Chapter 7 we demonstrate that small-angle neutron scattering can also be used for the investigation of structure of thylakoid membranes in algal and cyanobacterial cells *in vivo*. Furthermore, we reveal small but well discernable light-induced reversible reorganizations in thylakoid membranes of *Phaeodactylum tricornutum* and in the PAL mutant of the *Synechocystis* PCC 6803 cells.

In Chapter 8 incoherent elastic neutron scattering is employed for the dynamical characterization of photosystem II membrane fragments. The experiments, performed in the physiological and relevant super-physiological temperature region, reveal a hydration sensitive transition in the membrane, which is proposed to be related to the heat induced removal of the oxygen evolving complex.

Finally, Chapter 9 contains the summary of the main results as well as an outlook and future perspectives for further application of neutron scattering for the investigation of photosynthetic membranes.

1.1 Introduction Générale en Français

La présente thèse de doctorat est préparée pour la soumission d'une thèse au programme doctoral de Physique pour les Sciences du Vivant de l'Ecole Doctorale de Physique du PRES «Université de Grenoble» (Grenoble, France) et au programme doctoral de Physique Statistique, Physique Biologique et Physique des Systèmes Quantiques de l'Ecole Doctorale de Physique de l'Université des Sciences Eötvös Loránd (Budapest, Hongrie).

La thèse a été réalisée à l'Institut Laue-Langevin (Grenoble, France) sous la direction conjointe du Prof. Judith Peters et Dr. Peter Timmins et à l'Institut de Recherche de Physique du Solide et d'Optique (Budapest, Hongrie) sous la direction conjointe du Dr. Győző Garab et Dr. László Rosta.

L'un des défis scientifiques les plus importants de notre époque consiste à trouver des réponses et des solutions aux différentes questions et problèmes liés à la consommation d'énergie rapidement croissante de l'humanité. La prédominance actuelle des combustibles fossiles dans la production d'énergie mondiale ne peut pas être maintenue à long terme, en raison de la diminution rapide des ressources facilement exploitables et des conséquences potentiellement catastrophiques de la concentration croissante de dioxyde de carbone dans l'atmosphère. En conséquence, les études scientifiques sur l'utilisation des ressources renouvelables, de leur transformation en sources d'énergie écologiques facilement stockables et transportables deviennent de plus en plus importantes.

L'énergie solaire a un rôle exceptionnel parmi ces ressources. En effet, toutes les heures suffisamment de lumière atteint la surface de la Terre pour satisfaire aux besoins mondiaux annuels en énergie (Harnessing solar energy for the production of clean fuel (2008) Science Policy Briefing of the European Science Foundation). Dans la biosphère, la conversion d'énergie solaire en énergie chimique est réalisée par les organismes photosynthétiques. La photosynthèse sert d'entrée d'énergie pour la vie terrestre actuelle et elle équilibre la concentration de dioxyde de carbone et d'oxygène dans l'atmosphère. Des organismes photosynthétiques modifiés ou des appareils artificiels inspirés par la photosynthèse pouvant convertir l'énergie solaire ont le potentiel de contribuer de façon significative à la production d'énergie industrielle. Dans sa forme naturelle la photosynthèse est cependant loin d'être comprise. Ce constat est particulièrement vrai pour les différents mécanismes de régulation, qui permettent à l'appareil photosynthétique à s'adapter à diverses conditions environnementales.

Les membranes thylakoïdes sont les membranes les plus abondantes sur Terre et jouent donc un rôle central dans la photosynthèse par leurs réactions de lumière. Dans la présente thèse nous étudions les paramètres structuraux des membranes thylakoïdes, isolés des plantes supérieures et dans des différentes cellules d'algues et de cyanobacteria, par la diffusion de neutrons aux petits angles, et la dynamique des fragments de membranes thylakoïdes isolés, par diffusion incohérente élastique de neutrons. L'un de nos principaux objectifs a été d'étudier les échantillons aussi près que possible des conditions *in vivo* en profitant du caractère non-invasif de la diffusion

neutronique. Les résultats montrent des preuves claires de la présence de réorganisations petites, mais bien perceptibles dans les membranes des thylakoïde pendant la photosynthèse, et aussi une transition dans les membranes BBY à des températures physiologiques. Ils indiquent également des applications possibles de diffusion des neutrons à l'étude des échantillons biologiques *in vivo*.

Cette thèse est composée de neuf chapitres. Après cette introduction générale sur la motivation du travail, certains aspects importants des neutrons, de la production neutronique et les bases théoriques de la diffusion des neutrons thermiques sont présentés dans le Chapitre 2, avec une introduction courte des deux types d'instruments utilisés dans nos expériences. Dans le Chapitre 3 un bref aperçu de la photosynthèse est donné avec une présentation des réactions lumineuses et des complexes protéiques participants et avec une discussion plus détaillée de la structure de la membrane thylakoïde qui accueille ces complexes.

Ensuite, les protocoles de préparation des échantillons, l'analyse de la composition de certains des échantillons étudiés, la description des techniques expérimentales appliquées sont présentés dans le Chapitre 4, et une description brève des différentes méthodes et des calculs utilisés dans l'interprétation des données expérimentales est donnée.

Des études structurales des membranes thylakoïdes extraites de feuilles d'épinard par diffusion de neutrons aux petits angles sont présentées dans les Chapitres 5 et 6. Nous commençons la discussion par l'identification des deux pics caractéristiques présents dans les courbes de diffusion moyennées radialement à l'aide des résultats présentés dans la littérature et de nos données expérimentales, ensuite nous étudions l'influence des différents paramètres environnementaux, tels que l'osmolarité, la force ionique ou la phosphorylation sur la structure des lamelles du stroma et du granum. Dans le Chapitre 6, nous présentons nos résultats qui révèlent des réorganisations structurales des thylakoïdes du stroma pendant la photosynthèse, avec une résolution temporelle de plusieurs secondes. Nous montrons que les changements sont plus prononcés lorsque le transport cyclique des électrons autour de PSI fonctionne et qu'ils sont générés par le ΔpH transmembranaire produit pendant la photosynthèse.

Dans le Chapitre 7, nous démontrons que la diffusion de neutrons aux petits angles peut également être utilisée pour l'étude de la structure des membranes thylakoïdes de cellules d'algues et de cyanobactéries *in vivo*. En outre, nous révélons des réorganisations petites mais bien discernables et réversibles, induites par l'illumination, dans les membranes thylakoïdes de *Phaeodactylum tricornutum* et de PAL mutante des cellules *Synechocystis* PCC 6803.

Dans le Chapitre 8 la diffusion incohérente élastique des neutrons est utilisée pour la caractérisation dynamique des fragments de membranes du Photosystème II. Les expériences ont été réalisées dans la région de température physiologique et ultra-physiologique pertinente et révèlent une transition dépendante de l'hydratation de la membrane. Ceci peut être lié à l'enlèvement induit par la chaleur du complexe évolutif de l'oxygène.

Enfin dans le Chapitre 9 les résultats, présentés dans cette thèse, sont résumés et quelques perspectives sont proposées pour la poursuite de ce projet en l'appliquant la diffusion de neutrons à l'étude des membranes photosynthétiques.

2. Neutron Scattering, a Tool to Study the Structure and Dynamics of Biological Systems

Neutron scattering is a widely used technique for studying the structure and dynamics of biological systems. Structure determination studies range from monitoring conformational changes of proteins upon interacting with different molecules, or the elucidation of the protein oligomeric state in solution or kinetic studies of protein-protein interactions with small-angle scattering, to e.g. neutron protein crystallography providing precise information about the organization of water molecules present in a crystal. Incoherent neutron scattering experiments can provide information e.g. about the dynamical behavior of entire proteins, of their specific subunits or of the hydration water or the diffusion of proteins in solution.

In this chapter basic characteristics of the neutron and neutron scattering will be summarized along with the two neutron scattering techniques, used in the present studies.

2.1 Neutrons, Neutron Scattering

2.1.1 General Properties of Neutrons

Table 1: Basic physical parameters of the neutron (Dianoux and Lander 2003).

Charge	0
Mass	$m = 1.674928(1) \cdot 10^{-27}\, kg$
Spin	$s = -\hbar / 2$
Magnetic moment	$\mu = -9.6491783(18) \cdot 10^{-27}\, JT^{-1}$
β-decay lifetime	$\tau = 885.9 \pm 0.9 s$
Quark structure	udd

Neutrons along with protons form the nuclei of all the atoms in nature (with the exception of ^{1}H). Neutrons are subatomic particles, without electrical charge, and with a mass slightly higher than that of the protons. They were discovered in 1932 by James Chadwick (Chadwick 1932). Basic parameters for the neutrons can be found in Table 1. Due to their electrical neutrality neutrons can penetrate deeply into matter and, since

they do not experience a Coulomb-barrier, they can get into close interaction with the atomic nuclei. Scattering of neutrons by matter is thus governed by nuclear forces. There is no complete theory describing these forces, but experimental results show that the ability of a specific atom to scatter neutrons is not a simple function of the atomic number. On the contrary, it can be significantly different even for different isotopes of the same atom (Sears 1992).

2.1.2 Production of Neutrons

There are currently two means of producing neutrons in significant quantities for scattering experiments. In research reactors with a constant flux (e.g. Institut Laue-Langevin, Budapest Neutron Center, etc.), uranium-235 splits into smaller nuclei while emitting on average about 2.5 neutrons (Martin 2006). About 1.5 neutrons are needed to maintain the chain reaction, so only 1 neutron can be used for experiments. In spallation sources a heavy metal target is bombarded by protons accelerated to energies of about 1 GeV. As a result the heavy metal atoms undergo a spallation process, producing several nucleons and about 25-30 neutrons per proton (for instance 28 n/p in case of spallation with 1.33 GeV protons on a mercury target (Conrad 2005)).

The most important difference between the above mentioned neutron sources is the time distribution of the neutron flux. In high flux reactors the time-averaged flux ($\overline{\Phi} = 1.2 \cdot 10^{15} cm^{-2} s^{-1}$ at ILL, Grenoble) is higher than in spallation sources ($\overline{\Phi} = 2 \cdot 10^{13} cm^{-2} s^{-1}$ at ISIS, Chilton, $\overline{\Phi} = 1.7 \cdot 10^{14} cm^{-2} s^{-1}$ at SNS, Oak Ridge, $\overline{\Phi} = 6 \cdot 10^{14} cm^{-2} s^{-1}$ - predicted at ESS). But as the neutrons in a spallation source are produced in pulses, the so-called peak flux in spallation sources ($\hat{\Phi} = 2.4 \cdot 10^{15} cm^{-2} s^{-1}$ at ISIS, Chilton, $\hat{\Phi} = 1.7 \cdot 10^{16} cm^{-2} s^{-1}$ at SNS, Oak Ridge, $\hat{\Phi} = 1.4 \cdot 10^{17} cm^{-2} s^{-1}$ - predicted at ESS) (Conrad 2005) is higher than the average flux in reactors. The choice of the instrument type depends thus often on the source characteristics. Time-of-flight instruments, which can exploit the time structure of the beam and hence use most of the available neutrons, are in general favored at spallation sources, whilst monochromatic instruments, where a large portion of the available neutrons is discarded, are best used at reactor sources. However, an important disadvantage of time of flight (TOF) instruments built on pulsed sources is the fact that the I(t) distribution of the neutrons arriving on the

detectors is quite asymmetric, compared to a TOF instrument built on a continuous source (see (Loong et al. 1987; Peters et al. 2006)).

Since in many fields of science neutrons and x-rays are investigation methods used in parallel, it is interesting to discuss the fluxes of some of the x-ray sources. The flux of these sources is characterized by a different unit than for neutrons; by the $brightness = \frac{spectral\ flux}{solid\ angle}$, $[] = \frac{photons}{s \cdot mrad^2} / \left(\frac{\Delta\lambda}{\lambda} = 0.1\% \right)$ or by the $brilliance = \frac{spectral\ flux}{solid\ angle \cdot surface}$, $[] = \frac{photons}{s \cdot mrad^2 mm^2} / \left(\frac{\Delta\lambda}{\lambda} = 0.1\% \right)$. At the European Radiation Facility in Grenoble (ESRF) the available brilliance is $10^{20} - 10^{21} \frac{photons}{s \cdot mrad^2 mm^2} / \left(\frac{\Delta\lambda}{\lambda} = 0.1\% \right)$ (ESRF 2011), and at the Free-electron Laser in Hamburg the peak brilliance is $10^{29} - 10^{30} \frac{photons}{s \cdot mrad^2 mm^2} / \left(\frac{\Delta\lambda}{\lambda} = 0.1\% \right)$ (Tiedtke et al. 2009). Although they are not directly comparable we can state that x-ray sources offer much higher fluxes than neutron sources.

There are few exceptions from the above mentioned classification of neutron sources. The Swiss Spallation Neutron Source is an almost continuous spallation source while the IBR-2 reactor in Dubna, Russia, is a fast pulsed reactor.

The wavelength or the related energy of the neutrons is a crucial parameter for the different neutron scattering techniques. Neutrons produced by either of the above mentioned techniques have typical energies of the order of MeV (Harroun et al. 2006). However only slow neutrons ($E < 1keV$) can be used for structural and dynamical investigations (Conrad 2005). The energy distribution of the neutrons is modified by thermalization in different moderators, placed close to the source of the neutrons. Supposing a thermodynamic equilibrium with the moderator, neutrons have a Maxwellian distribution of velocities. The relationship between the wavelength, λ, the kinetic energy calculated with the most probable velocity (Profio 1976), E, the velocity, v and the wavevector, k, of a neutron, thermalized in a moderator with temperature, T, can be described by

$$E = k_B T = \frac{1}{2} m v^2 = \frac{h^2}{2m\lambda^2} = \frac{\hbar^2 k^2}{2m}, \qquad \textbf{2.1}$$

where $k_B = 1.380\,6504(24)\cdot 10^{-23}\,\frac{J}{K} = 8.617\,343(15)\cdot 10^{-5}\,\frac{eV}{K}$ is the Boltzmann's constant and m is the mass of the neutron (Squires 1978). If we use the following variables with the given dimensions: $[E] = meV, [T] = K, [v] = \frac{km}{s}, [\lambda] = \text{Å}, [k] = \frac{1}{\text{Å}}$, we get the following relations without dimensions (Squires 1978)

$$\lambda = 6.283\frac{1}{k} = 3.956\frac{1}{v} = 9.045\frac{1}{\sqrt{E}} = 30.81\frac{1}{\sqrt{T}}. \qquad \textbf{2.2}$$

The wavelength distribution can thus be influenced by the application of moderators with different temperatures. Commonly used moderators and corresponding temperature and neutron energy values can be found in Table 2 (Lovesey 1984). Neutrons, thermalized in different moderators, can be used for different experimental techniques.

Table 2: Terminology and kinetic energy of neutrons thermalized in different moderators.

	Neutron energy	Moderator material and temperature
Cold neutrons	$E \le 10\,meV$	Liquid H_2 or D_2, $T = 20K$
Thermal neutrons	$10\,meV \le E \le 100\,meV$	H_2O and D_2O, $T = 290K$
Hot neutrons	$100\,meV \le E \le 500\,meV$	Graphite, $T = 2000K$
Epithermal neutrons	$500\,meV \le E$	

2.1.3 General Neutron Scattering Experiments

In order to understand the different neutron scattering experiments, we need to know what type of information we can obtain during the experiments. For simplicity we consider a monochromatic beam of incident neutrons hitting the sample under investigation. Neutrons can be absorbed by the sample, can be scattered by it or can traverse it without interaction. The number of neutrons per second absorbed by the sample, I_a, and the number of neutrons per second scattered by the sample, I_s, can be expressed by $I_a = 4\pi\Phi\sigma_a$ and $I_s = 4\pi\Phi\sigma_s$, where σ_a, and σ_s are the absorption and

scattering cross-section, respectively, their usual unit is the barn ($1\,barn = 10^{-24}\,m^2$), and Φ is the flux of the incoming neutron beam in $neutrons/(cm^2\,s)$.

Neutrons scattered at a sample can be characterized by the incident wavevector ***k***, the wavevector of the scattered neutron, ***k'*** and with the corresponding *E* and *E'* neutron energies (see equation 2.1). Important parameters of the scattering process are the energy transfer from the neutron to the sample:

$$\hbar\omega = E - E' = \frac{\hbar^2 k^2}{2m} - \frac{\hbar^2 k'^2}{2m} \qquad \textbf{2.3}$$

and the scattering vector:

$$\boldsymbol{Q} = \boldsymbol{k} - \boldsymbol{k'}. \qquad \textbf{2.4}$$

The latter one is shown in Figure 1.

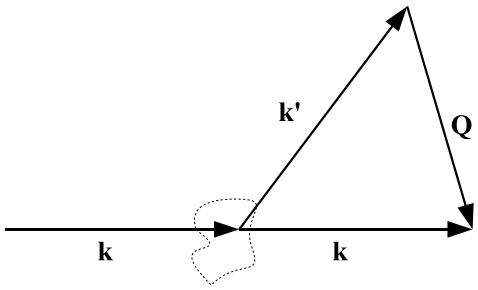

Figure 1: Scattering of a neutron with an incident wave vector ***k*** and a scattered wave vector ***k'***. The momentum transfer corresponds to the scattering vector $\boldsymbol{Q} = \boldsymbol{k} - \boldsymbol{k'}$.

In a typical scattering experiment (see Figure 2) neutrons are scattered anisotropically in different directions. The number of neutrons, N, scattered in a specific direction, characterized by the angles θ and φ, into a solid angle, dΩ, can be described by the differential scattering cross-section (Harroun et al. 2006):

$$\frac{d\sigma_s}{d\Omega} = \frac{N(\theta,\varphi)}{\Phi d\Omega}. \qquad \textbf{2.5}$$

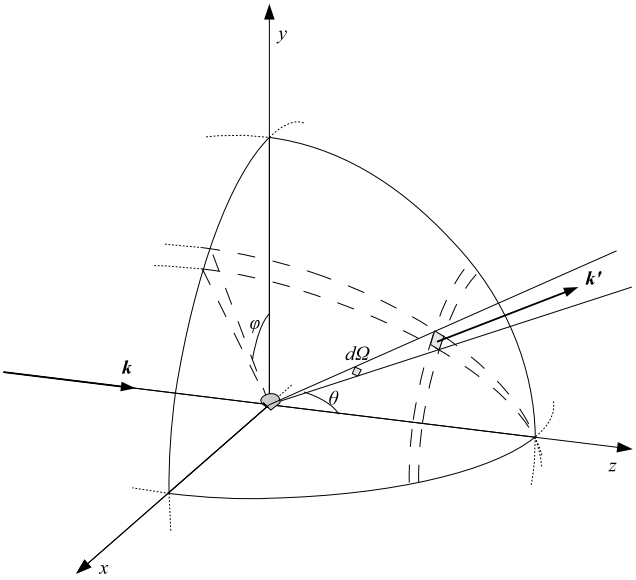

Figure 2: Schematic geometry for a scattering process.

Considering a change in the neutron energy during the scattering process, equation 2.5 is modified to give (Squires 1978):

$$\frac{d^2\sigma_s}{d\Omega dE'} = \frac{N(\theta,\varphi,E')}{\Phi d\Omega dE'}, \qquad \textbf{2.6}$$

where all the neutrons have a final energy between *E'* and *E'+dE'*. In the neutron scattering experiments presented in the following chapters, we either measure the number of scattered neutrons independently from their energy as described by equation 2.5 or we analyze also the energy of the scattered neutrons as described by equation 2.6.

2.1.4 Scattering of Neutrons by a Sample

In a typical neutron scattering experiment the instrument and the sample are tens of meters away from the neutron source. The connection between the source and the sample is provided by a set of fixed and/or exchangeable elements of neutron guides and collimators.

Neutron guides usually consist of mirrors, for example nickel coated glass plates arranged around a rectangular form under vacuum, capable of totally reflecting neutrons, which hit the mirror at an angle below the critical angle of the mirror-material (Sears

1989). The critical angle for a non-multilayer surface is wavelength dependent and can be calculated as

$$\phi_c = \lambda\sqrt{\left(\frac{\rho b}{\pi}\right)}, \qquad \textbf{2.7}$$

where ρ is the average number of atoms per unit volume and b is the coherent scattering length of the molecule or atom, of which the mirror is made (Sears 1989). In a more complicated system, called supermirror, a multilayer is used which is built up from unit bilayers of two different materials, with increasing unit bilayer thickness, providing nearly perfect total-reflection up to an angle several times higher than the critical-angle of usual neutron mirrors. Neutron guides have the advantage, apart from neutron transportation capabilities, that they selectively transmit longer wavelength neutrons, as the critical angle increases with neutron-wavelength. Shorter wavelength neutrons and γ rays, for which the guide is almost transparent, are absorbed by the radiation protection mounted around the guides, and are not transported to the instruments. With a properly curved neutron guide the background at the instruments can be significantly reduced.

Collimators (usually tubes under vacuum, surrounded by materials with high neutron absorbance, such as cadmium and different boron-compounds) are sometimes needed for the instrumentation in order to eliminate the diverging neutrons.

For distance within the sample less than $\frac{L}{2\pi a}\lambda$, (where L is the distance of the sample from the so-called virtual source of neutrons, and a is the size of the virtual source perpendicular to the neutron beam), the incident neutron can be considered as a plane wave (Gahler 2010). As a consequence the observable object-size in a neutron scattering experiment strongly depends on the selection and adjustment of the instruments.

2.1.4.1 Scattering of Neutrons from one Single Bound Nucleus

The simplest theoretical case of a scattering experiment is the scattering from one single atomic nucleus, at the origin position ($x = y = z = 0$) in the coordinate system. The wave function of the incident neutrons can be described as a plane wave

$$\psi_{inc} \sim e^{ikz}, \qquad \textbf{2.8}$$

where the z-axis is oriented along $\boldsymbol{k}$, the wave vector of the incident neutrons. As mentioned in 2.1.1, neutrons have almost no interaction with the electron cloud of the atom, and their scattering is governed by nuclear forces. Nucleon-nucleon forces have a range of $(1-2)\times10^{-15}\,m$ (Martin 2006), which is several orders of magnitude lower than the wavelength of neutrons used in scattering experiments, being $(0.4-30)\times10^{-10}\,m$ (Squires 1978). Thus the scattering is spherically symmetric and the wave function of the scattered neutrons can only contain an s-wave component (which only depends from $|\boldsymbol{r}|$). It can be characterized by a constant b, called the scattering length (Egelstaff 1965), and the outgoing wave function can thus be written in the form:

$$\psi_{scat} = -b\frac{e^{ik'r}}{r}. \qquad \textbf{2.9}$$

The negative sign of b is a convention accounting for a positive value of b for a repulsive potential. In a general case b is a complex number and one can show that the imaginary part of it is related to the absorption cross-section of the atom according to $\sigma_a = -\frac{4\pi}{k}\,\mathrm{Im}\,b$ (Lovesey 1984; Sears 1992).

Considering elastic scattering, and using equations 2.5, 2.8 and 2.9 we can calculate (Egelstaff 1965):

$$\sigma_s = \frac{4\pi r^2 \cdot v \cdot \left|-b\frac{e^{ik'r}}{r}\right|^2}{v\cdot\left|e^{ikz}\right|^2} = 4\pi|b|^2. \qquad \textbf{2.10}$$

The only form of potential which can cause an isotropic scattering into a spherical wave is a delta function, which, with the proper parameters, is called the Fermi pseudo-potential (Squires 1978):

$$V(\boldsymbol{r}) = \frac{2\pi\hbar^2 b}{m}\delta(\boldsymbol{r}). \qquad \textbf{2.11}$$

In case the potential is repulsive, which is true for about 90% of the atoms in nature (Cser 2010), we obtain positive values for b (Squires 1978). Experimentally measured values of b for different isotopes of all the elements can be found in (Lovesey 1984).

2.1.4.2 Coherent and Incoherent Scattering

For a more appropriate approach of a real scattering experiment we consider now the scattering from a system of N atoms of the same element at positions R_j having a scattering length b_j where $j \in [1, N]$. The b_j values can be different due to the possible existence of different isotopes of the same element in the sample or due to the relative spin orientation of the neutrons and the scattering atom (in the case of a non-zero atom-spin, since the scattering length of the neutron is different depending on the atom- and neutron-spin being parallel or not). Using equation 2.11 the Fermi pseudo-potential of this system becomes:

$$V(\boldsymbol{r}) = \frac{2\pi\hbar^2}{m}\sum_j b_j \delta(\boldsymbol{r} - \boldsymbol{R_j}). \qquad \textbf{2.12}$$

If we use Fermi's Golden rule for calculating the probability of the transition of a plane wave state defined by $\boldsymbol{k}$ to another defined by $\boldsymbol{k'}$ and we use the Born approximation (i.e. that the initial wave is only slightly perturbed by the scattering) and we assume that the spatial coordinates and scattering lengths are not correlated, it follows (Richter 2005) that

$$\frac{d\sigma_s}{d\Omega} = \sum_{jj'} e^{i\boldsymbol{Q}(\boldsymbol{R_j} - \boldsymbol{R_{j'}})}\overline{b_{j'}^{*} b_j}, \qquad \textbf{2.13}$$

where $\overline{b_{j'}^{*} b_j}$ represents the average of $b_{j'}^{*} b_j$ over random isotope distributions and spin orientations of the scatterer elements. $\overline{b_{j'}^{*} b_j}$ equals $\left|\bar{b}\right|^2$ if $j \neq j'$ and $\overline{|b|^2}$ if $j = j'$, which gives for the differential scattering cross-section:

$$\frac{d\sigma_s}{d\Omega} = \sum_{j,j'}\left[\left|\overline{b}\right|^2 + \delta_{j,j'}\left(\overline{\left|b\right|^2} - \left|\overline{b}\right|^2\right)\right]e^{i\boldsymbol{Q}(\boldsymbol{R}_j - \boldsymbol{R}_{j'})}, \qquad \textbf{2.14}$$

which can be divided into a structure dependent part, called the coherent cross-section:

$$\left(\frac{d\sigma_s}{d\Omega}\right)_c = \left|\overline{b}\right|^2 \sum_{j,j'} e^{i\boldsymbol{Q}(\boldsymbol{R}_j - \boldsymbol{R}_{j'})} = \frac{\sigma_c}{4\pi}\sum_{j,j'} e^{i\boldsymbol{Q}(\boldsymbol{R}_j - \boldsymbol{R}_{j'})}, \qquad \textbf{2.15}$$

and a structure independent part, called the incoherent cross-section (Richter 2005):

$$\left(\frac{d\sigma_s}{d\Omega}\right)_i = N\left(\overline{\left|b\right|^2} - \left|\overline{b}\right|^2\right) = \frac{\sigma_i}{4\pi}N, \qquad \textbf{2.16}$$

where $\sigma_c = 4\pi\left|\overline{b}\right|^2$ and $\sigma_i = 4\pi\left(\overline{\left|b\right|^2} - \left|\overline{b}\right|^2\right)$. As 2.15 shows, the coherent cross-section gives information about the structure in the sample, and its intensity depends strongly on the angular directions, while 2.16 shows that the incoherent cross-section is structure independent and completely isotropic.

By introducing the static structure factor (Lechner and Longeville 2006):

$$S(\boldsymbol{Q}) = \frac{1}{N}\sum_{j,j'} e^{i\boldsymbol{Q}(\boldsymbol{R}_j - \boldsymbol{R}_{j'})} = \frac{1}{N}\left|\sum_j e^{i\boldsymbol{Q}\boldsymbol{R}_j}\right|^2 \qquad \textbf{2.17}$$

the coherent cross-section can be expressed as $\left(\frac{d\sigma_s}{d\Omega}\right)_c = \frac{\sigma_c}{4\pi}NS(\boldsymbol{Q})$.

The most important consequence of equation 2.16 can be found when applying it for hydrogen. The scattering length of hydrogen is very different in case the spins of the neutron and of the hydrogen atom are parallel or antiparallel, which results in the fact that hydrogen has the highest incoherent cross-section among the biologically relevant elements (Sears 1992; Schober 2010).

2.1.4.3 Scattering Function, Correlation Function

Neutrons can give us information not only about the structure of the sample, e.g. the time averaged spatial positions of the atoms, but also about the movement of the atoms, i.e. their dynamics. For the latter purpose we have to study the scattering vector dependence of the number of neutrons scattered without changing their energy

(elastically scattered neutrons), and of neutrons which gain or lose energy during the interaction with the sample (inelastically scattered neutrons). We can obtain the double differential cross-section of the sample in an energy exchange dependent form of equation 2.13, assuming that spatial coordinates and scattering lengths are not correlated (Squires 1978):

$$\frac{d\sigma_s}{d\Omega dE'} = \frac{k'}{k}\frac{1}{2\pi\hbar}\sum_{j,j'}\overline{b_{j'}^{*}b_j}\int_{-\infty}^{\infty}\left\langle e^{-i\mathbf{Q}\mathbf{R}_{j'}(0)}e^{i\mathbf{Q}\mathbf{R}_j(t)}\right\rangle \times e^{-i\omega t}dt \qquad \textbf{2.18}$$

where $\langle\cdots\rangle$ denotes the thermal average over all possible states of the sample, which in this case can be written as:

$$\left\langle e^{-i\mathbf{Q}\mathbf{R}_{j'}(0)}e^{i\mathbf{Q}\mathbf{R}_j(t)}\right\rangle = \sum_{\lambda_i} p(\lambda_i)\left\langle \lambda_i\left|e^{-i\mathbf{Q}\mathbf{R}_{j'}(0)}e^{i\mathbf{Q}\mathbf{R}_j(t)}\right|\lambda_i\right\rangle. \qquad \textbf{2.19}$$

$p(\lambda_i)$ is the population probability of the possible states $|\lambda_i\rangle$ (Schober 2010). The double differential cross-section can be divided into coherent and incoherent parts by the same method as detailed in 2.1.4.2., giving

$$\begin{aligned}\frac{d\sigma_s}{d\Omega dE'} &= \frac{k'}{k}\frac{1}{2\pi\hbar}\sum_{j,j'}\overline{b_{j'}^{*}b_j}\int_{-\infty}^{\infty}\left\langle e^{-i\mathbf{Q}\mathbf{R}_{j'}(0)}e^{i\mathbf{Q}\mathbf{R}_j(t)}\right\rangle \times e^{-i\omega t}dt = \\ &\frac{k'}{k}\frac{1}{2\pi\hbar}\left(\bar{b}\right)^2\sum_{j,j'}\int_{-\infty}^{\infty}\left\langle e^{-i\mathbf{Q}\mathbf{R}_{j'}(0)}e^{i\mathbf{Q}\mathbf{R}_j(t)}\right\rangle \times e^{-i\omega t}dt + \\ &+\frac{k'}{k}\frac{1}{2\pi\hbar}\left(\overline{b^2}-\left(\bar{b}\right)^2\right)\sum_{j}\int_{-\infty}^{\infty}\left\langle e^{-i\mathbf{Q}\mathbf{R}_j(0)}e^{i\mathbf{Q}\mathbf{R}_j(t)}\right\rangle \times e^{-i\omega t}dt\end{aligned} \qquad \textbf{2.20}$$

By substituting σ_c and σ_i we get

$$\left(\frac{d\sigma_s}{d\Omega dE'}\right)_c = \frac{\sigma_c}{4\pi}\frac{k'}{k}\frac{1}{2\pi\hbar}\sum_{j,j'}\int_{-\infty}^{\infty}\left\langle e^{-i\mathbf{Q}\mathbf{R}_{j'}(0)}e^{i\mathbf{Q}\mathbf{R}_j(t)}\right\rangle \times e^{-i\omega t}dt \qquad \textbf{2.21}$$

for the coherent double differential cross-section and

$$\left(\frac{d\sigma_s}{d\Omega dE'}\right)_i = \frac{\sigma_i}{4\pi}\frac{k'}{k}\frac{1}{2\pi\hbar}\sum_{j}\int_{-\infty}^{\infty}\left\langle e^{-i\mathbf{Q}\mathbf{R}_j(0)}e^{i\mathbf{Q}\mathbf{R}_j(t)}\right\rangle \times e^{-i\omega t}dt \qquad \textbf{2.22}$$

for the incoherent part.

One can define1954 $S_c(\boldsymbol{Q},\omega)=\frac{1}{N}\frac{1}{2\pi\hbar}\sum_{j,j'}\int_{-\infty}^{\infty}\left\langle e^{-i\boldsymbol{Q}\boldsymbol{R}_{j'}(0)}e^{i\boldsymbol{Q}\boldsymbol{R}_j(t)}\right\rangle\times e^{-i\omega t}dt$, called coherent scattering function and $S_i(\boldsymbol{Q},\omega)=\frac{1}{N}\frac{1}{2\pi\hbar}\sum_{j}\int_{-\infty}^{\infty}\left\langle e^{-i\boldsymbol{Q}\boldsymbol{R}_{j}(0)}e^{i\boldsymbol{Q}\boldsymbol{R}_j(t)}\right\rangle\times e^{-i\omega t}dt$, called incoherent scattering function, which are independent of the number of scattering atoms in the system, to obtain:

$$\left(\frac{d\sigma_s}{d\Omega dE'}\right)_c=\frac{\sigma_c}{4\pi}\frac{k'}{k}NS_c(\boldsymbol{Q},\omega) \qquad \textbf{2.23}$$

$$\left(\frac{d\sigma_s}{d\Omega dE'}\right)_i=\frac{\sigma_i}{4\pi}\frac{k'}{k}NS_i(\boldsymbol{Q},\omega). \qquad \textbf{2.24}$$

The scattering functions are defined in reciprocal and energy space. However, to obtain a structure of a macromolecule, or to compare the results with molecular dynamics simulation, the information about the samples is needed in real and time space. For this purpose a method, presented first by Van Hove (1954), can be used. One can introduce the so-called intermediate function:

$$I_c(\boldsymbol{Q},t)=\frac{1}{N}\sum_{j,j'}\left\langle e^{-i\boldsymbol{Q}\boldsymbol{R}_{j'}(0)}e^{i\boldsymbol{Q}\boldsymbol{R}_j(t)}\right\rangle=\hbar\int_{-\infty}^{\infty}S_c(\boldsymbol{Q},\omega)\times e^{-i\omega t}d\omega \qquad \textbf{2.25}$$

and the self-intermediate function:

$$I_s(\boldsymbol{Q},t)=\frac{1}{N}\sum_{j}\left\langle e^{-i\boldsymbol{Q}\boldsymbol{R}_{j}(0)}e^{i\boldsymbol{Q}\boldsymbol{R}_j(t)}\right\rangle=\hbar\int_{-\infty}^{\infty}S_i(\boldsymbol{Q},\omega)\times e^{-i\omega t}d\omega, \qquad \textbf{2.26}$$

the time-dependent pair correlation function:

$$G_c(\boldsymbol{r},t)=\frac{1}{(2\pi)^3}\int_{-\infty}^{\infty}I_c(\boldsymbol{Q},t)\times e^{-i\boldsymbol{Q}\boldsymbol{r}}d\boldsymbol{Q} \qquad \textbf{2.27}$$

and the self time-dependent pair-correlation function, also called auto-correlation function:

$$G_s(\boldsymbol{r},t)=\frac{1}{(2\pi)^3}\int_{-\infty}^{\infty} I_s(\boldsymbol{Q},t)\times e^{-i\boldsymbol{Q}\boldsymbol{r}}\,d\boldsymbol{Q}\,, \qquad \textbf{2.28}$$

which are consecutive Fourier transforms of the scattering function. One can calculate from the equations above, that in the case of a classical approximation, if the amount of the exchanged energy and momentum in the scattering process is sufficiently small (Lechner and Longeville 2006), i.e. if $\frac{(\hbar\boldsymbol{Q})^2}{2M}\langle\langle\frac{1}{2}k_BT$ and $|\hbar\omega|\langle\langle\frac{1}{2}k_BT$, where M is the mass of the scattering atom, the pair correlation functions can be written as:

$$G_c(\boldsymbol{r},t)=\frac{1}{N}\sum_{j,j'}\left\langle\delta\left(\boldsymbol{r}-\boldsymbol{R}_j(t)+\boldsymbol{R}_{j'}(0)\right)\right\rangle \qquad \textbf{2.29}$$

$$G_s(\boldsymbol{r},t)=\frac{1}{N}\sum_{j}\left\langle\delta\left(\boldsymbol{r}-\boldsymbol{R}_j(t)+\boldsymbol{R}_j(0)\right)\right\rangle, \qquad \textbf{2.30}$$

which for equivalent atoms in the scattering system simplifies to (Squires 1978):

$$G_c(\boldsymbol{r},t)=\sum_{j}\left\langle\delta\left(\boldsymbol{r}-\boldsymbol{R}_j(t)+\boldsymbol{R}_0(0)\right)\right\rangle \qquad \textbf{2.31}$$

$$G_s(\boldsymbol{r},t)=\left\langle\delta\left(\boldsymbol{r}-\boldsymbol{R}_0(t)+\boldsymbol{R}_0(0)\right)\right\rangle. \qquad \textbf{2.32}$$

Scattering functions based on this classical approximation of the correlation functions would however not fulfill the detailed balance distribution. One has thus to consider the energy dependence of the level occupation, i.e. that $S(-\boldsymbol{Q},-\omega)=e^{\frac{\hbar\omega}{k_BT}}S(\boldsymbol{Q},\omega)$ (Boltzmann 1872; Lechner and Longeville 2006). A correction factor is needed to take this into account, and the classical scattering functions calculated from equation 2.29 and 2.30 have to be multiplied by $e^{-\frac{\hbar\omega}{2k_BT}}$.

2.1.5 Incoherent Neutron Scattering

Incoherent neutron scattering gives us access to the movement of individual atoms of the sample in a certain time window, defined by the characteristics of the instrument. Since the incoherent scattering cross-section of hydrogen is two orders of magnitude higher than that of any other biologically relevant element, the incoherent scattering function

represents mainly the averaged movement of individual hydrogen atoms in biological samples. As hydrogen constitute usually about 50% of the atoms in biological macromolecules and are homogeneously distributed over the sample, they give a good overview over dynamics.

Corresponding to the characteristic neutron energy transfer values we can define three separate regions of the scattering function, associated with elastic, quasielastic and inelastic scattering, as shown in Figure 3.

In case of elastic scattering the neutrons do not exchange energy with the sample ($\hbar\omega=0$). The elastic peak, theoretically a delta function, is broadened by the instrument resolution. Rotational or translational diffusive motions present in the sample cause the appearance of the broad quasielastic feature, which is centered around the elastic peak position. Furthermore, transitions between different vibrational modes in the sample can be induced by the scattered neutrons. This process is represented by the inelastic satellite peaks of the scattering function, symmetrically located at $+\hbar\omega$ and $-\hbar\omega$ around the elastic position.

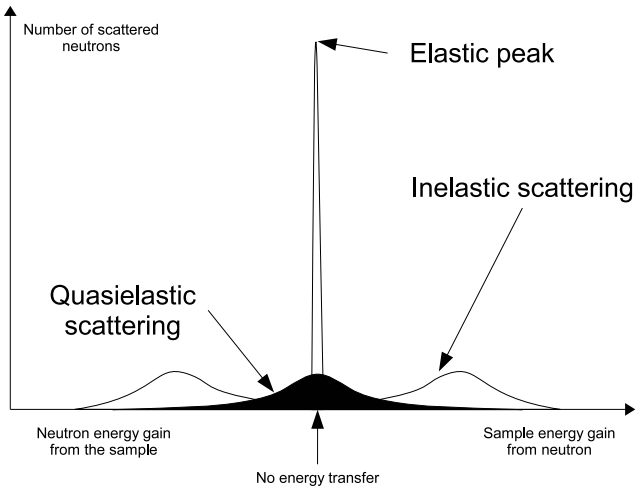

Figure 3: Different possible contributions to neutron scattering.

2.1.5.1 Elastic Incoherent Scattering Function

For simplicity we first consider only translational and rotational diffusive motions in the sample. We divide the self time dependent pair-correlation function into two terms: the

so called time independent part $G_s(\boldsymbol{r}, t \to \infty)$ and the time dependent part $G_s^{\,1}(\boldsymbol{r}, t) = G_s(\boldsymbol{r}, t) - G_s(\boldsymbol{r}, t \to \infty)$. The time independent part can vanish or have a finite value depending on the volume, in which the investigated atoms can move. If the volume is not restricted during the investigated time-window, as in case of liquids, $G_s(\boldsymbol{r}, t \to \infty)$ vanishes. One can show that the incoherent scattering function calculated from these two terms takes the following form (Bee 1988):

$$S_i(\boldsymbol{Q}, \omega) = S_i^{\,el}(\boldsymbol{Q})\delta(\omega) + S_i^{\,in}(\boldsymbol{Q}, \omega), \qquad \textbf{2.33}$$

where $S_i^{\,el}(\boldsymbol{Q})\delta(\omega)$ denotes the elastic incoherent scattering function (corresponding to the time independent part in the time space) and $S_i^{\,in}(\boldsymbol{Q}, \omega)$ denotes the inelastic incoherent scattering function. For the calculation of the elastic incoherent scattering function, we consider that in 2.22 $R_j(t)$ has an equilibrium position R_j, and thus we can define $u(t) = R_j(t) - R_j$, assuming that deviation u has a Gaussian distribution, which is an appropriate approximation e.g. for harmonic oscillations.

If we apply this approximation for 2.22 and 2.24 we get

$$\left(\frac{d\sigma_s}{d\Omega dE'}\right)_i = \frac{\sigma_i}{4\pi}\frac{k'}{k}\frac{1}{2\pi\hbar}\sum_j \int_{-\infty}^{\infty} \left\langle e^{-i\boldsymbol{Q}\left(\boldsymbol{R_j}+\boldsymbol{u}_j(0)\right)} e^{i\boldsymbol{Q}\left(\boldsymbol{R_j}+u_j(t)\right)} \right\rangle \times e^{-i\omega t} dt \qquad \textbf{2.34}$$

and

$$S_i(\boldsymbol{Q}, \omega) = \frac{1}{N}\frac{1}{2\pi\hbar}\sum_j \int_{-\infty}^{\infty} \left\langle e^{-i\boldsymbol{Q}\boldsymbol{u}_j(0)} e^{i\boldsymbol{Q}u_j(t)} \right\rangle \times e^{-i\omega t} dt\,. \qquad \textbf{2.35}$$

According to (Schober 2010) $\left\langle e^{-i\boldsymbol{Q}\boldsymbol{u}(0)} e^{i\boldsymbol{Q}u(t)} \right\rangle$ can be expressed as

$$\left\langle e^{-i\boldsymbol{Q}\boldsymbol{u}(0)} e^{i\boldsymbol{Q}\boldsymbol{u}(t)} \right\rangle = e^{-\frac{1}{2}\left\langle (\boldsymbol{Q}\boldsymbol{u}(0))^2 \right\rangle} e^{-\frac{1}{2}\left\langle (\boldsymbol{Q}\boldsymbol{u}(t))^2 \right\rangle} e^{\langle (\boldsymbol{Q}\boldsymbol{u}(0))(\boldsymbol{Q}\boldsymbol{u}(t)) \rangle} = e^{-\left\langle (\boldsymbol{Q}\boldsymbol{u}(t))^2 \right\rangle} e^{\langle (\boldsymbol{Q}\boldsymbol{u}(0))(\boldsymbol{Q}\boldsymbol{u}(t)) \rangle}. \qquad \textbf{2.36}$$

If $t \to \infty$, the second exponential in 2.36 becomes 1. Introducing the so-called Debye-Waller factor:

$$W(\boldsymbol{Q}) = \frac{1}{2}\left\langle (\boldsymbol{Q}\boldsymbol{u})^2 \right\rangle, \qquad \textbf{2.37}$$

one obtains:

$$S_i(\boldsymbol{Q},\omega=0)=\frac{1}{N}\sum_j e^{-2W_j(\boldsymbol{Q})} \quad \textbf{2.38}$$

.

$\left\langle \boldsymbol{u}^2 \right\rangle$ represents the vibrations of the atoms around their equilibrium positions. Assuming isotropic motions (Kittel 1967): $\left\langle (\boldsymbol{Qu})^2 \right\rangle \approx \frac{1}{3}\left\langle \boldsymbol{Q}^2 \right\rangle \left\langle \boldsymbol{u}^2 \right\rangle$ and

$$S_i(\boldsymbol{Q},\omega=0)=\frac{1}{N}\sum_j e^{-\frac{1}{3}\left\langle \boldsymbol{Q}^2\right\rangle\left\langle \boldsymbol{u}^2\right\rangle} \quad \textbf{2.39}$$

.

In the literature we can find two different versions of equation 2.39. In the above detailed definition u describes the displacement of an atom from the equilibrium position. If we consider $\left\langle \boldsymbol{x}^2 \right\rangle$ as mean square displacement (MSD), where we refer to the full amplitude of the motion (Smith 1991; Serdyuk et al. 2007) we obtain the following equation:

$$S_i(\boldsymbol{Q},\omega=0)=\frac{1}{N}\sum_j e^{-\frac{1}{6}\left\langle \boldsymbol{Q}^2\right\rangle\left\langle \boldsymbol{x}^2\right\rangle} \quad \textbf{2.40}$$

.

Equation 2.40 is strictly valid for $Q \to 0$ and is a good approximation if $\left\langle x \right\rangle^2 Q^2 \le 2$ (Reat et al. 1997).

One can remark that the expression found in 2.39 is similar to the Guinier-approximation used in small-angle neutron scattering for calculating the radius of gyration in the sample (Guinier and Fournet 1955; Krueger et al. 2006).

In most of the calculations above we considered the presence of one single element in the sample. In real samples one usually has different atoms with different MSD values and different neutron cross-section values, thus equation 2.40 must be generalized to:

$$S_i(\boldsymbol{Q},\omega=0)=\frac{1}{\overline{|b|^2}-|\bar{b}|^2}\sum_j\left(\overline{|b_j|^2}-|\overline{b_j}|^2\right)e^{-\frac{1}{6}\left\langle \boldsymbol{x}_j^2\right\rangle \boldsymbol{Q}^2} \quad \textbf{2.41}$$

.

However, when working with hydrogenated biological samples 2.40 is an appropriate approximation, taking into account the high incoherent cross-section value of hydrogen.

Having obtained the $S_i(\boldsymbol{Q},\omega=0)$ value from an experiment the MSD values can finally be calculated through:

$$\langle x^2\rangle(T) = -6\frac{d\ln(S_i(Q,\omega=0))}{d(Q^2)} \quad \textbf{2.42}$$

.

2.1.5.2 Mean Force Constant

The mean square displacement values, measured at different temperatures, can reveal important characteristics of the dynamics of biological samples. It is generally accepted that protein dynamics are strongly correlated with the functionality of the protein (Zaccai 2000a). In Figure 4 MSDs are plotted as a function of temperature and show the onset of diffusive protein motions at ~ 250K in photosystem II. Below this dynamical transition the dynamics of proteins is usually described as harmonic motions within potential wells, and represented by their effective mean force constant. In the higher temperature region the dynamics of the proteins can be best described as the sum of harmonic motion within potential wells, and jump diffusion between the different wells and are best represented by a pseudo force constant, which describes the resilience of the system towards the jumps between the wells (Zaccai 2000a). Both types of the above mentioned effective mean force constants, (notion introduced by Giuseppe Zaccai in 2000) can be calculated according to (Zaccai 2000a):

$$\langle k\rangle = \frac{0.00276}{d\langle x^2\rangle / dT}, \quad \textbf{2.43}$$

where <k> is in units of Newtons per meter and $<x^2>$ in Angstroms squared and T is the absolute temperature.

2.1.6 Neutron Spectrometers

Neutron spectrometers are used to provide information about the double differential cross-section $\frac{d^2\sigma_s}{d\Omega dE'}(\boldsymbol{Q},\omega)$. In most of the instruments this is done by defining the energy distribution of the incoming neutrons, and measuring their angular and energy distribution after the scattering process. However, the experimental techniques used to

perform these tasks, and the accessible (Q, ω)-ranges and resolution values are different for all instruments and can thus be used for specific studies (see Figure 5).

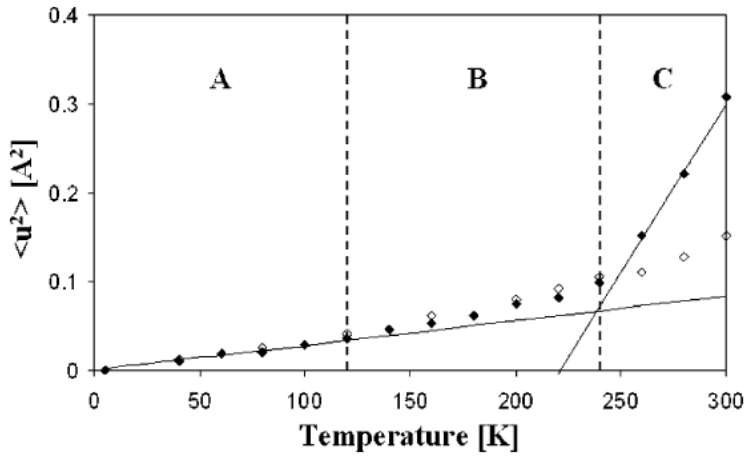

Figure 4: Temperature dependence of MSD obtained from elastic intensity of hydrated (full squares) and dry (open squares) photosystem II samples. (From (Pieper et al. 2007)).

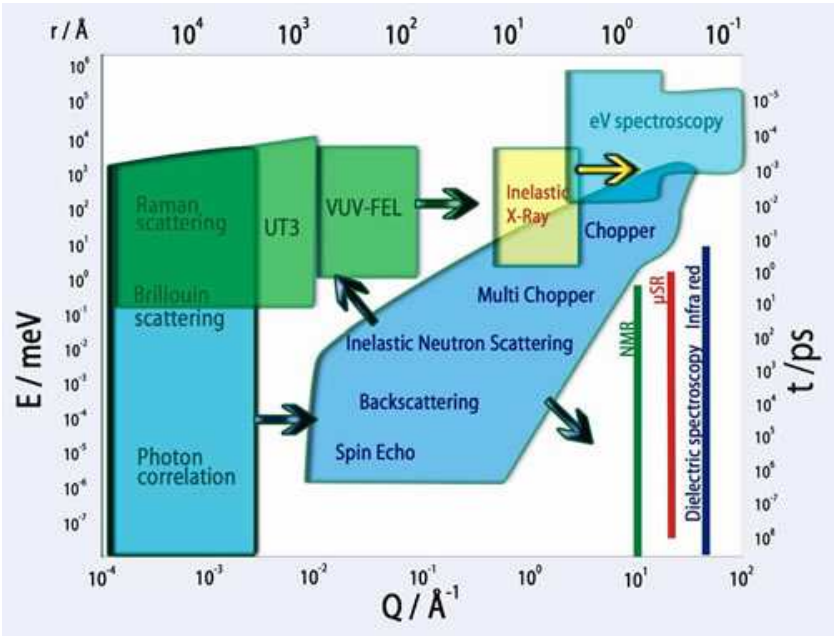

Figure 5: Scattering vector and energy range covered by different neutron scattering techniques, in comparison with other experimental methods (copied from (Buttaro 2005)).

2.1.6.1 Backscattering Spectrometers

Backscattering (BSC) instruments achieve an energy resolution of the order of several μeVs. During Bragg reflection of a plane-wave on a perfect crystal, the energy resolution

of the reflected neutrons will be the highest if the wave vector is perpendicular to the scattering plane (Alefeld 1966; Lechner and Longeville 2006). In BSC instruments the analyzer crystals are placed circularly around the sample position, thus those scattered neutrons which have the proper energy (defined by the Bragg equation) are reflected back onto the sample by the analysers. A detailed description of the IN13 instrument at the ILL can be seen in Figure 6.

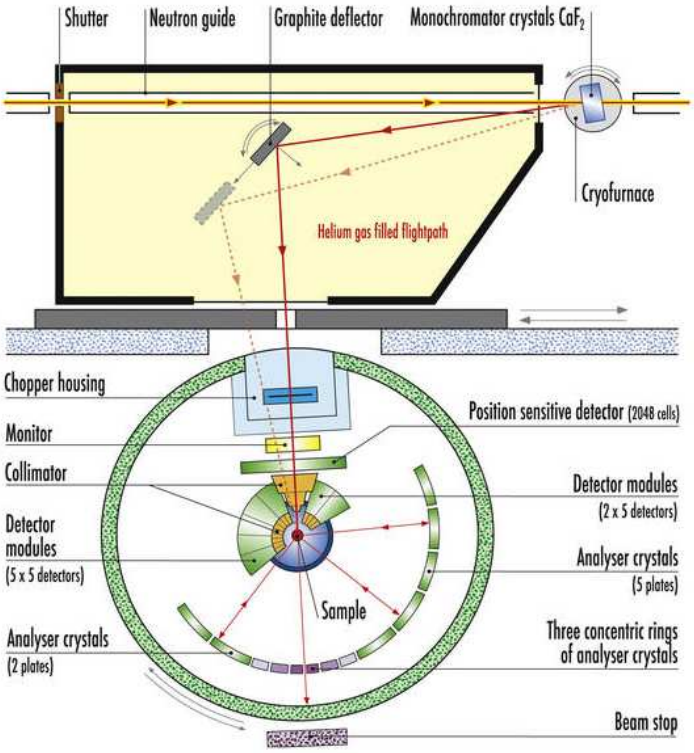

Figure 6: Instrument layout of the IN13 backscattering spectrometer at the ILL. (From The Yellow Book 2008, Guide to Neutron Research Facilities, ILL.) The neutron energy is selected by the monochromator crystals, and can be varied by changing the d spacing via controlling the temperature of the crystal. A vertically curved graphite deflector reflects and focuses the neutrons on the sample. A low efficiency uranium-based monitor which detects the number of incoming neutrons, is used for normalization. Neutrons scattered by the sample are analyzed by the analyzer crystals, and reflected back onto the sample if they have the appropriate energy. After traversing the sample a second time, they are detected by He^3 gas counter detectors. The number of neutrons not originating from backscattering is reduced by the application of collimator cones in front of the detectors. Neutrons scattered from the sample directly to the detectors are not counted due to synchronization of a chopper forming pulses in the incoming neutron beam and of the detector electronics. The energy resolution of the instrument is usually set to 8 μeV (FWHM), corresponding to a time window of about 100 ps. The wavelength of the detected neutrons (defined by the analysers) is 2.23 Å. The momentum transfer range of 0.19 $Å^{-1}$ – 4.9 $Å^{-1}$ makes the instrument appropriate to probe length scales ranging from 1.28 to 33.4 Å, considering the equation of $R \sim \frac{2\pi}{Q}$ (Natali et al. 2008).

2.1.7 Small-Angle Neutron Scattering

A schematic view of the D22 SANS instrument at the Institut Laue-Langevin can be seen in Figure 7. SANS instruments built on a reactor source usually use neutrons moderated in cold sources. The instruments are situated preferably far from the neutron source in order to reduce the background of the experiments. Neutrons, transported through neutron guides are monochromatized by a velocity selector, whose rotation speed determines the average wavelength (λ) of the transmitted neutrons. The wavelength distribution ($\Delta\lambda/\lambda$) of the monochromatized neutron beam depends on the design and orientation of the selector, and its full width at half maximum (FWHM) is usually in the range of 10-30%. After passing the selector, the neutrons pass through a neutron guide and a collimator with variable length. The length of the collimation is chosen in accordance with the specific detector distance, in order to optimize the flux and the resolution of the instrument. The neutron beam is shaped by different diaphragms before arriving to the sample position.

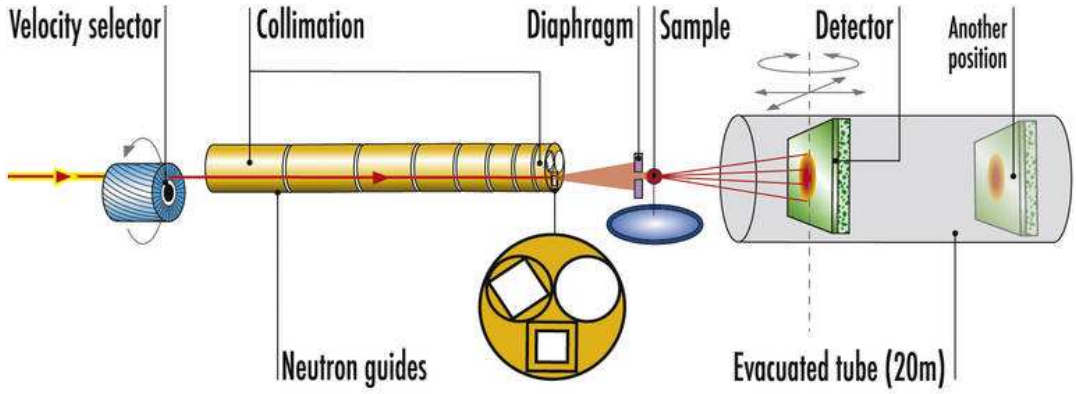

Figure 7: Schematic view of the D22 SANS instrument at the Institut Laue-Langevin (copied from (ILL 2011)).

Samples can be mounted into different sample holders and in different sample environments. The temperature of the sample can be controlled and a magnetic field, different illumination levels and high pressure can be established at the sample position. Neutrons scattered from the sample are detected by a two-dimensional detector. The sample-to-detector distance can be varied, by moving the detector in a tube, under vacuum. This, in combination with the incident neutron wavelength determines the Q-range covered by the scattered neutrons.

3. Thylakoid Membrane, the Site of Light Reactions in Photosynthesis

During the following section I give a short overview of the basic features of photosynthesis, paying special attention to the structural organization of the photosynthetic apparatus and to the ultrastructure of the thylakoid membranes. The overview is based on (Gunning and Steer 1975; Blankenship 2002).

3.1 Principles of Photosynthesis

What is photosynthesis? The definition given in (Blankenship 2002) is "*Photosynthesis is a process in which light energy is captured and stored by an organism, and the stored energy is used to drive cellular processes*." To emphasize the importance of this process, which converts the energy of light coming from the Sun, to chemical energy, one has to remark that most of our energy resources, even the food we consume, are or were created by using energy provided by photosynthesis.

The variety of organisms benefiting from photosynthesis is enormous and includes primitive bacteria up to organisms as big as the *Sequoiadendron giganteum*. The prevalent form of photosynthesis is the so called chlorophyll-based photosynthesis. Bacteriorhodopsin-based photosynthesis is also known, but is not the subject of this thesis.

Photosynthesis, which we can observe now in nature is a result of billions of years of evolution, and thus shows variance in different organisms. However, we can form an overall division of the so-called light reaction processes into four principal parts, being valid for all these organisms:

1. The light reaching the plant is mainly gathered by antenna complexes, specialized for the absorption and transfer of the light energy. The energy of the photon is primarily stored in the form of excited states of different accessory pigments or chlorophylls in the antenna, and funneled towards the photosynthetic reaction center through several intermediate pigments. The directionality of the funneling process is maintained by the decreasing energy level of the consecutive excited states. The existence of the antenna complexes is crucial for increasing the efficiency of the photosynthesis and the adaptation properties of the organism for different light conditions.

2. The transformation of the energy of the light into chemical energy occurs in the reaction centers through light driven electron transfer reactions. In these membrane-embedded pigment-protein complexes a dimer of chlorophylls is involved in the primary charge separation processes; the donor chlorophyll molecule(s) of the reaction center get(s) into excited state and become(s) a highly reductive agent in the vicinity of an acceptor molecule. As a result, one electron is transferred to the primary acceptor molecule, during the primary photochemical process of photosynthesis. Due to their physical vicinity the oxidized primary donor and the reduced acceptor form a highly unstable system because of the possibility of recombination, i.e. the back transfer of the transferred electron. Recombination results in the formation of heat and the loss of useful energy for photosynthesis.
3. The stabilization of the chemical energy occurs through several consecutive secondary reactions, being faster than the recombination process. Through these reactions the positive and negative charges, formed during the primary photochemical processes, are physically separated from each other and the chance of their recombination is thus reduced.
4. During the secondary processes of the light reactions of photosynthesis energy transfer molecules, ATP and NADH or NADPH, are produced, this way storing the solar energy transformed by the photosynthetic apparatus. The energy and the reducing power stored in these molecules are used in the process of carbon fixation, during which CO_2 and water are converted to carbohydrates.

The different processes involved in photosynthesis are far from being completely understood, and have been extensively studied by scientists from various fields of expertise. In this thesis, my work was related to two specific aspects of the photosynthesis and therefore the overview of literature will be confined to these areas. In particular, I will deal in detail with the structural parameters of the thylakoid membranes, a complex multilamellar membrane system where virtually all photosynthetic light reactions take place and with the relationship between the functionality and the composition of this system with its structure. A short description of

the photosynthetic electron transport chain and especially the involvement of the photosystem II in it will also be given.

3.1.1 Granal Chloroplasts

In higher plants photosynthesis takes place in an organelle of the plant cell, called the chloroplast (see Figure 8). The inner part of the chloroplast is filled with an aqueous phase, called the stroma liquid, which surrounds a multilamellar lipid bilayer membrane assembly, the thylakoid membrane.

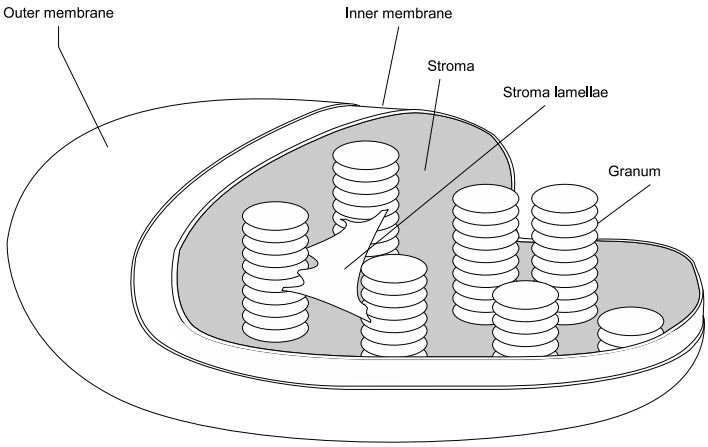

Figure 8: Simplified three-dimensional model of granal chloroplast.

Carbon fixation, the 'dark reactions', happen in the stroma, while thylakoid membranes are the site for the light reactions of photosynthesis. This connection of the primary steps of photosynthesis with membranes can be found even in the simplest chlorophyll based photosynthetic organisms.

The existence of the thylakoids in the chloroplast is known since 1883 when Meyer found small grains (grana) in the chloroplast in light microscopy measurements. The existence of several layers in the grana was shown first in 1940 (Kausche and Ruska 1940). Membranes interconnecting the grana stacks, the stroma thylakoids, were first

found in 1956 (Leyon 1956). The currently accepted structural representation of the thylakoid membrane assembly is a result of research over several decades, in which the main experimental method used was electron microscopy of ultra-thin sections of chloroplasts. The results on the morphology of the thylakoid membranes can be summarized by the following points:

1. The grana are constituted of circular discs of stacked thylakoid membranes aligned on top of each other.
2. Each disc can be considered as a flattened lipid bilayer vesicle, resulting in the inversed directionality of the upper and lower lipid bilayer of the disc.
3. The bilayers separate the inner (lumen) and outer (stroma) liquid phases from each other.
4. The diameter of the discs is 300-600 nm.
5. The lumenal phases of the granum thylakoid discs being on top of each other are interconnected by stroma thylakoids winding around the grana membranes.
6. The lumenal phases of cylindrical sets of stacked granum thylakoid discs are also interconnected by stroma thylakoids that interconnect adjacent grana.
7. The structure of the stroma thylakoids at the vicinity of the granum thylakoid discs can be described as a right handed helix.
8. Contiguous lumenal space.

A computerized model, created on the basis of electron micrographs of serial sections of thylakoid membrane assemblies, presented in Figure 9, shows a currently accepted model of the thylakoid membrane system, granum thylakoids with stroma thylakoids, helically wound around them. One has to keep in mind that this representation is a highly idealized picture of the thylakoids, not showing the irregularities in the structure, revealed by recent electron tomography data (Mustárdy et al. 2008; Austin and Staehelin 2011).

Basic parameters defining the model are:

1. The height of the central grana disc column, in other terms the number of discs stacked together is usually found to be 10-20 in higher plants.
2. A grana disc is built up from two approximately 4 nm thick membranes, a 4.5 nm thick lumenal and a 3.2 nm thick interthylakoidal space (Daum et al. 2010)

providing 15.7 nm for the repeat distance in spinach chloroplasts, but the various results in the literature for the repeat distance range from 14 to 24 nm (Dekker and Boekema 2005). Furthermore the parameter strongly depends on the sample environment (Murakami and Packer 1970).

3. If we consider a cross-section of the grana disc column along the axis, on one margin of the granum discs stroma thylakoids are joining to approximately every 2-2.5th granum disk (Paolillo and MacKay 1969).
4. The angular tilt between the stroma and granum thylakoids is found to be in average 22º in *Lolium multiflorum* (Brangeon and Mustárdy 1979); recent studies found this value to be ~ 10 to 15º in spinach thylakoids (Daum et al. 2010).

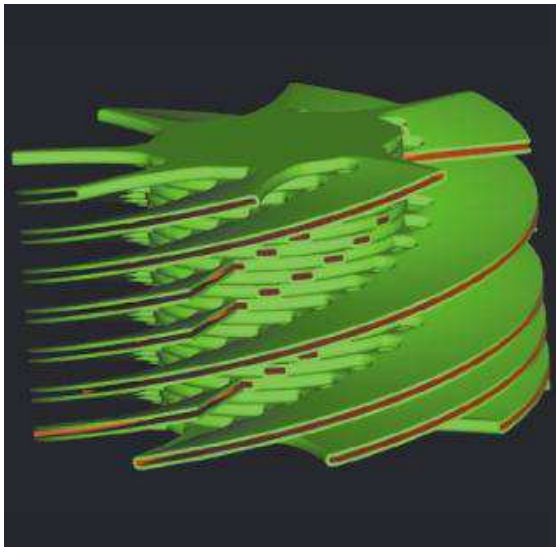

Figure 9. Idealized model of the granum-stroma thylakoid membrane assembly, with stroma lamellae helically wound around the multiple granum thylakoid discs (copied from (Mustárdy and Garab 2003)).

3.1.2 Protein Complexes Incorporated in the Thylakoid Membrane

The thylakoid membrane has a crucial role in the primary steps of photosynthesis. The membrane separates two aqueous phases (the stroma and the lumen) and incorporates virtually all protein complexes involved in the light reactions of photosynthesis. These proteins, their role in the photosynthetic electron transport or in the energy conversion are presented in Figure 10, together with the schematic presentation of the flow of electrons and of the formation of ATP and NADPH.

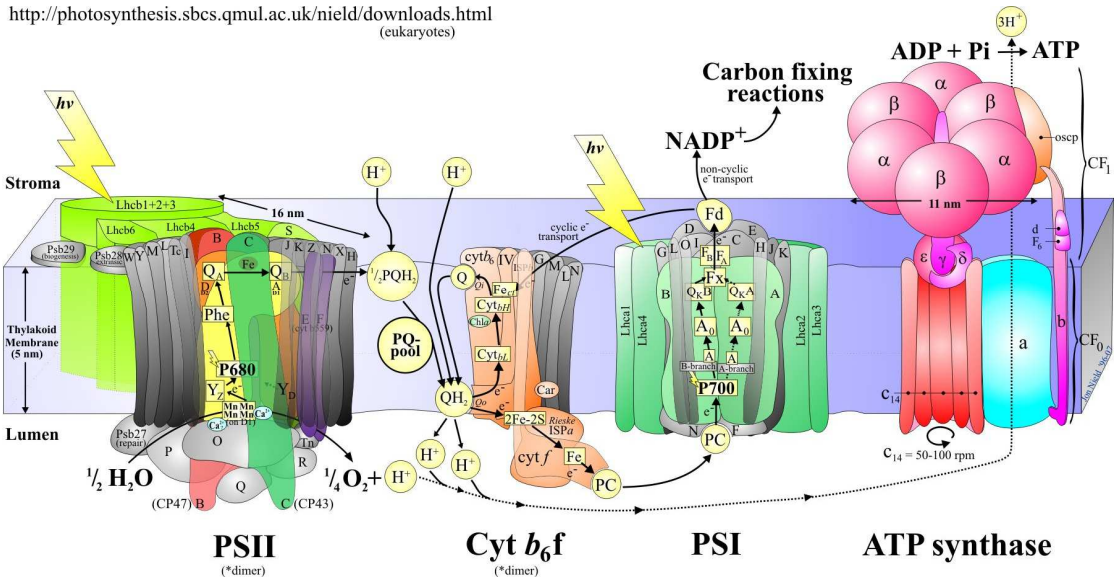

Figure 10: Schematic representation of the thylakoid membrane with the major protein complexes involved in photosynthesis (copied from (Nield 2010)). In higher plants the 'light reactions' of photosynthesis take place in the thylakoid membrane. Photochemical reactions in plants occur in two different photosystems. The reaction centers are capable of absorbing light themselves. However most of the light energy is absorbed by the surrounding light-harvesting antenna complexes and transferred towards the reaction centers. In the second photochemical reaction center (PSII) the energy of the absorbed light generates an excited state of P_{680} (chlorophyll in a special environment). The primary electron acceptor is reduced by P_{680}^*, forming a $P_{680}^+A^-$ ion-pair[1]. P_{680} is the strongest biological oxidizing agent. The charge separation is stabilized by secondary processes. P_{680}^+ is reduced to its original state by electrons obtained ultimately from the oxygen evolving complex (OEC), located at the lumenal side of the PSII, which performs the $H_2O \rightarrow 2H^+ + \frac{1}{2}O_2 + 2e^-$ reaction. The reaction decreases the pH of the lumen. Electrons obtained during the photochemical reaction are transferred to the stromal side of the thylakoid membrane and reduce the primary stabile quinone acceptor (Q_A) and the secondary quinone acceptor (Q_B), forming QH_2 with protons obtained from the stroma. Fully reduced quinones (quinols) diffuse to the lumenal side and release H^+ further decreasing the pH of the lumen. Electrons are carried further to the lumenal side of the first photochemical reaction center (PSI) by plastocyanin, which is a soluble electron carrier protein. In PSI the absorbed light generates a highly reductive state of P_{700}. The primary electron acceptor is reduced by P_{700}^*, forming a $P_{700}^+A^-$ ion-pair. The electron transported by the plastocyanin reduces P_{700}^+ to its original state, while the electron on the acceptor is transferred, in several steps, to the ferredoxin at the stromal side of the thylakoid, and finally to the ferredoxin-$NADP^+$ oxidoreductase. The latter reduces $NADP^+$ to NADPH. The large electrochemical (pH and electrical potential) gradient between the lumenal and stromal side of the thylakoid membrane, formed during photosynthesis, is used for ATP production via the chloroplast ATP synthase. ATP and NADPH formed during the first steps of photosynthesis are energy and redox power carrier molecules, respectively, used during CO_2 fixation. There exists another pathway of electron flow driven by the energy of absorbed light, than the above detailed linear electron transport. In the case of the so-called cyclic electron transport, ferredoxin reduces the quinone complex, after which the process continues until the ferredoxin as detailed above. In the case of PSI cyclic electron transport, only PSI is active, the energy of the absorbed light is used for increasing the proton gradient, and thus for ATP production. Since the ferredoxin reduces the quinone complex, there is no NADPH production. Furthermore there is no O_2 produced since PSII is not involved in this process (Lodish et al. 1995; Nield 2010).

[1] * represents the excited state.

In higher plants the distribution of the different protein complexes, presented in Figure 10, is not homogenous. PSII is mainly found in the granum while PSI and the ATP synthase only in the stroma thylakoids and the end membranes of grana. The location of the cytochrome b_6f complex is not yet elucidated in the literature (see Figure 11). This lateral separation of the protein complexes allows the formation of the different structure of the stroma and granum thylakoids. The light harvesting complexes connected to PSII (LHCII) actively participate in the close packing of granum thylakoids (Garab and Mustárdy 1999; Albertsson 2001).

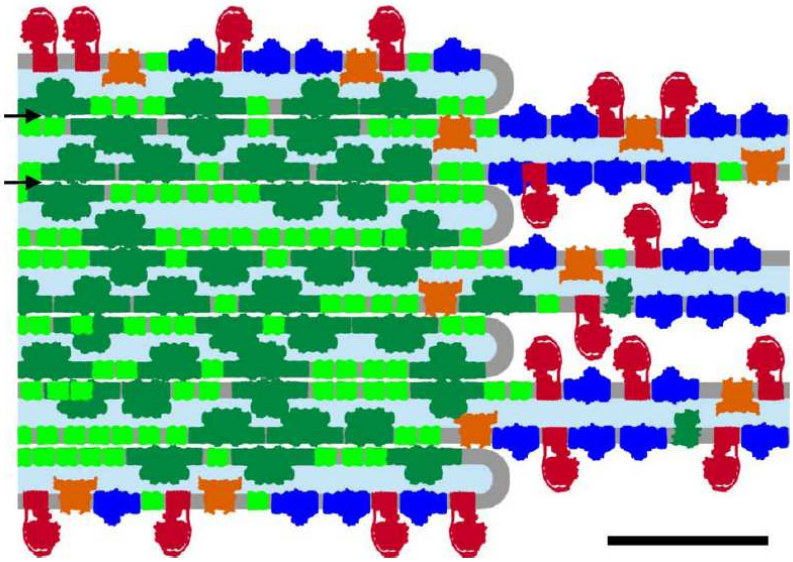

Figure 11: Heterogenous distribution of different photosynthetic membrane protein complexes in the granum and stroma thylakoid membranes (copied from (Dekker and Boekema 2005)). PSI (dark blue) and the ATP synthase (red) can be found only in stroma thylakoids and the end membranes of grana. The PSII (dark green) can be mainly found in granum thylakoids. The cytochrome b_6f complex (bright green) can be found both in stroma and granum thylakoids. Exact location of the latter, however, is still debated. It is often assumed (as on this figure) that cytochrome b_6f is present in the stroma and granum parts of the thylakoid (Albertsson 2001). However, it was shown in (Berthold et al. 1981) that isolated PSII membranes do not contain this complex. It is proposed in (Allen and Forsberg 2001) that cytochrome b_6f is predominantly localized in grana margins, and the possibility of a similar spatial distribution is indicated by (Dekker and Boekema 2005). The lumen is marked by bright blue. The bar is 50 nm.

The biological advantage of the structural and functional separation of the two different thylakoid membranes, a unique feature for plants, is a widely investigated question in photosynthesis. In cyanobacterium, for example, where no lateral separation of the protein complexes is observed, thylakoid membranes do not form granal structures. Further aspects of the lateral heterogeneity of thylakoid membranes in higher plants will be discussed in Paragraph 5.2.

3.1.3 Structural Flexibility of the Thylakoid Membranes

The multilamellar thylakoid membrane assembly is not a rigid structure, but a highly flexible system easily influenced by different environmental parameters. These parameters can be best investigated on isolated thylakoids. Changes in the composition of the suspending medium in the isolated thylakoids can be considered as models for effects which change the composition of the stroma, *in vivo*, and the following observations have been recorded:

1. The thickness of the interthylakoidal space can be influenced by the amount of monovalent and divalent cations in the suspending medium (Murakami and Packer 1971). The phenomenon can be understood if we consider the net negative charge of the thylakoid membranes' surface. The coulombic repulsion of adjacent thylakoid membrane surfaces can be screened by an appropriate, valency dependent amount of cations and affect the membrane stacking (Barber 1982).
2. The thickness of the thylakoid lumen can be varied by the osmolarity of the suspending medium, in case the thylakoid membrane is impermeable for the given osmotic compound. Upon increasing the concentration of sucrose in the suspending medium the shrinkage of the lumenal space, and thus the repeat distance of the granum thylakoids, can be observed (Murakami and Packer 1970).
3. The effect of the proton concentration of the suspending medium on the granum thylakoid structure is also known. Changing the pH of the medium from 7.7 to 4.7 decreases the repeat distance of granum thylakoids (Murakami and Packer 1970).
4. The repeat distance of granum thylakoids in the presence of phenylmercuric acetate (PMA) was found to decrease upon illumination. The changes were found to be reversible upon subsequent dark adaptation (Murakami and Packer 1970).

The above presented results and articles are all based on electron microscopy studies of chemically fixed and stained thylakoid membranes.

3.1.4 Photosystem II – Structure and Function

The basic role of the photosystem II is to oxidize water molecules on the lumenal side, and to reduce quinones at the stromal side of the thylakoid membrane by using the energy of absorbed photons as driving force. During the last decade electron and X-ray crystallography studies have provided more and more detailed information about this multisubunit protein complex achieving already a resolution of 1.9 Å (Rhee et al. 1998; Ferreira et al. 2004; Guskov et al. 2009; Umena et al. 2011). The overall structure of PSII is shown in Figure 12. PSII is formed by a dimer of two almost identical monomers, each built up from 19 subunits (Umena et al. 2011). Each of the monomers contains one oxygen evolving complex (Ferreira et al. 2004).

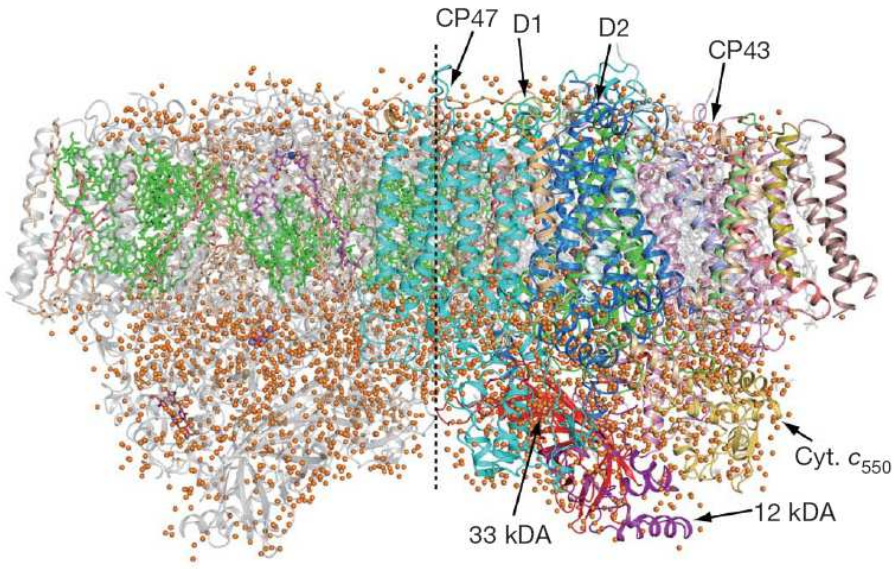

Figure 12: Overall structure of PSII dimer from *Thermosynechococcus vulcanus* (copied from (Umena et al. 2011)), viewed from a direction perpendicular to the membrane normal. In the right-hand monomer the protein subunits are colored and the cofactors are in light grey, while in the left hand monomer the cofactors are colored and the protein subunits are in light grey. The orange balls represent the water molecules.

The OEC is the site of the water splitting in the PSII; it contains four manganese ions, two Cl^- ion and a Ca^{2+} ion (Umena et al. 2011) and is surrounded by a protein microenvironment (Govindjee et al. 2010). These ions play a crucial role in the oxidation and splitting of water as detailed in (Vrettos et al. 2001). The detailed structure of the OEC revealed by X-ray studies can be seen in Figure 13.

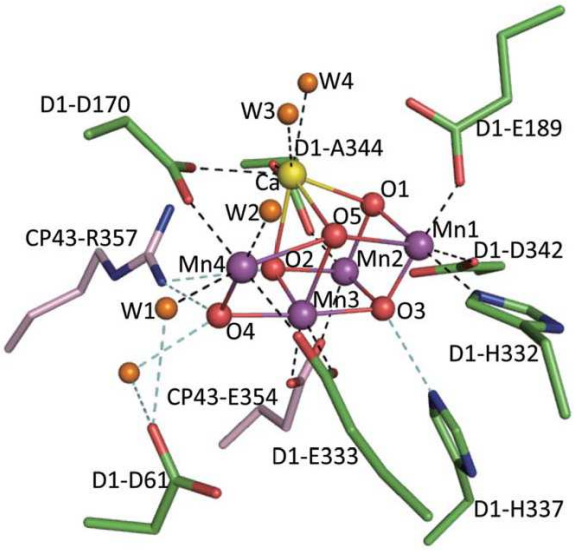

Figure 13: Structure of the Mn_4CaO_5 cluster (copied from (Umena et al. 2011)). Color code for the protein subunits: D1, green; CP43, pink.

As was shown in Figure 10 the absorption of one photon by PSII can transfer one electron from the OEC. For the formation of one O_2 molecule two H_2O molecules are needed to be oxidized, therefore four electrons are needed to be removed. The absorption of a single photon cannot result in a water splitting event. Therefore the OEC cycle goes through five different states (S_0 –S_4) where indices represent increasing oxidation states. The transition between each state is induced by the absorption of one photon, only the S_4 –S_0 transition is spontaneous and coincides with the release of O_2.

The above detailed delicate structure and function of the OEC is the most heat-sensitive component of PSII as revealed by the temperature dependence of the oxygen evolution activity. This method shows us that in PSII membrane fragments the oxygen evolution activity starts to decrease at ~ 40 ºC and half inactivation occurs at 47 ºC (Nash et al. 1985).

4. Materials and Methods

4.1 Sample Preparation

4.1.1 Intact Thylakoid Membranes

4.1.1.1 SANS measurements

Thylakoid membranes were isolated by a method which preserves their structure and composition the closest possible to their natural state. Samples were prepared freshly before the experiment and were used for 4-5 hours after the isolation.

Spinach and pea leaves were used as starting materials. Pea seedlings were grown at the greenhouse of the Biological Research Center in Szeged. Spinach leaves were purchased from the local markets in the towns adjacent to the experimental places. The preparation afterwards was identical for spinach and pea.

Leaves, after main ribs being removed, were homogenized in ice cold grinding medium containing 20 mM Tricine (pH 7.6), 0.4 M sorbitol, 10 mM $MgCl_2$, 10 mM KCl and filtered with 6 layers of medical gauze pads. Remaining debris was removed by centrifugation at 200×g for 2 min. The supernatant was centrifuged for 5 min at 4000×g. The pellet was resuspended and soaked in an osmotic shock medium of 20 mM Tricine (pH 7.6), 5 mM $MgCl_2$ and 5 mM KCl to destroy the chloroplasts' outer membrane. It was then centrifuged for 5 min at 7000×g. The pellet was resuspended and soaked in a D_2O containing grinding medium (20 mM Tricine (pD 8), 0.4 M sorbitol, 10 mM $MgCl_2$, 10 mM KCl in ~ 100% D_2O), centrifuged for 5 min at 7000×g, and resuspended in media, different for the various samples.

4.1.1.2 EINS Measurements

For EINS measurements the thylakoid isolation protocol was identical. As a final step the sample was resuspended and soaked once again in a D_2O containing grinding medium at a temperature of 5 ºC for the control sample and at a temperature of 50 ºC for 5 min for the heat treated sample. Both samples were centrifuged for 5 min at 7000×g, and the pellets were used for the experiments.

4.1.2 Algal Cultures

Phaeodactylum tricornutum (1090-1a, obtained from the Culture Collection of Algae, Göttingen (SAG)) was cultivated by Dr. Milán Szabó (BRC, Szeged, Hungary) as described in (Lepetit et al. 2007) at a photon flux density of 40 μmol photons m^{-2} s^{-1} with light/dark periods of 16h/8h at 19 °C.

Wild type and PAL (completely devoid of phycobilisomes (Ajlani and Vernotte 1998)) mutant cells of *Synechocystis* PCC 6803 were grown photoautotrophically by Dr. Bettina Ughy in BG 11 medium (Wilson et al. 2006) supplemented with 5 mM HEPES NaOH (pH 7.5) at 30 ºC under continuous illumination at a photon flux density of 30 μmol photons m^{-2} s^{-1}.

Cells were harvested from the logarithmic growth phase, by centrifugation (5000 g, 5 min) and resuspended for SANS measurements in ~ 95% (v/v) D_2O-containing culture medium to a chlorophyll content of 200-500 μg/ml.

4.1.3 Photosystem II Particles

4.1.3.1 SANS measurements

Photosystem II particles (BBY – named after the authors, Berthold et al., who first described its preparation in 1981) were isolated from spinach leaves with the commonly used method (Volker et al. 1985) in the Biological Research Center (Szeged, Hungary), were frozen and sent to the ILL and stored at -80 ºC until use. After thawing, samples were centrifuged for 5 min at 7000×g. For SANS measurements samples were resuspended in media containing 20 mM Tricine (pD 8), 5 mM $MgCl_2$, 5 mM KCl and 0.4 M sorbitol; D_2O content was set to 40 or 100 %.

4.1.3.2 EINS Measurements

For elastic incoherent neutron scattering (EINS) measurements the pellet was resuspended in different D_2O-containing reaction media. Control and heat-treated samples were washed and resuspended in the grinding medium (20 mM Tricine (pD 8), 0.4 M Sorbitol, 10 mM $MgCl_2$, 10 mM KCl in ~ 100% D_2O). For heat treatments the samples were incubated at 323 or 333 K water baths for 5 min while continuous stirring was applied. For TRIS-treatment the samples were suspended in 1 M TRIS (tris-

(hydroxymethyl)aminomethane) buffer (pH 8.0), incubated for 1 hour on ice, centrifuged for 5 min at 7000×g, and washed twice in the grinding medium. All samples were finally centrifuged for 5 min at 7000×g and the pellets were used for the experiments - after adjusting their relative humidity (r.h.), for which the samples were placed in an open sample holder in a desiccator with 57% r.h. (adjusted by oversaturated D_2O solution of NaBr (O'Brien 1948)) and were equilibrated. One of the control (no heat or TRIS treatment applied) samples was then hermetically closed and used for the experiment. The remaining samples were placed into a desiccator with 75% r.h. (adjusted by oversaturated D_2O solution of NaCl (Adams and Merz 1929)), equilibrated (controlled by the lack of mass change) and closed hermetically. Thermoluminescence studies performed on dry films of pea chloroplasts of various humidity have shown that partially dehydrated samples retain their photochemical activity (Knox and Garab 1982), suggesting that in our samples with 57 and 75 % r.h. the PSII complex also remains functional.

The masses (m) of the BBY samples were as follows: 57% r.h. sample, $m \approx 0.14$ g; TRIS-treated (75% r.h.) sample, $m \approx 0.35$ g, 75% r.h. control and heat treated samples, $m \approx 0.2$ g.

Table 3: List of the electron donors, acceptors and inhibitors used during our experiments, together with a short description of their function, the used concentration and the applicable solvent. Information about the function was taken from (Allen and Holmes 1986).

Reagent	Function	Concentration used in our experiments	Soluble in
Ascorbate	Reducing agent	1 mM	Water
DCMU [Diuron; 3-(3,4-dichloprophenyl)-1,1-dimethylurea]	PSII inhibitor (of electron transport between Q_A and Q_B)	10 μM	>10 % Ethanol
Duroquinol (tetramethyl-*p*-hydroquinone)	Electron donor to plastoquinone pool	4 mM	Ethanol
Ferricyanide (K salt)	Terminal (PSI) electron acceptor; Oxidizing agent (after reduction it is not reoxidized)	5 mM	Water
Methyl viologen (1,1'-dimethyl-4,4'-bipyridylium dichloride)	Terminal PSI electron acceptor, autoxidizing (after reduction it is reoxidized through reaction with O_2)	1 mM	Water
PMS (N-methyl phenazonium methosulphate)	Co-factor of PSI cyclic electron flow	0.1 mM	Water

For the measurements samples were placed into flat rectangular Aluminum sample holders, with area (30 x 40 mm^2) adapted to the dimensions of the incident neutron

beam; the sample thickness, defined by the sample mass – due to the sample being stuck on the sample holder – was ~ 0.12 mm for the 57% r.h. sample; ~ 0.29 mm for the TRIS-treated sample; and ~ 0.17 mm for the remaining samples.

4.1.4 Reagents Used in the Experiments

In plants under normal conditions the entire electron transport chain (presented in Figure 10) is active. One can study different components of the electron transport chain in isolated thylakoid membranes by adding various combinations of inhibitors, electron donors and acceptors. Reagents, used in our different experiments are presented in Table 3.

Additionally we used NH_4Cl in 4 mM concentration or nigericin in 2.5 μM concentration as uncouplers to dissipate the ΔpH (Mills 1986).

4.2 Molecular and Chemical Composition of Thylakoid Membranes and Photosystem II Membrane Fragments

Considering that cross-section values (either coherent or incoherent) can be very different for different elements or even for different isotopes of the same element, detailed interpretation of the neutron scattering data requires the knowledge of the exact composition of the investigated sample. Here we present calculations about the composition of thylakoid membranes and PSII (BBY) membrane fragments.

A wealth of information is available on the protein and lipid contents of plant thylakoid membranes, but significantly less is known about BBY membranes. According to (Douce and Joyard 1996) the lipid/protein mass ratio in spinach thylakoid membranes is 0.6-0.8. The mass fraction of proteins in the thylakoid membrane can be calculated as ~ 70 and ~ 65 % according to (Duchene and Siegenthaler 2000) and (Dorne et al. 1990), respectively. Recent studies revealed that in BBY the protein content is increased compared to thylakoids, possessing ~ 80 % protein area fractions (compared to ~ 70 % in thylakoids) (Kirchhoff et al. 2002; Haferkamp and Kirchhoff 2008). In our calculations we chose 80% for the mass fraction of proteins in BBY and 70 % in intact thylakoids.

The chemical composition of the main proteins, i.e. LHCII and PSII (cf. (Kirchhoff et al. 2004)), present in BBY and LHCII, PSII, PSI, cytochrome b_6f complex and ATP

synthase, present in thylakoid membranes is calculated by using the crystal structure data contained in the RSCB Protein Data Bank. Structure of LHCII, PSII, PSI, cytochrome b_6f complex and ATP synthase are taken from (Standfuss et al. 2005), (Umena et al. 2011), (Amunts et al. 2010), (Yamashita et al. 2007) and (Stock et al. 1999), respectively. The proteins' H-atom containing structure was built by using the PHENIX ReadySet program (Adams et al. 2010); the same program was used for generating the D-atom containing structure, considering isotope exchange of the exchangeable H-atoms with the D_2O containing buffer. The chemical compositions of the samples were calculated using the CCP4 Program Suite 6.1.13 (Collaborative Computational Project 1994), with the RWCONTENTS subprogram. Relative molar contributions for the protein complexes were calculated from (Kirchhoff et al. 2002) for thylakoids and from (Kirchhoff et al. 2004) for BBY.

The lipid molar composition of thylakoid membranes and BBY were calculated from (Kirchhoff et al. 2002) and (Haferkamp and Kirchhoff 2008), respectively. The relative contribution and fatty acid composition of the four lipid classes have been found to be homogeneous in different parts of the thylakoid membrane (Duchene and Siegenthaler 2000). The fatty acid composition for the individual lipid classes used in the present calculation is taken from (Duchene and Siegenthaler 2000).

4.2.1 Estimation of the H-content for the Interpretation of EINS Measurements

In biological samples EINS is mainly reflecting the displacement of the hydrogen atoms. Therefore we estimated the hydrogen content in different constituents of the samples. The obtained hydrogen content of the individual protein subunits (calculated by considering H – D exchange between the proteins and the solution), and the relative molar contributions for the protein complexes are shown in Table 4. Taking into account these proportions and the molar mass of the different protein complexes, we can thus calculate the average hydrogen content of the proteins in thylakoids: $n_H/n_{all\ atoms}=33.3 \pm 1.1$ %; $m_H/m_{protein}=4.2 \pm 0.1$ % and in BBY: $n_H/n_{all\ atoms}=30.5 \pm 1.8$ %; $m_H/m_{protein}=3.8 \pm 0.2$ %.

The hydrogen contents of the main lipid classes (calculated by considering H – D exchange between the proteins and the solution) and the lipid molar compositions for

thylakoids and BBY are shown in Table 5. The presented results yield an average hydrogen content of the lipids in thylakoids: $n_H/n_{all\ atoms}$=53.6 ± 4.8 %; m_H/m_{lipid}=8.8 ± 0.8 % and in BBY: $n_H/n_{all\ atoms}$=53.8 ± 3.2 %; m_H/m_{lipid}=8.8 ± 0.5 %.

Table 4: H-contents of different proteins present in thylakoid membranes and BBY and their relative contribution in two different samples, calculated based on the protein structure data (Stock et al. 1999; Standfuss et al. 2005; Yamashita et al. 2007; Amunts et al. 2010; Umena et al. 2011) and the composition of the samples (Kirchhoff et al. 2002; Kirchhoff et al. 2004). [a]Molar contributions calculated for PSII monomers.

	Hydrogen content		Relative molar content in spinach-	
	[]=$n_H/n_{all\ atoms}$	[]=$m/m_{protein}$	thylakoid membranes	BBY membranes
PSI	40.6 %	5.6 %	5.5 ± 0.4 %	
PSII-core	35.9 %	4.9 %	7.3 ± 0.6 % [a]	7.7 ± 0.6 %
Cyt b6f	39.5 %	5.4 %	3.1 ± 0.1 %	
LHCII	28.7 %	3.3 %	81.8 ± 2.4 %	92.3 ± 5.5 %
ATP synthase	39.9 %	5.6 %	2.3 ± 0.2 %	

Table 5: H-contents of different thylakoid lipids with fatty acid compositions given by (Duchene and Siegenthaler 2000), and their relative molar contents in thylakoid membranes and BBY as in (Kirchhoff et al. 2002) and (Haferkamp and Kirchhoff 2008).

	Hydrogen content		Relative molar content in spinach-	
	[]=$n_H/n_{all\ atoms}$	[]=m_H/m_{lipid}	thylakoid membranes	BBY membranes
MGDG	54.1 ± 0.7 %	9.0 ± 0.1 %	43.1 ± 4.9 %	40.9 ± 3 %
SQDG	54.4 ± 1.5 %	8.8 ± 0.2 %	19.5 ± 1.8 %	12.4 ± 1.7 %
DGDG	51.5 ± 0.8 %	8.3 ± 0.1 %	26.2 ± 3.3 %	25.8 ± 1.9 %
PG	56.1 ± 1.1 %	9.3 ± 0.2 %	11.3 ± 1 %	20.8 ± 1.4 %

Based on calculated m/m % values, we estimate that in thylakoid membranes ~ 53% of the hydrogen atoms are associated with protein complexes and ~ 47% with lipid molecules while in BBY ~ 63% of the hydrogen atoms are associated with protein complexes and ~ 37% with lipid molecules. As a consequence ~ 53 % of the EINS signal of thylakoid membranes and ~ 63 % of the EINS signal of BBY is considered to originate from proteins, while the contribution of the lipid part is ~ 47 % and ~ 37 %, respectively.

4.2.2 Neutron Scattering Length Density Calculations for the Interpretation of SANS Measurements on BBY membranes

The lipid composition of the BBY membrane was used to calculate the average scattering length density (SLD) for the hydrocarbon chain and the headgroup region of the lipids. Calculations were performed for the case of the sample being suspended in 100 % H_2O (none of the exchangeable hydrogen atoms are replaced by deuterium) and 100 % D_2O (all of the exchangeable hydrogen atoms are replaced by deuterium) containing buffer and the obtained values were used to calculate the SLD in 40 % D_2O containing buffer (in which protein components of the sample has no contrast, as will be discussed in paragraph 5.2.2). As an approximation mass density of the lipids was considered to be 1 g/cm^3. Calculating with a lipid composition presented in Table 5 we obtain $1.39 \cdot 10^{-6}$ Å^{-2}, $1.67 \cdot 10^{-6}$ Å^{-2} and $2.09 \cdot 10^{-6}$ Å^{-2} for the average headgroup SLD in 0, 40 and 100 % D_2O containing buffer, respectively. Since the hydrocarbon chain does not contain exchangeable H atoms its SLD is considered as $-0.36 \cdot 10^{-6}$ Å^{-2} in all cases.

For the calculations, the Scattering Length Density Calculator of the NIST Center for Neutron Research was used (NIST 2011).

4.3 Small-Angle Neutron Scattering

4.3.1 Experimental Description

Small-angle neutron scattering experiments were performed on the D22 instrument at the Institut Laue-Langevin, on the Yellow Submarine instrument at the Budapest Neutron Centre, and on the SANS II instrument at SINQ at the Paul Scherrer Institut. The results of the latter experiment are not included in the present thesis.

4.3.1.1 D22 Experiments

For all the experiments on D22 the neutron wavelength was set to 6 Å. The neutron beam was defined by a $10mm \times 6.5mm$ aperture. Commonly used sample-to-detector distances were 8 m and 2.45 m with 8 m and 2.8 m collimation distances. Neutrons were detected by a 128×128 pixels detector with a pixel size of $0.8 \times 0.8 cm^2$. The different measurements covered the Q-range between 0.008 and 0.2 Å^{-1}.

In part of the experiments the samples were placed between electromagnets (see Figure 14), providing a ~ 1.5 T magnetic field at the sample position. For the experiments studying light induced structural changes a Schott KL 2500 light source was mounted near the sample position and the samples were illuminated through a light guide. Samples were measured in 1 mm and 2 mm quartz cuvettes, which were placed in a water-cooling based temperature controlled sample holder. The sample temperature was set to 288 K during most of the experiments in order to slow down any degradation effects.

For time resolved measurements, performed to obtain kinetic information about the investigated structural changes, scattering data were collected and stored after an acquisition time down to 1 s. Due to the time required for the readout of the detector the achievable time resolution was 2 s.

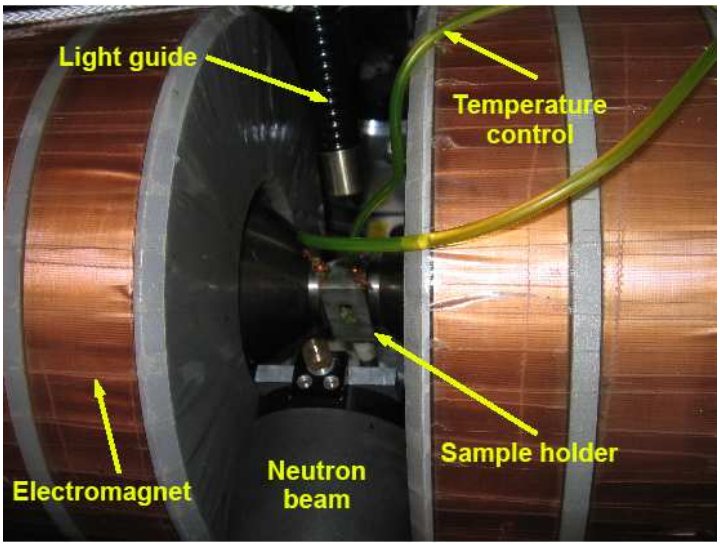

Figure 14: Sample environment on D22 in experiments for light induced reorganizations in the thylakoid membrane ultrastructure.

4.3.1.2 Yellow Submarine Experiments

During experiments on the Yellow Submarine instrument a 3.996 Å neutron wavelength was used. The applied sample-detector distance and collimation were 5.6 m and 6 m, respectively. Neutrons were detected by a 64×64 pixels detector with a pixel size of $1\times1cm^2$ (Rosta 2002).

During the experiments for the investigation of the phosphorylation induced changes in the thylakoid membrane a ~ 0.7 T magnetic field was achievable at the sample position. Samples were measured in 2 mm quartz cuvettes placed into water cooled temperature controlled sample holders. Sample temperature was set to 283 K. The neutron wavelength was set to 7.51 Å. The investigated Q-range was between 0.009 and 0.055 $Å^{-1}$. Each sample was measured for 30 min.

4.3.1.3 Magnetic Orientability of the Thylakoid Membranes

Fluorescence of magnetically oriented chloroplasts was observed to be polarized in a plane perpendicular to the external magnetic field > 1 T (Geacintov et al. 1972). The polarized fluorescence emission is explained by the preferentially in-plane orientation of the emission dipoles of the chlorophyll molecules and the alignment of the thylakoid membranes perpendicular to the magnetic field vector. The membrane itself is orientable in the magnetic field due to its diamagnetic anisotropy (Knox and Davidovich 1978).

Among the chlorophyll containing constituents of the thylakoid membrane, light-harvesting complexes contain about half of the chlorophyll molecules. Aggregates of LHCII have also been shown to be orientable by a magnetic field. Furthermore, the magnitude of the diamagnetic anisotropy of the thylakoid membranes was found to depend on their LHCII content, suggesting that the light harvesting complexes play an important role in the alignment of the thylakoid membranes in the external magnetic field (Kiss et al. 1986).

In our neutron scattering experiments we used ~ 0.7 T (Yellow Submarine) and ~ 1.5 T (D22) magnetic field strengths which are close to the saturation levels for the fluorescence polarization shown in (Geacintov et al. 1972)

4.4 SANS Data Treatment

4.4.1 SANS Data Treatment I – from 2D to 1D

During experiments on the Yellow Submarine instrument, part of the experimental parameters – such as sample detector distance and neutron wavelength - are stored only in logbooks. Using these parameters, the two dimensional detector data were rewritten in a format similar to standard format of the ILL, as provided by the D22 instrument. For

this purpose, for personal use, a transforming program code was written in Java programming language. Further data treatment was thus identical for data obtained from the two instruments.

Primarily data treatment on two dimensional scattering data recorded during the experiments was performed by a Graphical Reduction and Analysis SANS Program written in Matlab™ (GRASP), developed by Charles Dewhurst at the ILL. The raw data counts for each pixel, n, and errors, $\sqrt{n}$, were normalized for the number of beam monitor counts and multiplied by a constant (standard monitor – set to be 10^7). Correction for detector efficiency and absolute calibration was performed by a 1 mm H_2O sample. Buffer, sample holder scattering and instrument background were subtracted from the sample scattering taking into account the corresponding transmission values according to equation 4.1.

$$I_{corrected} = \frac{1}{T_{sample}T_{buffer}}\left[I_{sample} - I_{Cd}\right] - \frac{1}{T_{buffer}}\left[I_{buffer} - I_{Cd}\right] \quad \textbf{4.1}$$

,

where I_{sample}, I_{Buffer} and I_{Cd} denote the measured scattering intensities during the sample, buffer and instrument background measurement, respectively while T_{sample} and T_{buffer} denote the transmission values of the sample relative to the buffer and the buffer transmission, respectively.

The obtained 2-dimensional sample scattering signal was radially averaged around the beam centre position (defined by the analysis of an empty beam measurement), in a sector of a 360º opening angle in case of unoriented samples. In case of oriented samples the data was radially averaged in 2 sectors with 45º opening angles, the bisectors being aligned parallel to the magnetic field. Further data treatment was performed on the resulting $I(Q)$ radially averaged scattering curves.

Here we can explain the advantage of the magnetic orientation of the thylakoid membranes in our experiment. In a sample solution where the membrane sheets' normals are randomly oriented in a 4π solid angle, the membrane sheets have a significantly lower probability to be in a diffracting position (detailed below) than in the case where the membrane sheets' normals are preferentially perpendicular to the neutron beam.

Furthermore, magnetic orientation reduces the experimental background of the radially averaged scattering curves due to the fact that the lower opening angle of the 2D signal is averaged radially.

4.4.2 SANS Data Treatment II – from Radially Averaged Scattering Curves to Repeat Distances

Thylakoid membranes of higher plants, as shown in Chapter 3, form a highly organized structure with two significantly different sets of structural parameters in the stroma and the granum part. The primary information, we intend to obtain from neutron scattering data, are these structural parameters. Similar structural parameters of thylakoid membranes are of high interest in living algal cells.

There were previous neutron scattering experiments performed by Sadler and Worcester (1982) on chloroplasts isolated from spinach in order to obtain information about the arrangements of the thylakoid membranes. These authors drew the conclusion that the observed ~ 250 Å periodicity present in the thylakoid membranes investigated *in vivo* can be connected to the granum thylakoids, in accordance with some earlier electron microscopy studies (Izawa and Good 1966). At the time of their experiment, periodic arrangement of the stroma thylakoids was not yet widely accepted and known.

Recent investigations on spinach chloroplast suggest, however, granum repeat distances as low as 157 Å (Daum et al. 2010). This study does not provide numerical information about the repeat distance of the stroma thylakoids. Serial thin section electron micrographs of *Loloum multiflorum*, presented in (Brangeon and Mustárdy 1979), reveal that a stroma thylakoid is joint together with approximately every 2-2.5th granum. Paolillo and MacKay (1969) found this number to be on average 2.35 for the six species studied, and 2.4 for spinach. Accordingly we can expect a repetition of the stroma thylakoids along the axis perpendicular to the periodic granum membrane sheets to be found in the 300-400 Å range.

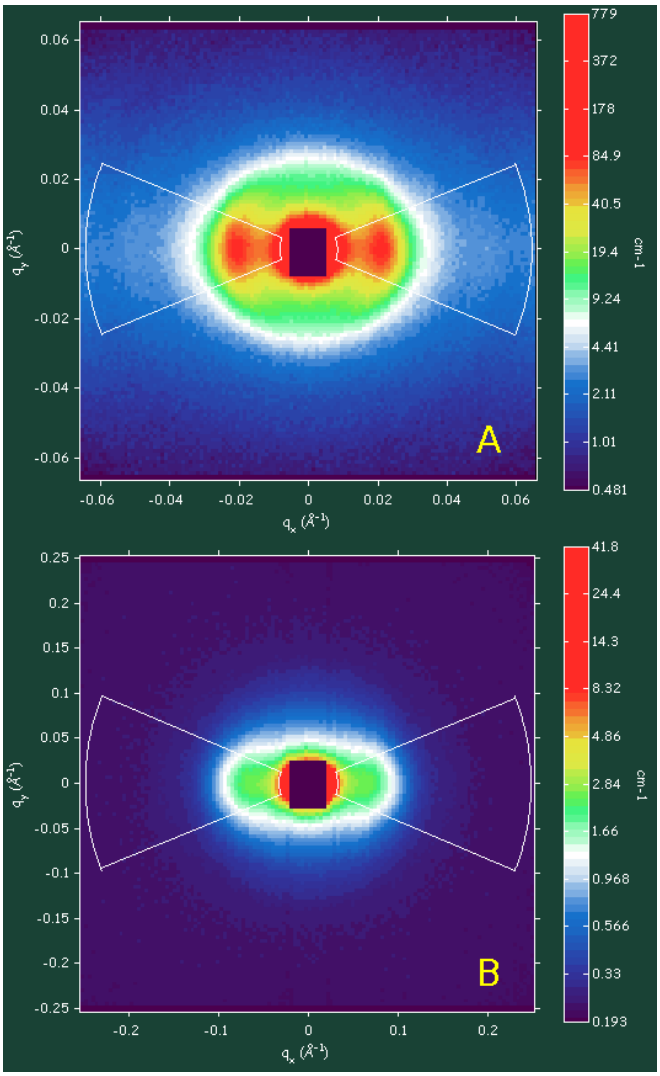

Figure 15: Scattering profile of thylakoid membranes isolated from spinach with the stroma Bragg peak (left) and the granum related feature (right) oriented with an external magnetic field of 1.5 T field strength and recorded with the 2D detector of the D22 SANS instrument. The instrument settings were: sample-to-detector distance, SD = 8 m, collimation, col = 8 m and λ = 6 Å (A); SD = 2.05 m, col = 2 m and λ = 6 Å (B). Corresponding instrumental and empty cell background measurements are subtracted and the results are corrected for detector efficiency. Colors are representing the differential scattering cross-section values in a logarithmic scale. Thylakoids are suspended in 20 mM Tricine (pD 8), 5 mM $MgCl_2$, 5 mM KCl and 0.4 M sorbitol in 100 % D_2O. The white sectors represent the area of radial averaging.

The most apparent feature of our radially averaged SANS curves of spinach thylakoids is a pronounced peak at Q ~ 0.02 Å^{-1}. This peak can clearly be identified also in the 2D scattering images (Figure 15 A). A less pronounced peak at Q ~ 0.07 Å^{-1} can also be observed on 2D scattering curves (Figure 15 B). These two characteristic peaks can hardly be recorded with the same instrument setting; their characterization requires two different settings (sample-to-detector distance, collimation) of the instruments.

Although we performed some test experiments to verify the continuity of the absolute calibrated, radially averaged scattering curves obtained in the two different experimental settings, as shown in Figure 16, in most of our experiments for technical reasons we focused our attention on only one of these signals. As a consequence the data treatment was performed separately on the different Q-ranges.

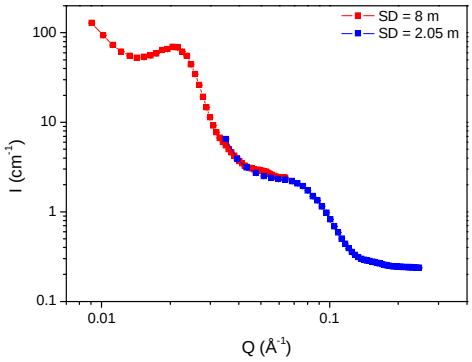

Figure 16: Radially averaged SANS scattering curve obtained from isolated thylakoid membranes suspended in 20 mM Tricine (pD 8), 5 mM KCl, 5 mM $MgCl_2$, 0.4 M sorbitol in 100 % D_2O. Red and blue curves were obtained with the SD=8 m, col=8 m and SD=2.05 m, col=2 m instrument setup, respectively. Curves are extracted from the 2D images presented in Figure 15. Absolute calibration, allowing the joint presentation of the two curves, was performed with a reference water sample.

Considering the peak at Q ~ 0.02 $Å^{-1}$ as a first order Bragg peak we calculated repeat distance values ranging from between 286 and 301 Å, under control conditions (20 mM Tricine, 5 mM KCl, 5 mM Mg Cl_2, 0.4 M sorbitol). This repeat distance cannot correspond to the granum thylakoids. Albeit it is slightly smaller then the repeat distance value expected for stroma thylakoids from EM, we connected it to the periodic structure of the stroma thylakoids, considering that the sample environmental conditions for EM and SANS are significantly different. The connection of the peak to the periodicity of the stroma thylakoids will be supported by multiple results presented in this work in latter chapters.

The information we desired to obtain from the scattering curves covering the low Q-range (usually from ~ 0.01 $Å^{-1}$ to ~ 0.06 $Å^{-1}$) is the peak position of the first order Bragg peak at Q ~ 0.02 $Å^{-1}$. As apparent e.g. in Figure 16, the Bragg peak is superimposed on a sample background signal decreasing with increasing Q values. Due to the highly complex composition of the sample we could not perform a detailed modeling of the

thylakoid membrane assembly and connect every parameter of the scattering curve to specific structural parameters. We found, however, that the curve can be well fitted with a Power function: $I(Q) = I_0 + A|Q|^p$. The resulting parameters of this function strongly vary for samples taken from different isolation, or for samples taken from the aliquots which were taken from the same stock solution, subjected to different environmental conditions. The stroma thylakoid Bragg peak was fitted with a Gaussian function, which is generally used on the D22 and Yellow Submarine SANS instruments for Bragg peak fitting. Therefore single scattering curves were fitted independently with the following function:

$$I(Q) = I_0 + A|Q|^p + \frac{B}{w\sqrt{\frac{\pi}{2}}} \exp\left(\frac{-2(Q-Q_c)^2}{w^2}\right), \qquad \textbf{4.2}$$

where the center position of the Gaussian function is defined by Q_c. Corresponding stroma thylakoid repeat distance (RD) values were calculated according to the Bragg equation:

$$RD = \frac{2\pi}{Q_c}. \qquad \textbf{4.3}$$

Standard errors of the RD values are representing the uncertainty of the peak position (Q_c) values.

4.4.3 Correction for the Helical Arrangement of the Stroma Thylakoids in the Vicinity of the Granum

The representation of the stroma thylakoid related peak on the radially averaged SANS curves, as it is presented in the paragraph 4.4.2, and the corresponding calculation method for the stroma thylakoid repeat distance do not take into account the helical arrangement of the stroma thylakoids around the granum shown in Figure 9. This structural model presented in (Mustárdy and Garab 2003) is a simplified representation of a complex biological structure. The recently refined model (Mustárdy et al. 2008) suggests a quasi-helical structure of stroma thylakoids around the granum with less periodicity then predicted by (Mustárdy and Garab 2003). Assuming an array of granal

thylakoid cylinders interconnected by stroma thylakoids, it is evident that the helical arrangement of the stroma thylakoid membranes can only be maintained in the vicinity of the granum cylinders. Therefore, I will discuss the comparison between the scattering from a helical line and the scattering observed during our neutron scattering experiments and present a possible correction of the stroma repeat distance values obtained during the data treatment.

We consider a single continuous helical line with its axis oriented parallel to the vertical axis z. The radius of the helix is r_h and the helix rises by P (pitch) for each 2π rotation around its axis; R and Z are reciprocal-space variables. The expected scattering intensity from such structure can be seen in Figure 17. According to (Cantor and Schimmel 1980) it can be described mathematically by Bessel functions of the first kind as presented in equation:

$$I_c(R, n/P) = J_n^2(2\pi r_h R) \quad \textbf{4.4}$$

The intensity is non-zero in a set of lines perpendicular to the axis Z with a distance of 1/P from each other. The intensity in the n^{th} line is proportional to the square of the n^{th} Bessel function.

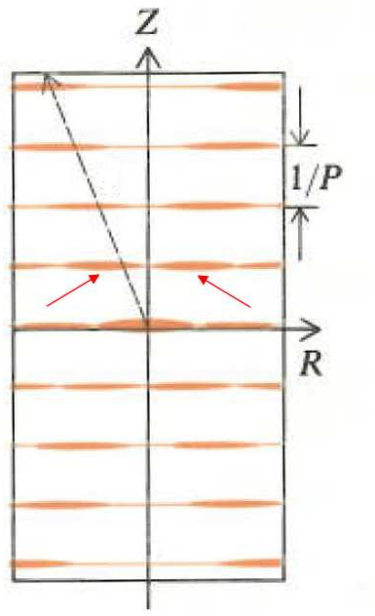

Figure 17: Scattering intensity from a continuous helical line (Cantor and Schimmel 1980). P is the pitch of the helix, Z and R are reciprocal-space variables.

We can compare the intensity scheme presented in Figure 17 with the one observed with neutron scattering presented in Figure 15 B, while keeping in mind that in our experimental setup the axis of the helical structure describing the stroma thylakoids in the vicinity of the granum is preferentially oriented parallel to the magnetic field, i.e. horizontally. We cannot observe any apparent similarity between the two figures. However, as a matter of fact neither the investigated helical structure nor the orientation of the axes of the helices are ideal. In Figure 17 the first horizontal line is situated 1/P away from the origin in the reciprocal space. Intensity along this line can be described by $J_1^2(2\pi r_h R)$ which is plotted at the $2\pi r_h R \in [0,10]$ interval in Figure 18. The first maximum of this function for $2\pi r_h R \geq 0$ is at $2\pi r_h R \approx 1.84118 \rightarrow R \approx \frac{1.84118}{2\pi r_h}$. We can calculate the distance of this first maximum position from the origin in Figure 17:

$$D \approx \sqrt{\left(\frac{1}{P}\right)^2 + \left(\frac{1.84118}{2\pi r_h}\right)^2} = \frac{1}{P}\sqrt{1+\left(\frac{1.84118 * P}{2\pi r_h}\right)^2} = \frac{1}{P}\sqrt{1+1.84118^2 * \left(\frac{P}{2\pi r_h}\right)^2} \quad \textbf{4.5}$$

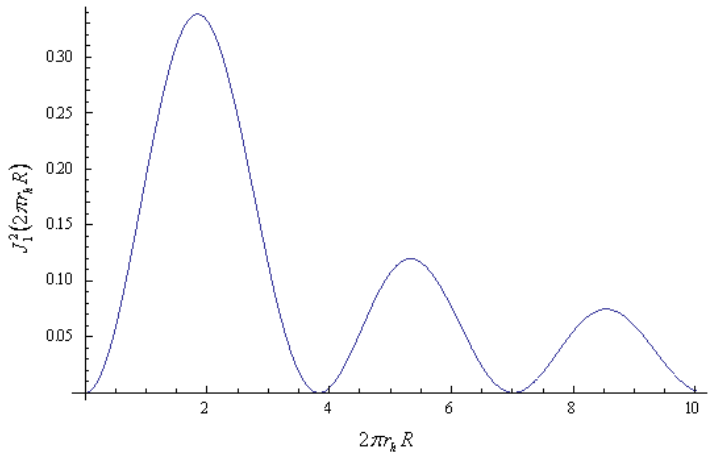

Figure 18: The Bessel function $J_1^2(2\pi r_h R)$.

We have to note that $\frac{P}{2\pi r_h}$ is equal $tg(\alpha)$ where α is the angle of inclination, i.e. the angle between the helical line and any plane perpendicular to the helix axis. We know from (Paolillo and MacKay 1969) that for thylakoids isolated from *Spinacia*

oleracea the average value α for the stroma thylakoids is 19º. Substituting this value into equation 4.5 we obtain

$$D \approx \frac{1}{P}\sqrt{1+1.84118^2 * tg^2(19°)} \approx \frac{1.18403}{P} \quad \textbf{4.6}$$

Equation 4.6 provides connection between the pitch of the helix and D (the distance of the maxima, marked by red arrows in Figure 17, and the origin).

In the non ideal system of thylakoids we have to consider multiple physical parameters which will result in a scattering pattern, which is significantly different from the one presented in Figure 17. We mentioned already that the quasihelical organization of the stroma thylakoids is valid only in the vicinity of the granum stacks. The granum stacks themselves do not form a perfect cylinder. The different granum stacks are interconnected by stroma thylakoids, therefore cannot orient independently in an external magnetic field. We do not have detailed information about the angle between the axes of the cylinder of the different granum stacks in an interconnected thylakoid membrane assembly. Therefore we may expect that the first maxima (marked by red arrows) in Figure 17 will be smeared out to form an arc as shown in Figure 15 A. As a consequence the repeat distance value which we calculate based on equation 4.3 will be approximately 1.18 times (see equation 4.6) smaller than the characteristic value P for the helix of stroma thylakoids.

The above presented calculation may provide an explanation for the slight inconsistency between the stroma thylakoid repeat distance values calculated from neutron scattering and expected repetition distances of the stroma thylakoids along the axes of the cylinder of granum thylakoids. The calculated repeat distance values for physiological conditions are in the range ~ 285 - 300 Å which along with the correction factor is changed to ~ 336 – 355 Å, being in perfect agreement with the expected 300 – 400 Å.

We do not include this correction factor in the further calculations. As mentioned above the stroma thylakoids can be described as a helical arrangement only in the close vicinity of the granum stacks. The stroma lamellae, farther from the granum thylakoids are better described as a set of parallel membranes characterized by the repeat distance of the stroma thylakoids as calculated in equation 4.3.

4.5 EINS Measurements and Data Treatment

EINS measurements were performed on the IN13 instrument (see Figure 6) at the Institut Laue-Langevin on samples scanned in the temperature range of 280 – 340 K, with 10 K steps, counting 3 hours at each temperature. The plane of the sample holders was oriented at 135° with respect to the incoming neutron beam.

The raw data collected on IN13 correspond to neutron intensities (I, which is proportional to the scattering function), as a function of the scattering angle (2θ), which can be converted into the momentum transfer **Q** through $Q = \frac{4\pi \sin(\theta)}{\lambda}$. Data reduction was performed using the Large Array Manipulation Program (LAMP) developed at the ILL (Richard et al. 1996).

The data have to be normalized and corrected for different factors. The scattering values were first normalized with respect to the incoming flux, measured by a low efficiency monitor placed in front of the sample. Scattering from the empty cell is subtracted and vanadium, a predominantly incoherent scatterer, is used for normalization.

Proper subtraction of the empty cell and vanadium normalization requires the information about the neutron transmission values of the samples, the empty cell and of vanadium. The obtained transmission values were all $T \geq 90\%$. Transmission values are kept high – by choosing the appropriate amount of sample for the measurement – in order to minimize multiple scattering effects in the sample.

MSD values were calculated based on equation 2.42. The domains for data fitting were chosen such that the linearity of the $\ln I(Q^2)$ curve was maintained. Data points were weighted when fitting by their statistical errors. The pseudo force constant, <k'> in the samples was calculated according to equation 2.43.

5. Structural Investigation of Plant Thylakoid Membranes Under Steady State Conditions

The main structural characteristics of the thylakoid membrane assembly in granal chloroplasts were presented in paragraph 3.1.1. In our experiments on thylakoid membranes of higher plants we wanted to obtain information about basic parameters of this system, such as the repeat distance of the stroma and granum thylakoids and the lumenal and interthylakoidal spaces of the granum thylakoid membranes (Figure 19).

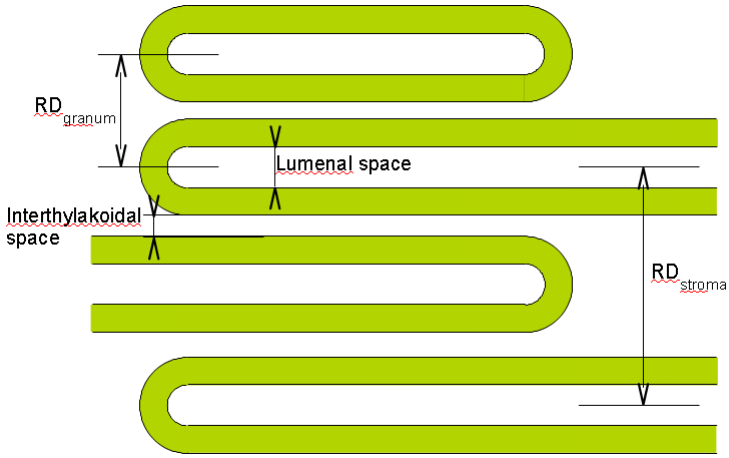

Figure 19: Schematic drawing of the granum-stroma membrane assembly of higher plants, showing the main structural parameters.

Small-angle neutron scattering curves of plant thylakoid membranes show two characteristic features in the investigated Q-range (between 0.008 and 0.2 $Å^{-1}$). A peak observed at Q ~ 0.02 $Å^{-1}$ originates from the periodic organization of the stroma thylakoids (as discussed earlier in paragraph 4.4). Another peak observed at Q ~ 0.07 $Å^{-1}$ appears to arise from the stacked membrane pairs of adjacent granum thylakoids. These features are usually investigated in two different configurations of the SANS-instruments.

5.1 Stroma Thylakoids

As mentioned above almost all our experiments on plant thylakoids were performed on oriented samples produced by applying a magnetic field to the sample. Figure 20 shows the effect of the magnetic field on the 2D detector images. The effect of the magnetic

field is evident as the characteristic signal originating from the stroma thylakoids is confined to a small angular region. Magnetic orientation can also be observed on the characteristic signal at Q ~ 0.07 $Å^{-1}$ (see Figure 15 B).

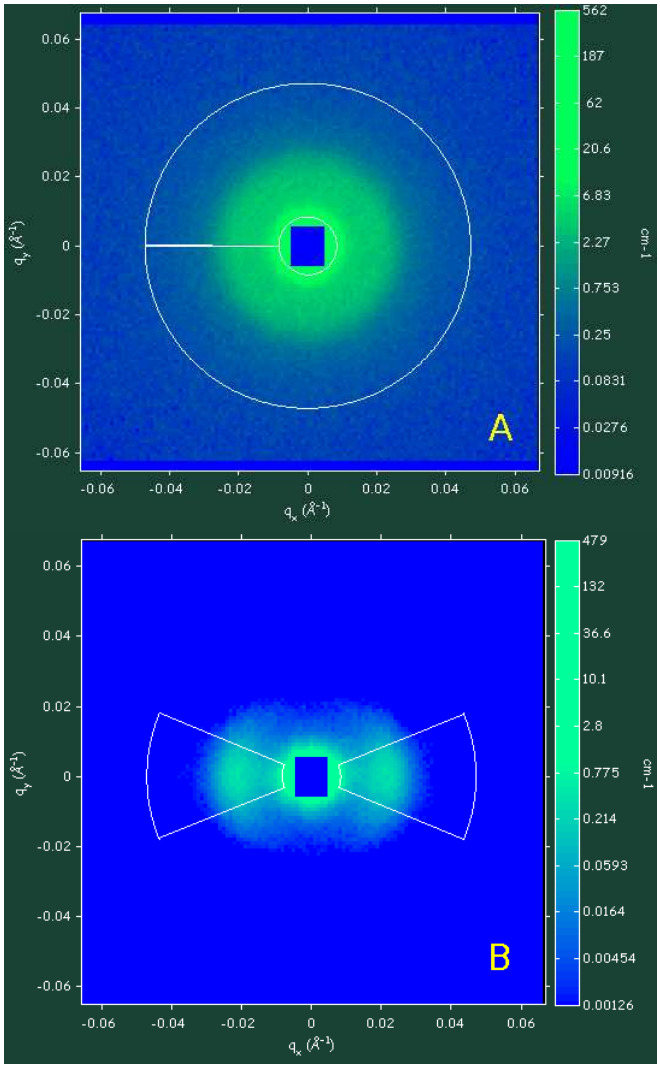

Figure 20: Scattering profile of isolated spinach thylakoid membranes, Bragg peaks attributed to the stroma thylakoid membranes; recorded with the 2D detector of the D22 SANS instrument (SD = 8 m, col = 8 m, λ = 6 Å). Corresponding instrumental and sample background measurements are subtracted and the results are corrected for detector efficiency. Colors are representing the differential scattering cross-section values in a logarithmic scale. Thylakoids are suspended in 20 mM Tricine (pD 8), 5 mM $MgCl_2$, 5 mM KCl, 0.4 M sorbitol and 100 µM PMS in 100 % D_2O. The applied magnetic field is 0 T (A) and 1.5 T (B). The white sectors represent the area of radial averaging in the two cases.

The comparison of the radially averaged scattering curves (Figure 21) reveals that in the case of magnetic orientation the characteristic peak around 0.02 $Å^{-1}$ is much more pronounced. As a consequence, the magnetically aligned samples allow us to observe

smaller changes in the peak position and allow time resolution measurements. Most of the experiments on spinach thylakoids, presented in this work, were performed in the presence of a magnetic field. The cases, when no magnetic field was applied will be indicated in the figure caption.

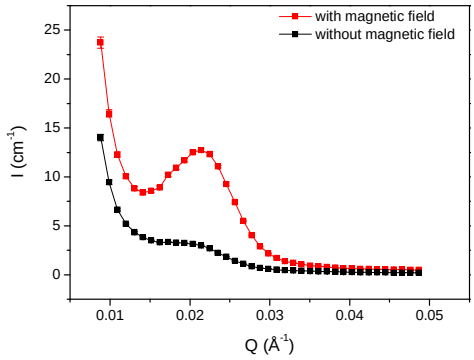

Figure 21: Effect of magnetic field on the radially averaged SANS signal of thylakoids. Curves are obtained from the 2D images presented in Figure 20.

5.1.1 Effect of Osmolarity and Ionic Strength

The structure of the thylakoid membranes can be influenced by the osmolarity of the suspending medium, as was mentioned in 3.1.3. The thylakoid membrane is relatively impermeable for ions and other solutes such as sorbitol, while being highly permeable for water, either due to its free diffusion or due to the presence of a specific transporter protein (aquaporin) in the membrane (Spetea and Schoefs 2010). According to the description of the *osmotic flow* (Serdyuk et al. 2007), water moves through the membrane from the liquid phase with lower osmotic pressure, towards the one with higher pressure. In our experiments the membranes of the isolated thylakoids remain intact and thus can be influenced by osmotic pressure. The effect of osmolarity on the granum thylakoid structure was investigated by electron microscopy (Murakami and Packer 1970) showing shrinkage and flattening of the grana upon increasing concentration of sucrose. Structural parameters of the stroma thylakoids strongly depend on the structure of the granum thylakoids according to the model, presented in (Mustárdy and Garab 2003), which predicts that a shrinkage of the granum is accompanied by a decreased repeat distance of the stroma thylakoids. SAXS

investigations of thylakoids isolated from pea leaves also predict significant changes in the membrane ultrastructure upon changing the osmolarity (Holm 2004). These experiments, however, could not resolve the Bragg-peak associated with the stroma thylakoids due to the available Q-range. Neutron scattering measurements performed at the Yellow Submarine SANS instrument (BNC, Budapest) suggested a shrinkage of the stroma thylakoids upon increasing osmolarity (Holm 2004). During our experiments on the D22 SANS instrument we could complete these results and obtain more detailed information about the osmolarity induced structural changes.

We investigated the SANS signal of thylakoids in buffers containing 20 mM Tricine, 10 mM KCl, 10 mM $MgCl_2$ dissolved in 40 % D_2O / 60 % H_2O with sorbitol concentrations of 0, 0.1, 0.4, 1 and 2 M. The radially averaged scattering curves are presented in Figure 22. The obtained curves were fitted with the function 4.2. Calculated Bragg peak positions and corresponding stroma thylakoid repeat distance values are presented in Table 6. The stroma thylakoid repeat distance decreases monotonically with increasing osmolarity. The total repeat distance change when osmolarity is increased from 0 M sorbitol to 2 M sorbitol is (38 ± 2) Å. These results also verify that the samples contain thylakoid membranes, relatively impermeable for sorbitol, i.e. they are intact.

EM revealed that in spinach chloroplasts isolated in low salt media the thylakoids lose their grana structure and form loosely attached lamellae (Izawa and Good 1966). The low salt induced structural changes were found to be partly reversible, moreover they were found to be non-osmotic. Application of a digitonin treatment for the determination of the degree of stacking in thylakoids revealed a more precise view about the role of cations in the stacking process (Barber and Chow 1979; Chow et al. 1980). Mono-, bi- and trivalent cations can all induce or maintain the stacking of thylakoids, for which increasing concentrations are required as the valency of the ion is decreased. The most important details of the theory and significance of ionic strength induced changes in the macroorganization of thylakoid membranes, detailed in (Barber and Chow 1979; Barber 1982), are as follows. The surface of the thylakoid membranes is negatively charged, mainly due to the carboxyl groups of glutamic and aspartic acid residues. The two main forces present in the interaction between the stacked membranes are the van der Waals forces and the repulsive Coulomb forces. In case of an appropriate amount of

positively charged ions present in the buffer, proteins with smaller negative charge can aggregate and form patches, separated from the proteins with higher negative charge and the patches of adjacent thylakoids can form stacking. As a result stroma thylakoids possess a higher negative surface charge.

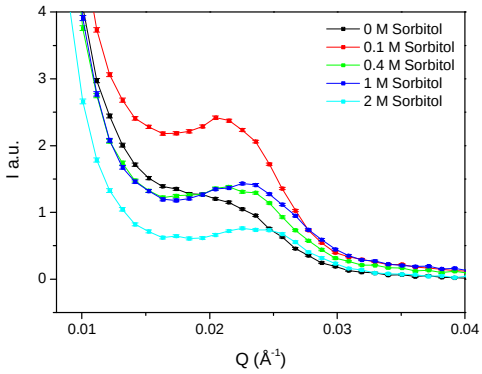

Figure 22: Effect of osmolarity on the radially averaged SANS signal of thylakoids in buffers containing 20 mM Tricine (pH 7.6), 10 mM KCl, 10 mM $MgCl_2$ dissolved in 40 % D_2O / 60 % H_2O with sorbitol concentrations of 0, 0.1, 0.4, 1 and 2 M. The measurements were performed on D22 (SD = 8 m, col = 8 m, λ = 6 Å).

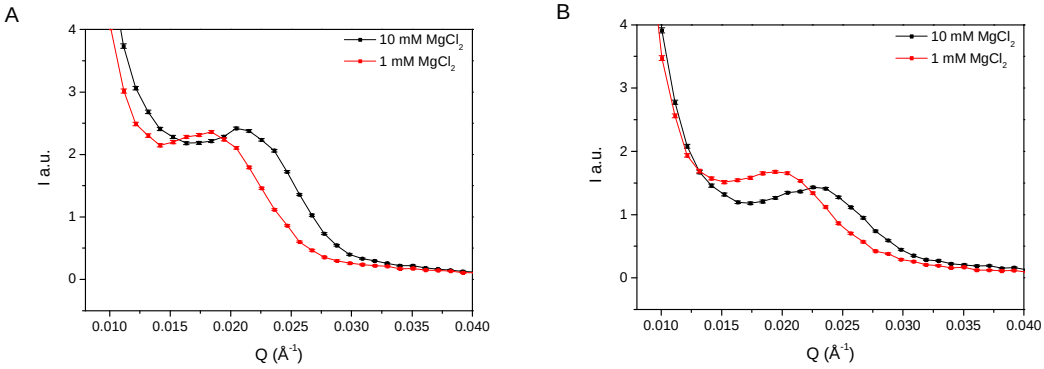

Figure 23: The effect of ionic strength on the radially averaged SANS signal of thylakoids in buffers containing 20 mM Tricine (pH 7.6), 10 mM KCl, 0.1 M (A) or 1 M (B) sorbitol, dissolved in 40 % D_2O / 60 % H_2O with $MgCl_2$ concentrations of 1 and 10 mM. The measurements were performed on D22 (SD = 8 m, col = 8 m, λ = 6 Å).

Due to the strong dependence of the stroma thylakoid periodicity on the granum thylakoid structure we can predict, as in the case of osmolarity changes, smaller repeat distance values of the stroma membranes upon increasing the concentration of Mg^{2+} ions in the buffer. We investigated the SANS signal of thylakoids in buffers containing 20 mM Tricine, 10 mM KCl dissolved in 40 % D_2O / 60 % H_2O with sorbitol

concentrations of 0.1 or 1 M and 10 mM $MgCl_2$ concentrations of 1 mM and 10 mM. The radially averaged scattering curves are presented in Figure 23. Calculated Bragg peak positions and corresponding stroma thylakoid repeat distances are presented in Table 6. Results reveal a (35 ± 1) Å and (40 ± 2) Å repeat distance decrease for stroma thylakoids, upon changing the $MgCl_2$ concentration from 1 mM to 10 mM for 0.1 and 1 M sorbitol content, respectively.

Table 6 Effect of osmolarity and ionic strength on the structure of stroma thylakoids.

40% D2O		**Peak position** [ ]=10^{-2} $Å^{-1}$	**Repeat distance** [ ]=Å
10 mM $MgCl_2$ 10 mM KCl 20 mM Tricine	**sorbitol** 0 M	2.04±0.01	307±2
	0.1 M	2.12±0.01	297±1
	0.4 M	2.2±0.01	286±1
	1 M	2.27±0.01	277±1
	2 M	2.34±0.01	269±1
0.1 M sorbitol 10 mM KCl 20 mM Tricine	**$MgCl_2$** 1 mM	1.89±0.01	332±1
	10 mM	2.12±0.01	297±1
1 M sorbitol 10 mM KCl 20 mM Tricine	**$MgCl_2$** 1mM	1.99±0.01	317±2
	10 mM	2.27±0.01	277±1

Earlier the degree of stacking was found, by W. S. Chow and coworkers, to be strongly dependent on the $MgCl_2$ concentration between 0.1 and 1 mM, and only slightly increased by raising the $MgCl_2$ concentration further to 10 mM as shown on Fig. 1 in (Chow et al. 1980). In a later experiment performed in the presence of KCl in an amount (10 mM) identical to our experiments, the change in the stacking of the thylakoids upon increasing the $MgCl_2$ concentration from 1 to 5 mM was found to be more pronounced (Chow et al. 2005). When comparing our results to the digitonin fractionation, we have,

however, to be aware that the technique used by W. S. Chow and coworkers is sensitive to the existence of the stacking of membranes, while SANS provides information about the changes in the distance between the stacked granum thylakoids (only indirectly) through the repeat distance values of stroma thylakoids.

5.1.2 Effect of Phosphorylation

Photosynthetic organisms are subject to continuously changing light conditions. In order to maintain their optimal growth and also to protect themselves from damage induced by excess light, they need to be able to adapt to the different levels of illumination on short and long timescales (Rochaix 2007).

Photoprotection against a rapid (timescale of seconds to minutes) increase in the light intensity is achieved by a ΔpH regulated high-energy-state quenching (qE). This process facilitates the deactivation of the singlet excited state of chlorophyll-a ($^1Chl^*$), and emit the excess absorbed energy as heat, preventing the formation of triplet chlorophyll ($^3Chl^*$) molecules which can react with oxygen and form highly reactive oxygen species (Holt et al. 2004).

In case of the accumulation of these highly reactive radicals, different subunits of PSII may be damaged, which can result in the inactivation of PSII. The most light sensitive part of PSII is the D1 subunit. After irreversible damage of the D1 subunit PSII migrates in a monomeric form to the stroma thylakoids, where degradation and synthesis of the D1 protein and reassembly of the PSII occurs, providing another level of photoprotective mechanism for the plants (Aro et al. 1993; Kanervo et al. 2005). Furthermore a non-functional fraction of PSII also serves as protection for the surrounding active PSII by dissipating the excess energy as heat (Lee et al. 2001).

Photosynthetic organisms can adapt on the longer timescale to illumination with different wavelength distributions by adjusting the stoichiometry of the photosystems. Thylakoid membranes isolated from pea leaves, grown under red light (which preferentially excites PSI), showed an increase of the PSII/PSI ratio compared to those isolated from leaves grown under yellow light (which preferentially excites PSII) (Chow et al. 1990). Plants are also observed to adapt to different levels of light intensity by

adjusting the macroorganization of their thylakoid membranes by forming more stacked membranes in low light than in high light intensity (Anderson 1999).

During adaptation on the timescale of minutes to light conditions which result in the unbalanced functioning of PSII and PSI a redox-controlled energy redistribution occurs between the two photosystems, a process known as state transition, during which large structural reorganizations have been shown to occur (Allen and Forsberg 2001; Allen 2003; Rochaix 2007; Chuartzman et al. 2008; Iwai et al. 2010). During these state transitions (see Figure 24) LHCII is redistributed between PSII (situated in the granum) and PSI (situated in the stroma thylakoids) by a plastoquinone pool redox-state controlled LHCII kinase (Allen 2003; Rochaix 2007). This redistribution requires the mobility of the LHCII complexes which probably cannot be maintained in the strongly appressed granum thylakoids, which thus predicts a high structural flexibility of the thylakoid membrane assembly. Indeed large structural reorganizations are proposed on the level of macro-domains of protein complexes and of the stacking of the thylakoid membranes (Allen and Forsberg 2001). In *Chlamydomonas reinhardtii* thylakoid membranes were found to be relatively unstacked in State 2 compared to the ones in State 1 (Iwai et al. 2008). The reorganization of the macrodomains and of the thylakoid membranes is proposed to be governed by the change in the phosphorylation state of LHCII (Allen 1992). This process, i.e. the way in which LHCII phosphorylation affects the dynamic architecture of photosynthetic membranes, is however not fully understood (Allen 2003).

We investigated the phosphorylation induced changes in the dynamic architecture of the thylakoid membranes with SANS. In the studies presented above, the reduced state of the plastoquinone pool which activates the kinase enzyme, responsible for the phosphorylation of LHCII, is the result of specific illumination conditions. Illumination however, also has an influence on the LHCII phosphorylation, independent of the reduced state of the plastoquinone pool; it exposes the phosphorylation site of LHCII (preferentially of the trimeric form) to the kinase enzyme (Zer et al. 1999). Illumination can also induce reorganizations in the chiral macrodomains of LHCII lamellar aggregates, resulting in an increased energy dissipation (Barzda et al. 1996), through a so called thermo-optic process (Cseh et al. 2005). Duroquinol (tetramethyl-*p*-

hydroquinone, hereafter DQH_2) is known to reduce the plastoquinone pool (Aro and Ohad 2003), therefore in the present study instead of illumination we used duroquinol-induced phosphorylation.

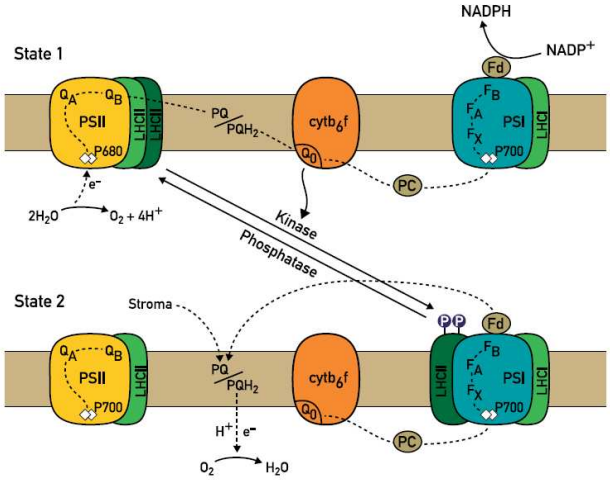

Figure 24: Schematic representation of photosynthetic complexes in thylakoid membranes, and their reorganization during state transition (Rochaix 2007). State I under light conditions when PSI is preferentially excited, the plastoquinone pool is in an oxidized state, which inactivates the LHCII kinase. The mobile fraction of LHCII is dephoshorylated via phosphatases (Aro and Ohad 2003), and binds to PSII. State II: under light conditions, when PSII is preferentially excited, the plastoquinone pool is in a reduced state, plastoquinol (PQH_2 is favorably docked to the cytochrome b_6f), which activates the LHCII protein kinase, and the latter phosphorylates LHCII, leading to the displacement of the mobile fraction of LHCII from PSII to PSI. In this state the electron transport chain is functioning mostly in a cyclic mode, when photosynthesis generates only ATP.

For SANS experiments thylakoid membranes were freshly isolated from leaves of 10-12 day old pea (*Pisum sativum*), as described in 4.1.1. The membranes were resuspended in a phosphorylation buffer containing 50 mM Tris-HCl (pD 8), 10 mM NaCl, 10 mM $MgCl_2$, 10 mM NaF in D_2O and were used for phosphorylation in 10 min or were stored on ice.

In our SANS experiments the investigated Q-range was between 0.009 and 0.055 $Å^{-1}$, therefore our data provide information only about the characteristic repeat distance of stroma thylakoids. We performed comparative SANS measurements on thylakoids from the same isolation suspended in phosphorylation buffer i) without additional DQH_2 or ATP, ii) with additional 4 mM DQH_2 and iii) with 4 mM DQH_2 and 0.2 mM ATP in order to differentiate between the effects of the different treatments. Representative radially averaged scattering curves obtained from one of the measured 4 different batches are presented in Figure 25. Scattering curves of the DQH_2-treated and of the

phosphorylated thylakoids are significantly different from the ones of control thylakoids. Calculated Bragg peak positions and corresponding stroma thylakoid repeat distances are presented in Table 7. Results reveal a (32 ± 7) Å and (28 ± 7) Å repeat distance increase (averaged over the 4 different samples) for stroma thylakoids upon DQH_2-treatment and phosphorylation, respectively. Phosphorylation did not result in a significant repeat distance change compared to the DQH_2-treatment, it only led to a ~ 15 % decrease in the intensity of the Bragg scattering.

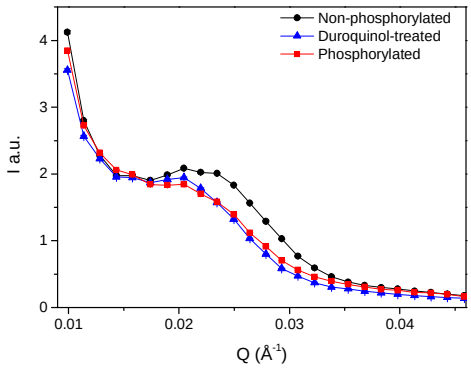

Figure 25 Effect of duroquinol-treatment and phosphorylation on the radially averaged SANS signal of pea thylakoids. Measurement was performed on Yellow Submarine (SD = 5.6 m, col = 6 m, λ = 7.51 Å).

Comparative CD measurements detailed in (Várkonyi et al. 2009) were performed by Zsuzsanna Várkonyi on control, DQH_2 treated and phosphorylated thylakoid membranes. The results (not presented here) show that at room temperature the CD spectra of each of the samples are very similar. A significant influence of the DQH_2-treatment cannot be revealed even with a temperature dependent CD measurement. Phosphorylation, however, was proven to influence the temperature dependence of the thylakoid membranes' CD spectra. The transition temperature of the CD band characterized by $\Delta CD_{688mm-672mm}$ was shifted from (47.5 ± 1.7) ºC in control thylakoids to (44.3 ± 1.0) ºC in phosphorylated thylakoids, suggesting that the disassembly of chiral macrodomains is facilitated by phosphorylation. Comparative CD spectroscopic and polyacrylamide gel electrophoresis studies showed that phosphorylation, by shifting the thermal stability to lower temperatures (from 55.6 ± 1.2 to 48.6 ± 1.6 ºC), facilitates the monomerization of LHCII in thylakoid membranes (Várkonyi et al. 2009).

Table 7: Effect of duroquinol treatment and phosphorylation on the structure of stroma thylakoids.

Batch	Treatment	**Peak position** [ ]=10^{-2} Å^{-1}	**Repeat distance** [ ]=Å
1	Control	2.31±0.01	272±1
	DQH_2-treated	2.11±0.01	298±1
	Phosphorylated	2.17±0.01	290±1
2	Control	2.24±0.01	280±1
	DQH_2-treated	2±0.01	314±1
	Phosphorylated	2±0.01	314±1
3	Control	2.17±0.01	290±1
	DQH_2-treated	2±0.01	314±1
	Phosphorylated	1.98±0.01	317±1
4	Control	2.3±0.01	273±1
	DQH_2-treated	1.99±0.01	316±1
	Phosphorylated	2.04±0.01	308±1

Comparing the results presented above, the interpretation of the SANS studies on the effect of phosphorylation on thylakoid membranes thus remains ambiguous. The periodic structure of the stroma thylakoids seems to be influenced more strongly by the redox state of the PQ-pool than by the phosphorylation process itself. We can exclude the presence of remnant ATP in the suspension of isolated thylakoids, since the synthesized ATP is situated in the stroma liquid which is washed away during the isolation procedure.

We also have to consider that our SANS measurements reveal changes in the multilamellar structure of the stroma thylakoids, while in the investigated Q-range they do not provide direct information about structural changes in the granum periodicity. The main structural reorganization of the thylakoid membranes during state transition is proposed to occur in the stacked regions or at the edge of the stacked regions (Allen 1992; Allen and Forsberg 2001; Posch et al. 2009); the influence of the state transitions on the stroma thylakoids is difficult to predict.

At the time of the experiments we were not completely aware of the interpretation of the granum related SANS signal, presented in 5.2, therefore we did not extend the Q-range of our experiments towards higher Q values. A possible continuation of the above

presented work would be to investigate the effect of DQH_2-treatment and phosphorylation on the granum related feature of the thylakoid SANS curves.

5.2 Granum Thylakoids

Lateral heterogeneity in the protein composition and in the packing density of the thylakoid membranes can be observed in many green algae and in some cyanobacteria (Mullineaux 2005). However, thylakoid granum in the highly structured form as shown e.g. in Figure 9, can be found only in higher plants. The biogenesis, the functional advantages and the evolutional necessity of this structure are not yet fully understood.

Granal thylakoids provide a space saving arrangement of the membranes. An average granum-stroma assembly requires ~ 16 times smaller space than a sphere defined by a membrane with an identical surface (Mustárdy and Garab 2003). Another important function of the differentiation of the thylakoid membrane might be facilitate the regulation and protection of different components of the electron transport chain (Albertsson 2001). This arrangement enhances the light capture, provides the ability of balanced distribution of excitation energy between the photosystems, facilitates the thermal dissipation of excess excitation energy, decreases the degradation-rate of different PSII subunits through protective mechanisms of photoinhibition, has a role in the regulation of cyclic and non-cyclic electron flows and facilitates the accommodation to different light conditions (Chow et al. 2005). By separating PSII and PSI, grana also provides a solution for preventing quenching of PSII by PSI, the latter having faster kinetics for the trapping of the excitation energy (Trissl and Wilhelm 1993).

Electron micrographs (see for e.g. Figure 9) revealed the highly organized structure of granum thylakoids. Based on this structure and considering repeat distances of ~ 157 Å (Daum et al. 2010), a Bragg peak can be expected at around $Q_c = \frac{2\pi}{RD} \approx 0.04\,\text{Å}^{-1}$. As shown in Figure 16, no characteristic peak can be observed at this Q region on isolated spinach thylakoids suspended in a ~ 100 % D_2O-containing buffer. We performed a number of experiments, where we attempted to detect this predicted Bragg-peak by varying the osmolarity or the ionic strength of the suspension buffer, by changing the D_2O content of the buffer and thus the contrast between the buffer and the different

compartments of the thylakoid membrane, or by decreasing the stacking of the adjacent granum thylakoid vesicles through the application of different isolation procedures. None of our efforts resulted in the appearance of a Bragg peak at Q ~ 0.04 $Å^{-1}$.

5.2.1 Neutron Scattering Length Density

As it can be seen in Figure 16, radially averaged scattering curves of thylakoid membranes display a characteristic peak at Q ~ 0.07 $Å^{-1}$. In order to identify the origin of this peak we performed contrast variation experiments.

In our SANS experiments the maximum observed value of the scattering vector Q is 0.2 $Å^{-1}$. This value defines the minimal d-spacing determinable by the experiment (Serdyuk et al. 2007). $\Delta x = \frac{2\pi}{Q_{\max}}$ is significantly higher than the distances between neighboring atoms in the investigated systems. Instead of considering our system as a set of i point scatterers with coherent scattering length b_i, we can define a scattering length density $\rho(\boldsymbol{R})$ under these conditions (Zaccai 2000b) through the equation: (Schwahn 2005)

$$\rho(\boldsymbol{R}) = \frac{b_k}{v_k}, \qquad \textbf{5.1}$$

where **R** points into a volume element (v_k), b_k is the scattering length of the volume element (obtained as the sum of the scattering lengths of the atoms in the volume element). The mean scattering density of the particle is $\rho = \sum_k \frac{b_k}{V}$ where V is the volume of the particle. As an example for water with a natural isotope composition the scattering length density can be calculated as follows:

$$\rho(\boldsymbol{R}) = \rho_0 = \frac{1}{V_{H_2O\ molecule}}(2b_H + b_O) = \frac{1}{\frac{M_{H_2O}}{\rho_{H_2O}}\frac{1}{A}}(2(-3.739)+5.803)\,fm = \\ = \frac{1}{\frac{18.01528\,g/mol}{1\,g/cm^3}\frac{1}{6.02214\times10^{23}\,1/mol}}(-1.675)\,fm == -5.5992\times10^{-7}\,Å^{-2} \qquad \textbf{5.2}$$

In the paragraph 2.1.4.2 and therefore in equation 2.15 we considered scattering from a system of N atoms of the same element with no correlation between the spatial coordinates and scattering lengths. If we do not use this presumption equation 2.15 is modified as:

$$\frac{d\sigma_s}{d\Omega} = \left| \sum_j \overline{b_j} e^{i\boldsymbol{QR}_j} \right|^2 \qquad \textbf{5.3}$$

and, by introducing the scattering length density (SLD) ρ, to:

$$\frac{d\sigma_s}{d\Omega} = \left| \int_V \rho(\boldsymbol{R}) e^{i\boldsymbol{QR}} d^3R \right|^2 . \qquad \textbf{5.4}$$

For a system with constant scattering length density equation 5.4 takes the form of $\frac{d\sigma_s}{d\Omega} = \rho_0{}^2 \left| \int_V e^{i\boldsymbol{QR}} d^3R \right|^2 = const \times \delta(Q)$ according to (Schwahn 2005), which will not be observed in the experiments due to the applied beam-stop (which absorbs neutrons with low momentum transfer). Therefore for a solution, consisting of a solvent with ρ_0 scattering length density and particles in it defined by ρ(**R**), equation 5.4 can be written as:

$$\frac{d\sigma_s}{d\Omega} = \left| \int_V (\rho(\boldsymbol{R}) - \rho_0) e^{i\boldsymbol{QR}} d^3R \right|^2 , \qquad \textbf{5.5}$$

where $(\rho(\boldsymbol{R}) - \rho_0)$ is the contrast of the particle.

Consequences of equation 5.5 are applied in neutron scattering experiments where samples are measured in buffer, containing various ratios of D_2O/ H_2O. By this way one reveals or hides different parts of a complex biological system (see Figure 26). The method is valid only in the case of sufficiently low resolution of the experiment, which does not allow distinguishing different parts of the specific macromolecule (Zaccai 2000b).

5.2.2 Contrast Variation Measurements

In our SANS experiments we performed contrast variation measurements on spinach thylakoid membranes suspended in buffer with D_2O concentrations of 0, 40, 70 and 100 %. The radially averaged scattering curves are presented in Figure 27. Due to the lack of SANS curves of all the corresponding buffers, only an empty cell subtraction was performed.

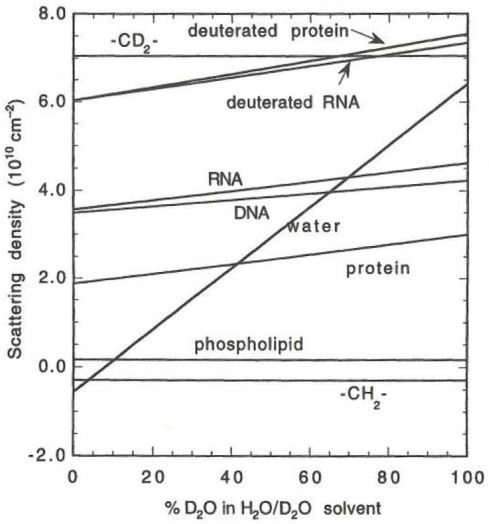

Figure 26: Averaged neutron scattering length density of different components of biological samples as a function of the D_2O/ H_2O ratio of the solvent, copied from (Zaccai 2000b). The slope of certain curves can be explained by the substitution of an increasing number of exchangeable H-atoms in the sample by D-atoms, as the D_2O content of the solvent increases. Some of the biological components can be matched with an appropriate solvent composition such as the proteins at ~ 40% D_2O content.

An apparent feature of the curves is the increasing incoherent background with increasing H_2O content of the buffer. At 0 % D_2O concentration, which is close to the match point (where the specific component of the sample has no contrast) of phospholipids, there is no peak observable on the scattering curves at Q ~ 0.07 Å^{-1}. The peak intensity is rising with increasing concentrations of D_2O, i.e. with increasing contrast for the phospholipid content of the thylakoid membranes. Furthermore, as shown in Figure 27 B, the peak is most marked at 40 % D_2O concentration, i.e. at the match point for proteins.

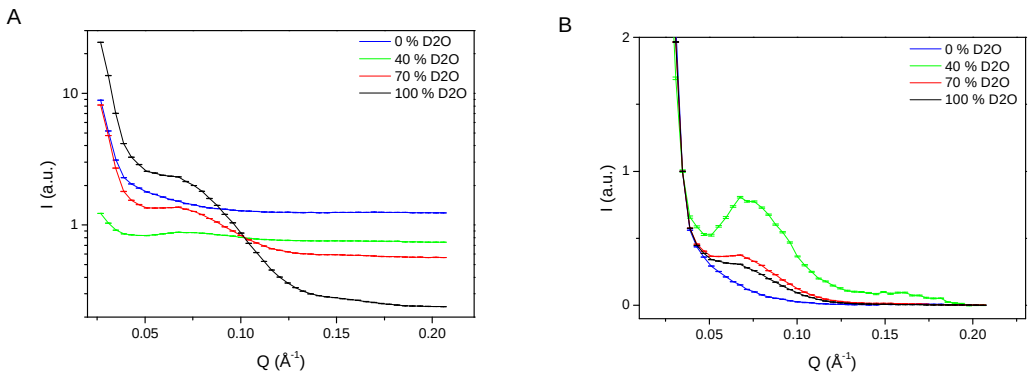

Figure 27: Effect of D_2O concentration of the solvent on the radially averaged SANS signal of thylakoids suspended in buffers containing 20 mM Tricine, 10 mM KCl, 10 mM $MgCl_2$, 0.4 M sorbitol with 0, 40, 70 and 100 % D_2O concentrations. Graph B was obtained as follows: constant values were subtracted to obtain I=0 at Q=0.21 $Å^{-1}$ and curves were normalized to 1 at Q=0.035 $Å^{-1}$ for a better comparison. Measurements were performed on D22 (SD = 2.05 m, col = 2 m, λ = 6 Å). In contrast to Paragraph 4.4.1, instead of a buffer subtraction an empty cell subtraction was performed on 1D scattering curves according to equation 4.1. In the measurements, performed on thylakoids suspended in buffer with 40 % D_2O concentration, apart from the peak at Q ~ 0.07 $Å^{-1}$ (discussed in the present paragraph) a further peak can be observed at Q ~ 0.16 $Å^{-1}$.

Radially averaged scattering curves of spinach thylakoids suspended in buffer with D_2O concentrations of 40 and 100 % after subtraction of the corresponding buffers (available for these two concentrations) can be seen in Figure 28.

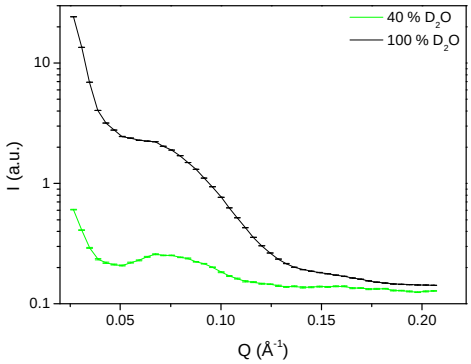

Figure 28: Effect of D_2O-concentration of the suspending medium on the radially averaged SANS signal of thylakoids suspended in buffers containing 20 mM Tricine, 10 mM KCl, 10 mM $MgCl_2$, 0.4 M sorbitol with 40 and 100 % D_2O concentrations. Measurements were performed on D22 (SD = 2.05 m, col = 2 m, λ = 6 Å). Buffer subtraction (instead of empty cell subtraction as in Figure 27) was undertaken on 1D scattering curves according to equation 4.1.

5.2.3 Effect of Osmolarity and Ionic Strength on the Characteristic Peak at Q ~ 0.07 Å^{-1}

Further experiments were performed in order to identify the origin of the peak at Q ~ 0.07 Å^{-1}. We investigated the influence on the peak position of a change in the osmolarity or in the ionic strength of the buffer at 40 % D_2O concentration. As shown in Figure 29 the peak cannot be properly described by one Gaussian function. However, the data were not suitable to apply a more subtle function (which could account for the background curve and the proper shape of the peak) for the fitting for all osmolarity and ionic strength values. Therefore, as a first approximation we used a Gaussian function with an asymmetrically defined Q range around the local maximum for the determination of the peak position; the center positions obtained are presented in Table 8.

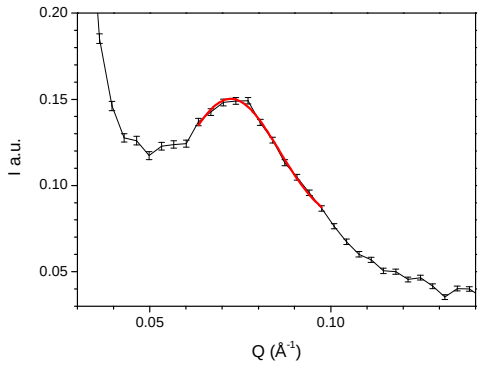

Figure 29: Radially averaged SANS scattering curve of thylakoids in buffers containing 20 mM Tricine (pH 7.6), 10 mM KCl, 10 mM $MgCl_2$ and 0.4 M sorbitol dissolved in 40 % D_2O/60 % H_2O. Measurements were performed on D22 (SD = 8 m, col = 8 m, λ = 6 Å). Fitted Gaussian function colored in red.

One possible interpretation of the peak at Q ~ 0.07 Å^{-1} could be, that it arises from the quasi periodicity of the lipid bilayers in the granum thylakoids. As shown in Figure 30 the distance of the lipid bilayers across the lumenal and interthylakoidal space is commensurate, and in a buffer with 40 % D_2O concentration the contrast of the interthylakoidal and lumenal space are both expected to be close to zero, independently from their protein content. Under control conditions (i.e. in buffer with 20 mM Tricine (pH 7.6), 10 mM KCl, 10 mM $MgCl_2$ and 0.4 M sorbitol) this interpretation would give ~ 87 Å for the lipid bilayer periodicity, i.e. ~ 174 Å for the total RD of the granum thylakoids. However, we find this interpretation less likely for several reasons. Although

the interthylakoidal and lumenal space thickness is commensurate (e.g. 32 and 45 Å, respectively in (Daum et al. 2010)), they are not identical. The variation of the peak upon changing the ionic strength and osmolarity (see below) also suggests that the interpretation is not appropriate.

Table 8: Effect of osmolarity and ionic strength on the peak positioned around Q ~ 0.07 $Å^{-1}$.

40% D2O		**Peak position** [ ]=10^{-2} $Å^{-1}$
10 mM $MgCl_2$	**sorbitol**	7.18±0.04
10 mM KCl	0 M	
20 mM Tricine	0.1 M	7.19±0.03
	0.4 M	7.24±0.03
	1 M	7.32±0.04
	2 M	7.42±0.04
0.1 M sorbitol	**$MgCl_2$**	6.85±0.06
10 mM KCl	1 mM	
20 mM Tricine	10 mM	7.19±0.03
1 M sorbitol	**$MgCl_2$**	6.96±0.05
10 mM KCl	1mM	
20 mM Tricine	10 mM	7.32±0.04

The results, presented in Table 8 reveal that upon increasing the osmolarity or the ionic strength of the buffer the peak position is shifted towards higher Q values. For comparison, it is interesting to recall that while the stroma related Bragg peak was shifted by ~ 15 % when the sorbitol content was increased from 0 M to 2 M (cf.Table 6), the changes induced at this higher Q peak were much smaller (about 3%).

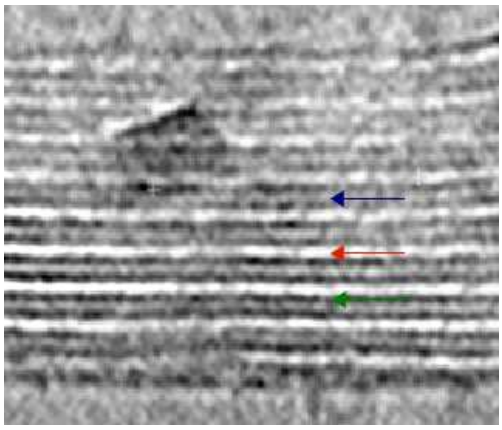

Figure 30: Electron Tomography image of granum thylakoids in a spinach chloroplast (copied from (Daum et al. 2010)). Black lines (green arrow) represent the thylakoid membranes, white areas (red arrow) the lumenal space, and grey regions (blue arrow) the interthylakoidal space.

With the variations in the ionic strength, 12 % (in the presence of 0.1 M sorbitol) and 14 % (in the presence of 1 M sorbitol) shifts were obtained for the Q peak related to stroma membrane repeat distance (Table 6), but only about 5 % for the peak at Q ~ 0.07 $Å^{-1}$, i.e. the changes in $MgCl_2$ concentration had a somewhat more pronounced effect on this peak position than the changes in the sorbitol concentration, but still much less that for the stroma peak. Considering these results and the fact that the change of osmolarity of the buffer is expected to influence the size of the lumenal space and the change in the Mg^{2+} concentration affects the stacking of membranes, i.e. the size of the interthylakoidal space, the Q peak at around 0.07 $Å^{-1}$ may be connected to the distance between the stacked membranes of adjacent thylakoids (see Figure 31). Nevertheless the obtained results are not sufficient to establish a clear-cut relation between the high angle scattering curves and any structural parameter of the investigated multilamellar membrane system.

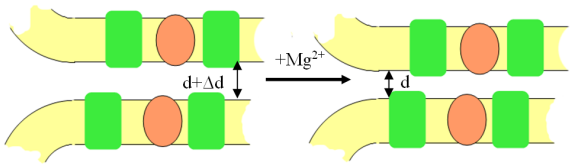

Figure 31: Schematic representation of the changes in the interthylakoidal space, induced by an increase in the ionic strength.

5.2.4 BBY as a Structural Element of the Granum Thylakoid Multilamellar Membrane System

In order to obtain further information on the origin of this peak we performed SANS experiments on PSII membrane fragments (BBY). During the isolation of the BBY membranes we obtain stacked membrane pairs, i.e. two membranes with an enclosed interthylakoidal space – a structural element of the granum thylakoid multilamellar membrane system, which is lacking the lumenal space (Figure 32).

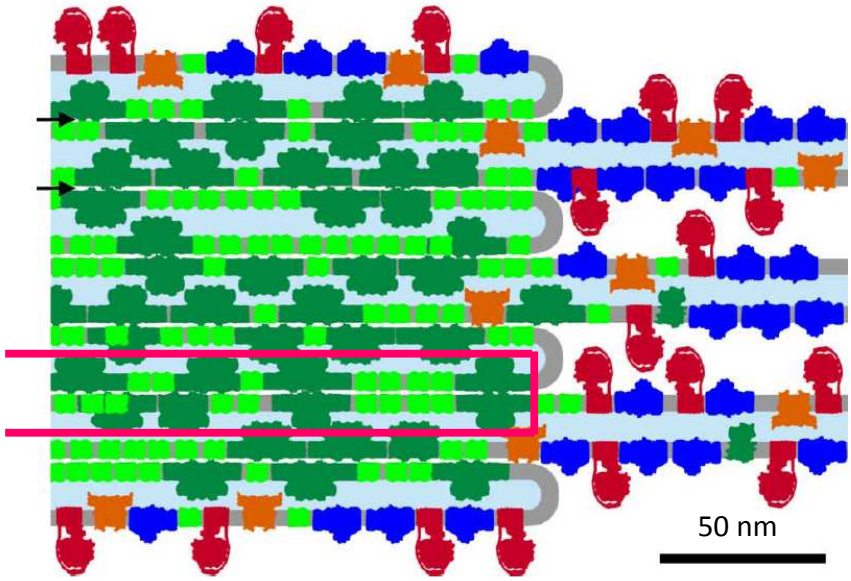

Figure 32: Schematic drawing showing the BBY (surrounded by pink line) as the structural element of the granum thylakoid. The drawing depicting the granum and stroma thylakoid membranes is copied from (Dekker and Boekema 2005). For further information see Figure 11.

The obtained BBY SANS curves, along with the corresponding thylakoid curves copied from Figure 28, are presented in Figure 33.

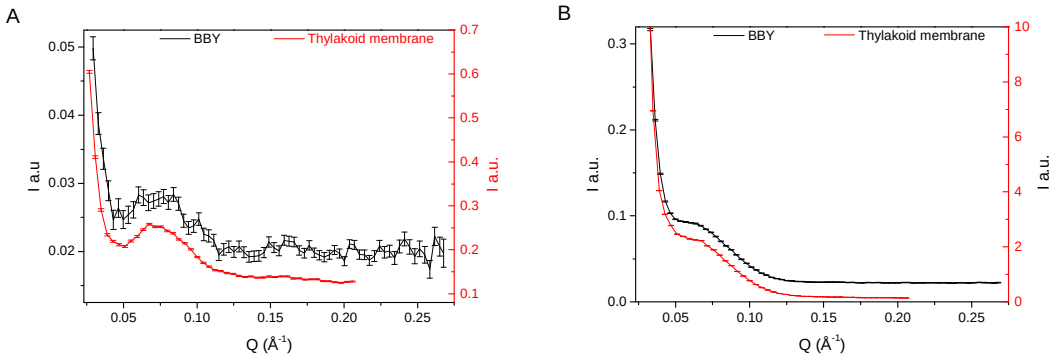

Figure 33: Radially averaged SANS scattering curve of BBY (black) and thylakoid (red) membranes suspended in buffers containing 20 mM Tricine, 10 mM KCl, 10 mM $MgCl_2$, 0.4 M sorbitol with 40 % (A) and 100 % (B) D_2O concentrations.

The very different signal to noise ratio and scattering intensity for the two samples can be explained, apart from the significantly different characteristics, by the fact that BBY samples were unoriented, while the thylakoid membranes were magnetically oriented. It is also to be noted that in the case of isolated thylakoid membranes the grana

contain several copies of the same structural element (which are spaced essentially periodically with respect to each other), in the BBY this structural unit is present freely in the suspension. Nevertheless the similarity between the scattering curves in the high Q range is apparent. This result confirms that the peak on the SANS curves of thylakoid membranes at Q ~ 0.07 $Å^{-1}$ is arising from the stacked membrane pairs of adjacent thylakoids. In the low Q range the BBY membrane does not show characteristic peaks. This is in accordance with the interpretation of the peak at Q ~ 0.02 $Å^{-1}$ for the thylakoid membranes, i.e. that it originates from the periodic arrangement of stroma thylakoids, since BBY does not contain this component of the thylakoid membranes.

5.2.5 SLD Profile and Corresponding Form Factor of BBY

In order to connect the SANS curve obtained from BBY membranes (suspended in buffer containing 20 mM Tricine, 10 mM KCl, 10 mM $MgCl_2$, 0.4 M sorbitol with 40 % D_2O) to specific structural parameters of the membrane pair, especially to the distance between the pair, we calculated a SLD profile perpendicular to the BBY membrane normal.

Based on Figure 26 we consider that proteins present in the sample have no contrast compared to the buffer. As detailed in paragraph 4.2.2 for the lipids the average headgroup SLD is $1.67 \cdot 10^{-6}$ $Å^{-2}$ while SLD of the hydrocarbon chain is $-0.36 \cdot 10^{-6}$ $Å^{-2}$ in 40 % D_2O containing buffer. SLD of the buffer with 20 mM Tricine, 10 mM KCl, 10 mM $MgCl_2$, 0.4 M sorbitol with 40 % D_2O concentration is $2.16 \cdot 10^{-6}$ $Å^{-2}$ when 1.07 g/cm^3 is considered for the buffer mass density. Therefore we obtain the mean SLD for the hydrocarbon chain as:

$\overline{\delta_{CH_2}} = \delta_{CH_2} - \delta_{Buffer} = (-0.36 - 2.16) \cdot 10^{-6} Å^{-2} = -2.52 \cdot 10^{-6} Å^{-2}$ and for the headgroup $\overline{\delta_{head}} = -0.49 \cdot 10^{-6} Å^{-2}$. As we are interested in the SLD profile along the membrane normal the SLD values have, however, to be averaged in the membrane plane. As detailed in paragraph 4.2 in BBY the protein area fraction is ~ 80 %, and this part is considered to have no contrast. Therefore we can obtain $\overline{\delta} \approx -0.5 \cdot 10^{-6} Å^{-2}$ for the central region and $\overline{\delta} \approx -0.1 \cdot 10^{-6} Å^{-2}$ for the headgroup region of the BBY membrane.

We have to note that the actual SLD is not constant in the above mentioned region. An example for a DPPC bilayer in D_2O is shown in Figure 34.

For our calculations we used an approximation, based on Fig. 6 in (Kucerka et al. 2004). (See Figure 35 A; in the case of buffer with 40 % D_2O m and h values are negative.) The connection between the scattering length density profile and the measured scattering intensity is provided by (Pabst et al. 2000):

$$I(Q) \sim \frac{\left\langle |f(Q)|^2 s(Q) \right\rangle}{q^2}, \qquad \textbf{5.6}$$

where I(Q) is the intensity scattered from a finite stack of unoriented bilayers and f(Q) is its form factor:

$$f(Q) = \int \rho(z) \exp(iQz) dz. \qquad \textbf{5.7}$$

$\langle\ \rangle$ denotes the average over the bilayer fluctuation, which we neglect in our approximation, due to the lack of complementary information.

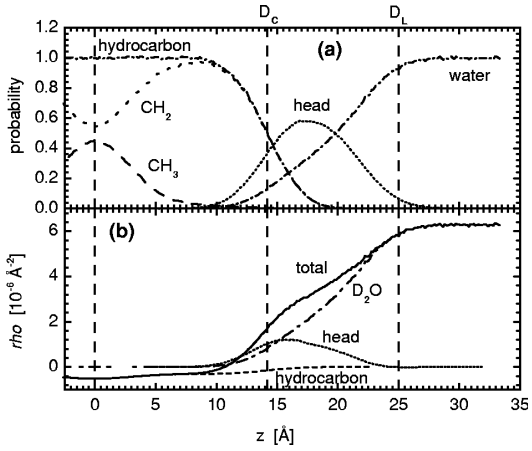

Figure 34: Volume fractions of different lipid components and D_2O for DPPC bilayers (a), and calculated neutron SLD values (copied from (Kucerka et al. 2004)).

In a buffer with 40 % D_2O content, i.e. when the proteins are matched out, the SLD profile of the stacked bilayers possess a translation symmetry. This symmetry is lost when we modify the model for other D_2O concentrations, since the transmembrane proteins are incorporated in opposite directions for the two membranes. For this reason we consider the basic unit of the calculation as two parallel rigid lipid bilayers (see Figure 35 B).

With such a definition of the unit cell in equation 5.6 $s(Q)$ becomes 1. Introducing the form factor of the membrane pair:

$$f(Q)=\left\{\frac{2h}{d\cdot Q^2}\cdot\{\cos(Qc)-\cos(Q(c+d))\}+\frac{2(m-h)}{Q}\sin(Qc)\right\}\cdot 2\cos(rQ),$$ into equation 5.6 we obtain:

$$I(Q)\sim\frac{\left[\left\{\frac{2h}{d\cdot Q^2}\cdot\{\cos(Qc)-\cos(Q(c+d))\}+\frac{2(m-h)}{Q}\sin(Qc)\right\}\cdot 2\cos(rQ)\right]^2}{Q^2} \quad \textbf{5.8}$$

and after substitution of the calculated contrast parameters:

$$I(Q)\sim\frac{\left[\left\{\frac{-0.2\cdot 10^{-6}A^{-2}}{d\cdot Q^2}\{\cos(Qc)-\cos(Q(c+d))\}+\frac{-0.8\cdot 10^{-6}A^{-2}}{Q}\sin(Qc)\right\}2\cos(rQ)\right]^2}{Q^2} \quad \textbf{5.9}$$

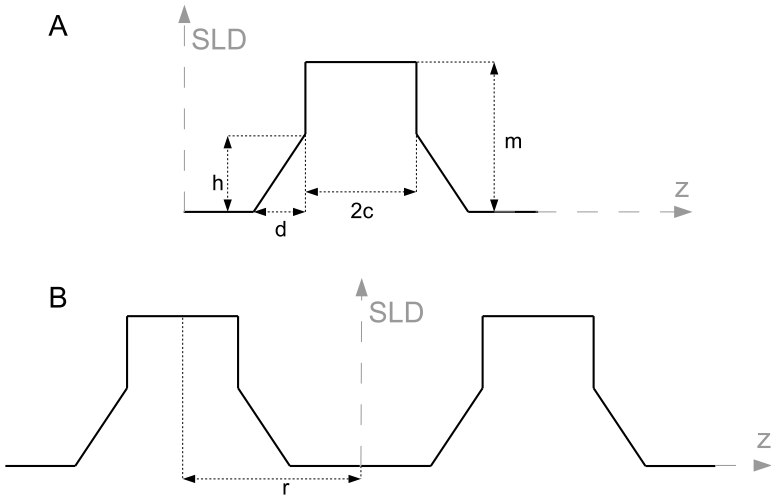

Figure 35: SLD profile of a single bilayer (based on (Kucerka et al. 2004)) (A) and of a pair of stacked parallel bilayers (B). h: averaged SLD of the headgroups relative to the buffer, m: averaged SLD of the hydrocarbon chain relative to the buffer, d: average headgroup thickness, c: average hydrocarbon chain length, r: half of the distance between the centers of the two bilayers.

Since the collected data (see Figure 33 A) has a low signal to noise ratio we are obliged to fix some of the parameters in equation 5.9. The membrane thickness 2(c+d) is approximately 40 Å (Daum et al. 2010), i.e. a lipid layer corresponds to a thickness of ~ 20 Å, which is in close accordance with parameters obtained for DGDG. The main bilayer forming lipid in the membrane (DGDG), has an ~ 8 Å thick headgroup region and a ~ 13 Å thick hydrocarbon region (McDaniel 1988). Therefore in our calculations d = 8 Å, c = 13 Å.

5.2.6 Comparison of Model Calculations with the Experimental Curves

Data fitting was performed by the SansView program from the DANSE project (Alina et al. 2011), which allowed to take into account the instrumental resolution (provided by the Grasp data treatment program). The experimental results in the Q range 0.029– 0.27 $Å^{-1}$ along with the fitted curve is shown in Figure 36. No perfect fit could be achieved with the applied model. The fitting provides $r = (33.1 \pm 0.28)\,Å$ corresponding to a distance of $(66.2 \pm 0.56)\,Å$ between the centers of the lipid bilayers ($2r$).

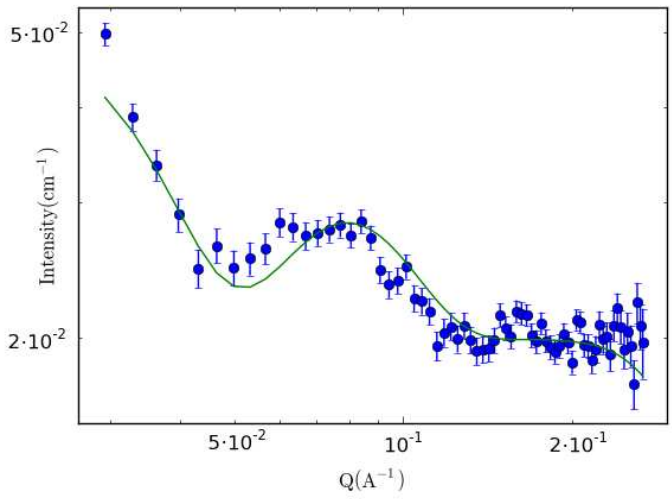

Figure 36: Radially averaged SANS scattering curve of BBY (data points, blue) suspended in buffers containing 20 mM Tricine, 10 mM KCl, 10 mM $MgCl_2$, 0.4 M sorbitol with 40 % D_2O concentration, and the calculated scattering profile (green curve) based on equation 5.9 Intensity is expressed in absolute value for the proper comparison of measurements performed at different Q ranges.

The experimental results in the Q range 0.0089 – 0.0833 Å^{-1} along with the fitted curve is shown in Figure 37. The fitting provides $r = (37.6 \pm 0.92)\,\mathring{A}$ corresponding to a distance of $(75.2 \pm 1.84)\,\mathring{A}$ between the centers of the lipid bilayers.

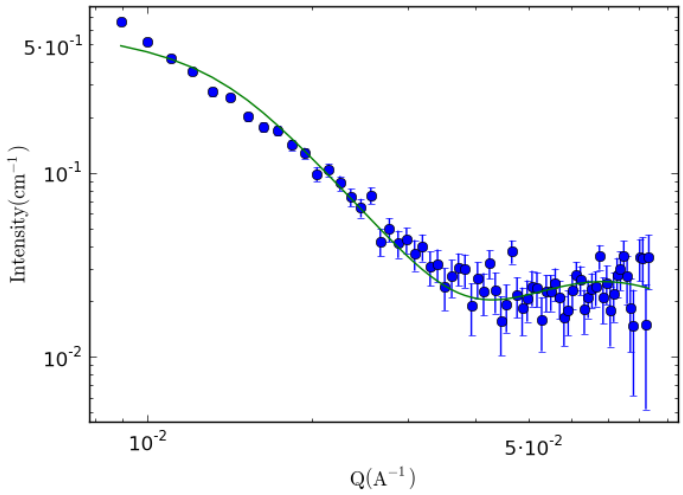

Figure 37: Radially averaged SANS scattering curve of BBY (data points, blue) suspended in buffers containing 20 mM Tricine, 10 mM KCl, 10 mM $MgCl_2$, 0.4 M sorbitol with 40 % D_2O concentration, and the calculated scattering profile (green curve) based on equation 5.9 (green).

Simultaneous fitting of the model in the whole Q range provides $r = (35.3 \pm 0.48)\,\mathring{A}$ corresponding to a distance of $(70.6 \pm 0.96)\,\mathring{A}$ between the centers of the lipid bilayers.

It is clear from the results that the proposed model cannot account for every feature of the measured scattering curves, and based on the model we cannot determine the accurate values of the distance between the membrane pairs. Nevertheless we can state, that change in the distance between the center of the lipid bilayers is reflected in the shift of the position of the peak at Q ~ 0.07 Å^{-1} as shown in Figure 38, thus change in the peak position provides qualitative information about shrinkage or swelling of the membrane pairs.

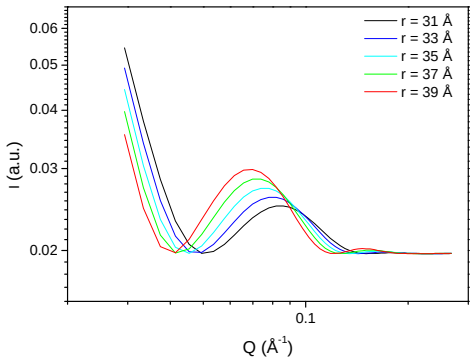

Figure 38: Evolution of the function described in equation 5.9 upon varying the values of r, when the parameters are taken from the fitting results in Figure 36.

We have to note that even slight deviation of the proteins' scattering length density in the BBY from the suspending medium can result in significant changes in the average SLD profile presented in Figure 35, due to the high protein content of the membrane. Consideration of this effect and data fitting with other models is underway. We are also planning to repeat the measurements with better signal to noise ratio.

In Chapter 5 typical SANS signals of plant thylakoid membranes were presented. We showed how the obtained radially averaged scattering curves provide information about the periodicity of the stroma thylakoid membranes. We demonstrated that SANS, due to its noninvasive nature can conveniently be used to investigate the effect of different environmental parameters on this periodic structure. We discussed the lack of the first order Bragg peak arising from the periodicity of granum thylakoid membranes on the radially averaged scattering curves. We proposed that a characteristic feature of the observed curves carries information about the arrangement of the adjacent membrane pairs in the granum and supported this interpretation by comparing the SANS signal of the thylakoid membranes with that of photosystem II (BBY) membrane fragments. In the following chapter we show how some of these structural parameters vary during the photosynthetic functions of the thylakoid membranes.

6. Light-induced Reorganizations of Plant Thylakoid Membranes

The structure of the thylakoid membranes can be influenced by illumination as was mentioned in 3.1.3. The effect of illumination on the thylakoid structure in isolated spinach chloroplasts was investigated with light scattering and electron microscopy (Deamer et al. 1967; Murakami and Packer 1970). Light scattering revealed thylakoid membrane reorganization upon illumination and provided the possibility also for the kinetic investigation of this phenomenon. Light scattering, however, does not contain direct information about the nature of the reorganization. Electron microscope images taken by Murakami and Packer from spinach chloroplasts are shown in Figure 39 revealing a tighter ordering of the thylakoid membranes in the grana region (Murakami and Packer 1970). Based on microdensitometric studies performed on the same samples it was proposed that the observed 32 % decrease in the spacing of the thylakoid membranes is accompanied by a 21 % decrease in the thickness of the thylakoid vesicle.

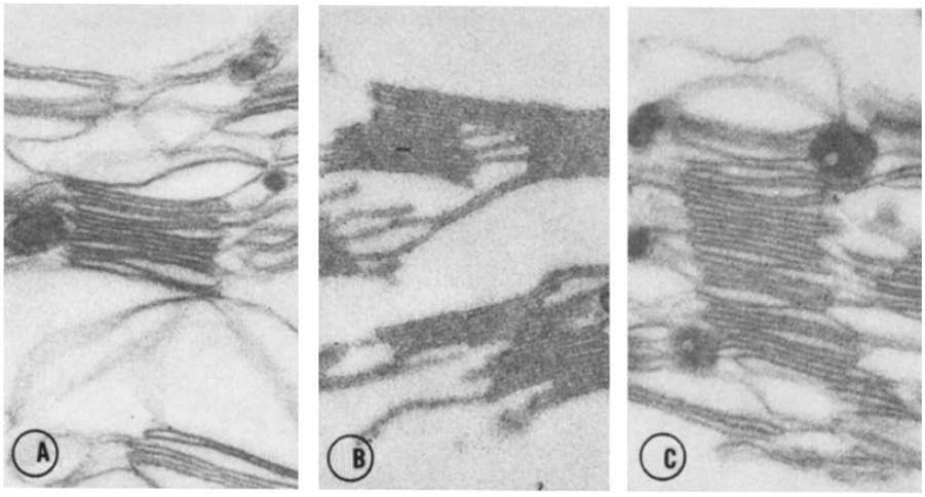

Figure 39: Light-induced changes in the ultrastructure of the thylakoid membrane system in isolated spinach chloroplasts, suspended in 100 mM NaCl 20 μM PMA (phenylmercuric acetate), pH 7.8 medium (taken from (Murakami and Packer 1970)). The electron micrographs were taken on samples, chemically fixed and stained before illumination (A), after 3 min illumination (B), after 4 min in the dark following illumination (C).

Electron microscopy studies provide direct information about structural parameters of the thylakoids, but can be influenced by artifacts resulting from the fixation, and do not provide information about the entire population of the investigated sample.

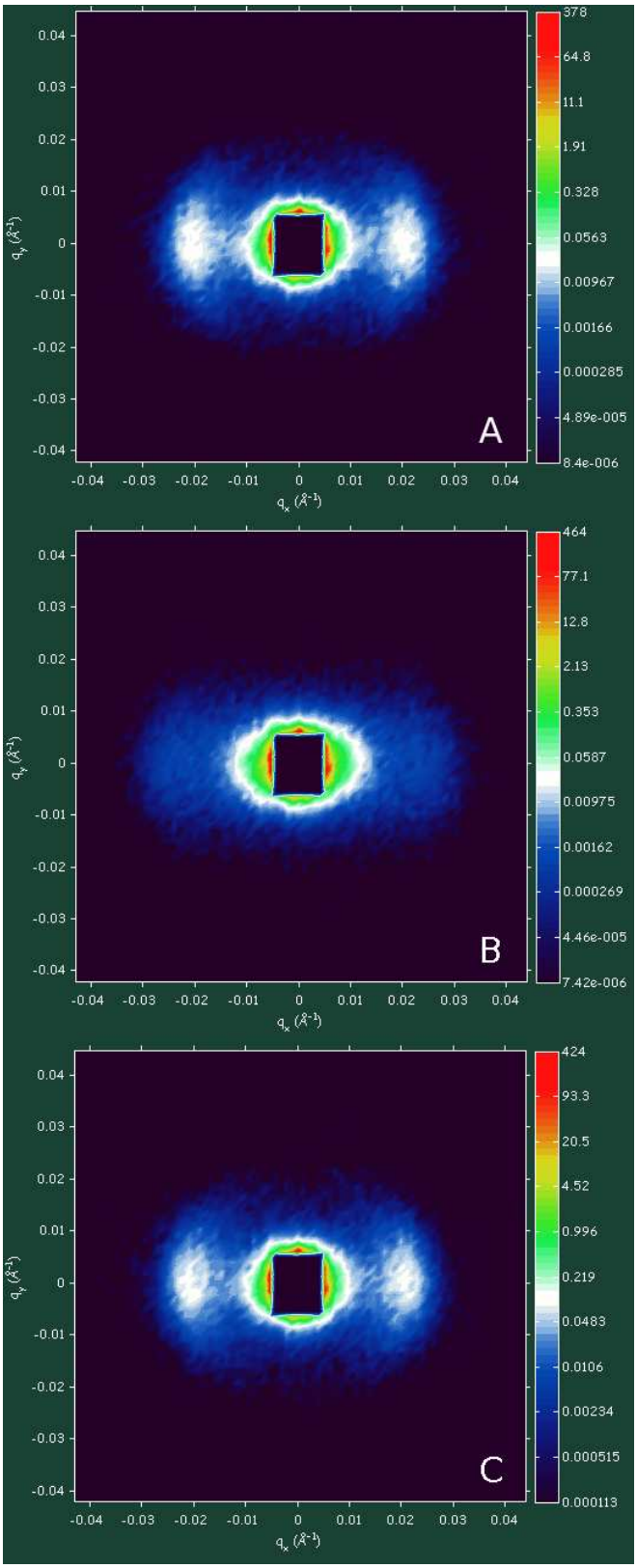

Figure 40: Effect of illumination on the two-dimensional SANS profile of magnetically oriented spinach thylakoid membranes, recorded with the 2D detector of the D22 SANS instrument. Sample-to-detector distance, SD = 8 m, collimation, col = 8 m, λ = 6 Å. Only part of the detector image is presented (Q-range: 0.0057-0.068 Å^{-1}); integration time is 20 s. Dark-adapted state (A), after illumination with white light of 1700 µmol photons m^{-2} s^{-1} photon flux density for 5 min (B), after 5 min light and 5 min dark (C). Colors are representing the differential scattering cross-section values in cm^{-1} in a logarithmic scale. Measurements were performed in the presence of 100 µM PMS.

SANS, as a noninvasive technique, capable of providing information about the periodical structure of biological membranes, is of great interest in the investigation of the light-induced changes of thylakoid membranes. Studies on this phenomenon were started before I joined the project, and the first results are described in the Ph.D. thesis of Jens Kai Holm (2004). Here I present the continuation of this work, in which we were able to carry out time-resolved measurements on the D22 SANS instrument at the ILL. By capitalizing on the high intensity neutron beam available at this instrument we could obtain more precise RD values and could also monitor the time course of the light-induced changes in the stroma thylakoid RD.

Reversible light-induced reorganization of the stroma thylakoids (in the presence of 100 μM PMS, i.e. during the functioning of the PSI cycle) is already observable in two-dimensional scattering profiles (see Figure 40).

Radially averaged scattering curves, corresponding to Figure 40 are presented in Figure 41. Upon illumination, the curves are significantly changed. The center position of the Bragg peak, connected to the periodicity of stroma thylakoids (see paragraph 4.4.2), is shifted towards higher Q values, and the peak intensity is decreased. The light-induced changes were found to be almost fully reversible.

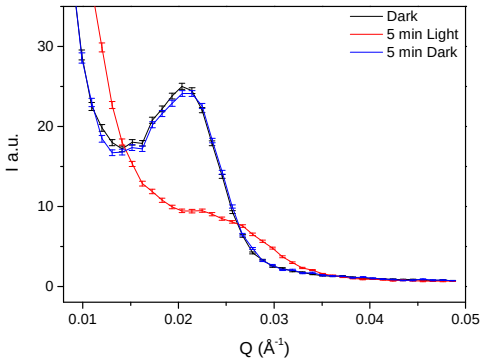

Figure 41: Effect of illumination with white light of 1700 μmol photons m^{-2} s^{-1} photon flux density on the spinach thylakoid membranes in the presence of 100 μM PMS.

We performed comparative experiments in order to test if the light-induced changes – due to some not known reason – can be observed only in magnetically oriented samples. As can be seen in Figure 42 similar light-induced changes can be observed also in samples where the magnetic orientation is absent. However, due to the significantly

better defined stroma thylakoid related Bragg peaks observed in oriented samples and due to the significantly lower required measuring time, further investigations were performed in the presence of magnetic orientation in all samples amenable for magnetic alignment.

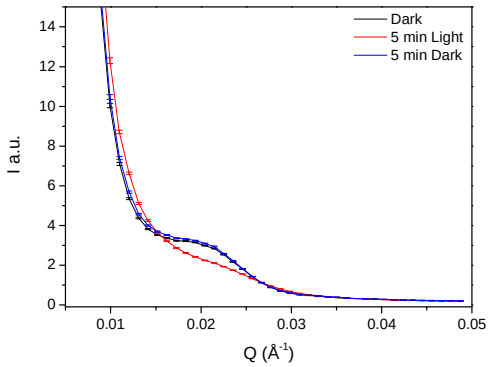

Figure 42: Effect of illumination with white light of 1700 µmol photons m^{-2} s^{-1} photon flux density on unoriented spinach thylakoid membranes in the presence of 100 µM PMS.

6.1 Time Resolved Investigation of the Light-induced Structural Changes of Stroma Thylakoids

During SANS investigation of different structural changes we are able to obtain the required structural information without modifying the tested sample. This allows us to observe the kinetics of the reorganization in the sample. In order to be able to follow the time course of the light-induced structural changes we performed time resolved measurements. The most important experimental parameter, defining the available time resolution is the available neutron flux, which – on the D22 SANS instrument – allowed us to achieve a resolution ranging from 5 min to 2 s. After the experiments, during the data treatment, the individual radially averaged scattering curves were regrouped if it was required to increase the statistical accuracy of the result.

A time parameter is associated with each scattering curve, which is usually defined by the time elapsed between the moment of the last change of the sample environmental parameters (e.g. start or end of illumination) and the moment the scattering data is read out from the detector. The radially averaged scattering curves thus obtained were fitted with the sum of a power function and a Gaussian, as described in paragraph 4.4.2. Each

of the obtained parameters (see equation 4.2) were plotted as a function of the time parameter along with the calculated RD values.

Figure 43 and Figure 44 show the time course of the light-induced changes and of the dark adaptation for isolated spinach thylakoid membranes along with the corresponding Bragg peak components. The latter was calculated by performing the fitting as detailed above and subtracting the resulting power functions from the corresponding scattering curves. The obtained figures better reveal the effect of the illumination on the Bragg peak, i.e. that upon illumination the center position of the peak is shifted towards higher Q values, accompanied with decreasing peak intensity and higher FWHM, and that these changes are reversible in the dark.

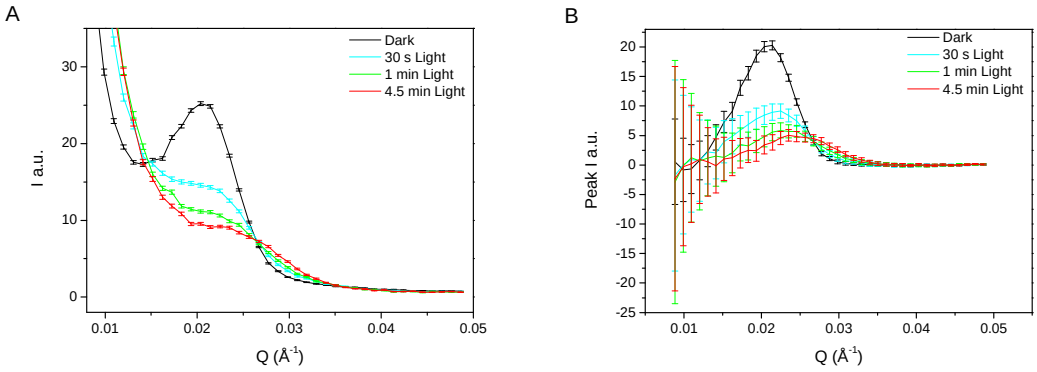

Figure 43: Time course of the radially averaged scattering curves of spinach thylakoid membranes during illumination with white light of 1700 µmol photons m^{-2} s^{-1} photon flux density (A) in the presence of 100 µM PMS. Time course of the scattering curves after subtraction of the fitted power function (B).

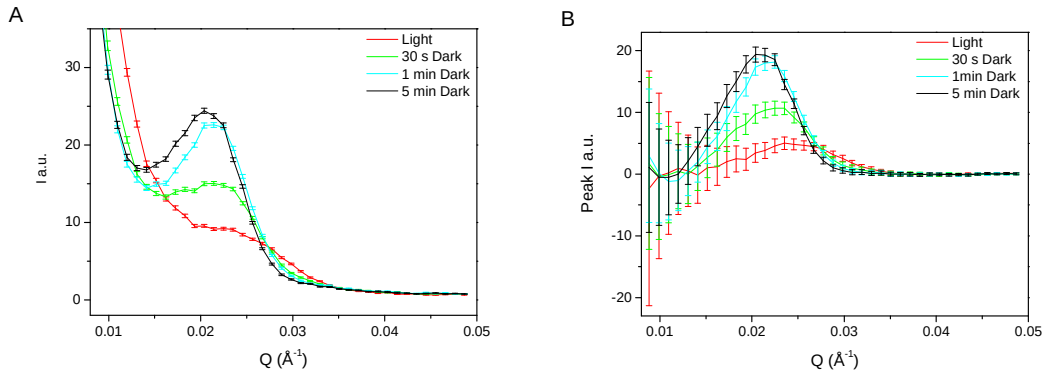

Figure 44: Time course of the radially averaged scattering curves of spinach thylakoid membranes during dark adaptation after a preillumination for 5 min with white light of 1700 µmol photons m^{-2} s^{-1} photon flux density (A) in the presence of 100 µM PMS. Time course of the scattering curves after subtraction of the fitted power function (B).

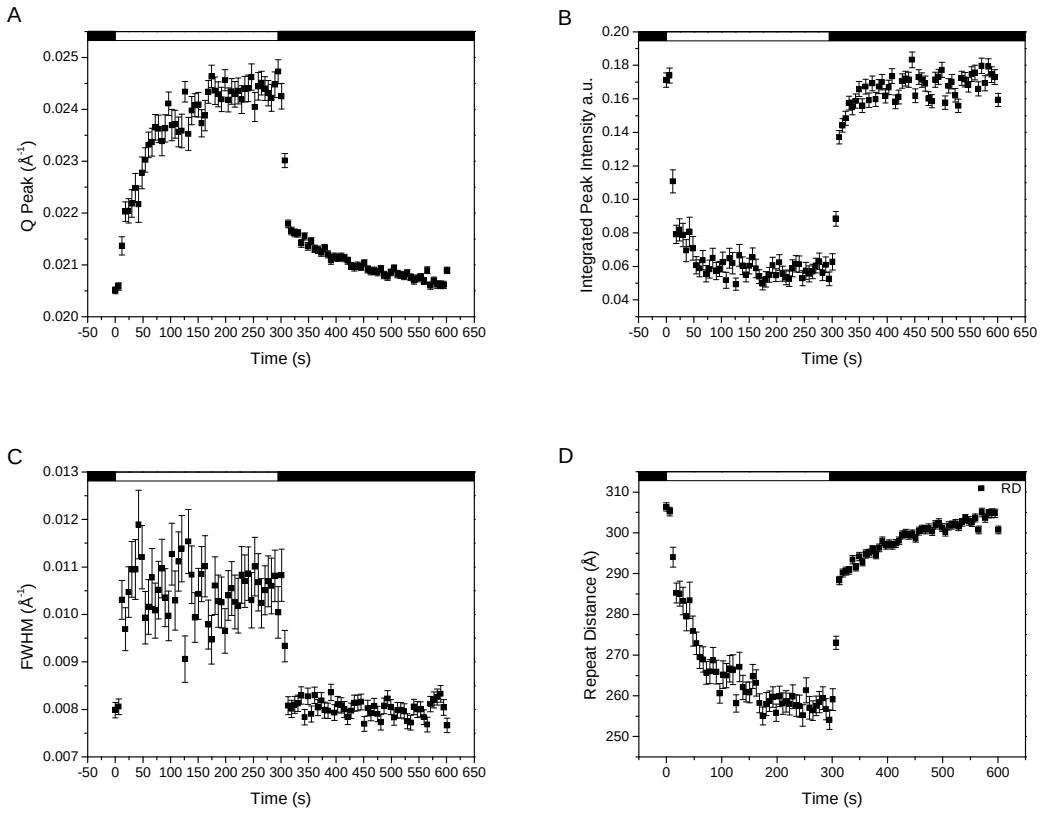

Figure 45: Time course of different fitted parameters: center position (A), integrated intensity (B), FWHM (C) and the corresponding RD values calculated from the center positions (D) of the Bragg peak for the scattering curves obtained during illumination (with white light of 1700 μmol photons m^{-2} s^{-1} photon flux density) and during the dark-recovery of the sample, isolated spinach thylakoid membranes (in the presence of 100 μM PMS).

The time course of some of the fitted parameters (center position, intensity and FWHM of the Bragg-peak and calculated RD) is presented in Figure 45. These figures demonstrate better the light-induced shrinkage of the stroma thylakoid membranes which is accompanied by a decrease in the long and short-range order of the stroma thylakoids, as indicated by the increased FWHM and the decrease in intensity. For the proper interpretation of the obtained FWHM values, we investigated the resolution function of the instrument as a function of Q, which is provided by the Grasp data treatment program, based on the equation (Grillo 2008):

$$\Delta Q^2 = Q^2\left(\frac{1}{2\sqrt{2\ln 2}}\frac{\Delta\lambda}{\lambda}\right)^2 + \left[\left(\frac{4\pi}{\lambda}\right)^2 - Q^2\right]\Delta\theta^2, \qquad \textbf{6.1}$$

where in our experiments $\frac{\Delta\lambda}{\lambda} = 0.1$, and $\Delta\theta$ is estimated by Grasp from the attenuated direct beam measurement, based on the equation (Grillo 2008): $\Delta Q(Q=0) = \left(\frac{4\pi}{\lambda}\right)\Delta\theta$. Estimated FWHM values for the instrument resolution are shown in Figure 46.

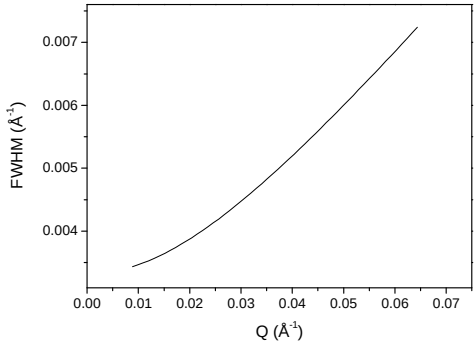

Figure 46: Q dependency of the calculated instrument resolution.

Figure 46 reveals that in the Q range 0.02 – 0.025 Å^{-1}, i.e. where the center position of the stroma Bragg peak can be found, the calculated FWHM is in the range of 0.0038 – 0.0042 Å^{-1}. We have to note that the shape of the direct beam is asymmetric in our experiments – being slightly wider in the vertical direction than in the horizontal direction. Therefore, when radial averaging is applied around the horizontal axis of the detector the FWHM is expected to be shifted to lower values. Furthermore, from the low Q dependency of the instrument resolution in the range of the possible Bragg peak center positions we can conclude that the increased FWHM of the Bragg peak cannot be the result of the shift of the Bragg peak alone; on the contrary, it reveals a decrease in the order of the stroma thylakoids. The origin of this phenomenon is yet unknown. This conclusion on the light-induced desorganization of the membrane system is supported by data in Figure 47, where normalized peaks are presented together with the instrument resolution (similar as described in (Demé et al. 2002)), allowing a better visualization of the widening of the Bragg peak during illumination.

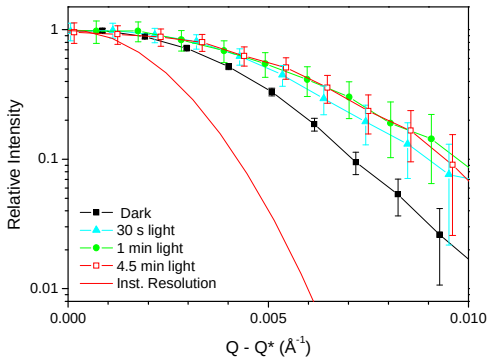

Figure 47: Bragg peak broadening in normalized representation, together with the calculated instrument resolution at Q=0.0215 $Å^{-1}$. Bragg peak curves are created from Figure 43 B via dividing by the maximum value of the fitted Gaussians and shifting the curves to be centered around 0.

6.2 Light-intensity Dependency of the Structural Changes of Stroma Thylakoids

The effect of the illumination on the structural rearrangements (observed by CD) was earlier found to be light intensity dependent (Barzda et al. 1996). As shown in Figure 48 the intensity and rate of the light-induced changes of the CD signal at 510 nm depends strongly on the illumination intensity. (For better comparison with the SANS measurements we note, that according to (Buschmann 2001) at a wavelength of 530 nm, at about the mean wavelength of photosynthetically active sunlight, 1 W m^{-2} corresponds to approximately 4.4 µmol photons m^{-2} s^{-1}.)

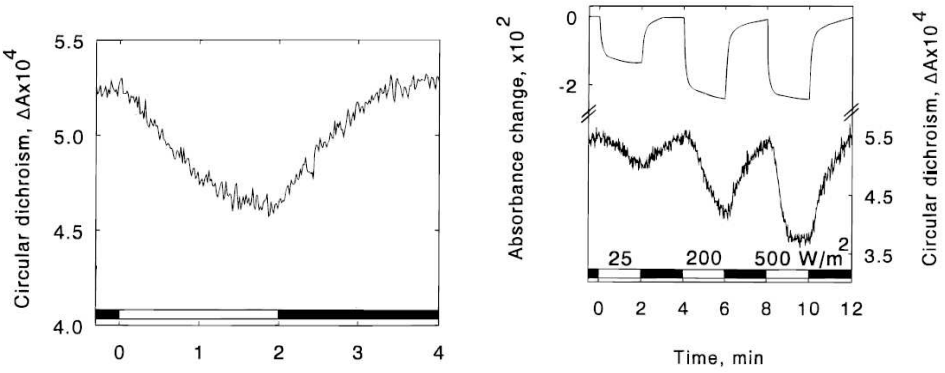

Figure 48: Light-induced changes in the CD at 510 nm of isolated pea thylakoid membranes suspended in 30 mM Tricine (pH 7.8) 330 mM sorbitol and 5 mM $MgCl_2$ (left). Black and white horizontal bars indicate dark and light (500 W m^{-2}) periods. Light-induced changes in the CD at 510 nm (lower curves) and absorbance changes of the pH indicator dye, neural red at 553 nm (upper curve) at three different intensities of the exciting light. Figures copied from (Barzda et al. 1996).

This CD change originates from changes in the long-range chiral order of the chromophores (and of the pigment-protein complexes) in granal thylakoid membranes, an overall structural rearrangement of the thylakoid membranes without affecting the short-range interactions (and the molecular architecture of the constituent complexes) of the membranes (Garab and van Amerongen 2009).

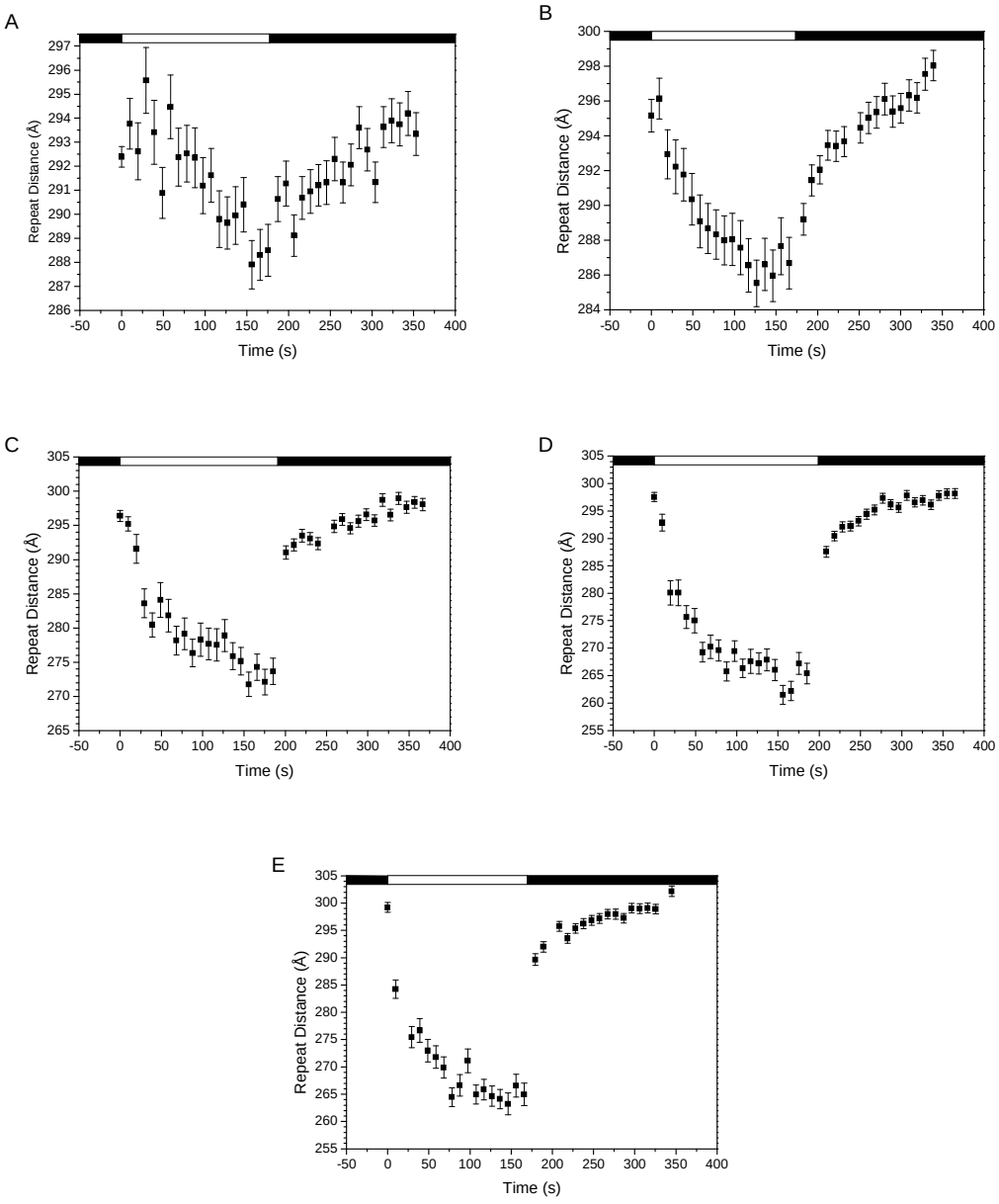

Figure 49: Time courses of the calculated stroma thylakoid RD values in isolated spinach thylakoid membranes in the presence of 100 µM PMS during illumination (with white light of 150 (A), 330 (B), 650 (C), 1200 (D) and 1700 (E) µmol photons m^{-2} s^{-1} photon flux density) and their dark recoveries.

Here we present SANS results with a sub minute time resolution about the light intensity dependency of the light-induced changes in thylakoid membranes.

Time course of the calculated stroma RD changes during the illumination and the consecutive dark period (Figure 49) reveal that increasing light intensities result in increased repeat distance changes and in significantly different kinetics. During these experiments the data acquisition time was 1 s which – including a ~ 1 s data storage time – results in a ~ 2 s time resolution. For a better representation we summed the radially averaged scattering curves in groups of 5, to obtain the curves in Figure 49, and performed the curve fitting and calculation of the RD values on these curves. The RD changes during the ~ 3 min light or dark time intervals were calculated by averaging two consecutive light-dark cycles for each light intensity (cf. Table 9).

Table 9: Calculated RD changes in isolated spinach thylakoid membranes during illumination with different light intensities and in the dark following the preillumination.

		Illumination intensity [ ]= μmol photons m^{-2} s^{-1} photon flux density				
		150	330	650	1200	1700
RD change [ ]= Å	Illumination	-5 ± 1	-11 ± 1	-22 ± 1	-33 ± 1	-37 ± 2
	Dark adaptation	6 ± 1	11 ± 1	23 ± 1	33 ± 1	37 ± 2

As shown e.g. in Figure 49 E there are major RD changes, especially in the dark adaptation period during ~ 10 s. Therefore we used the original ~ 2 s time resolution for the investigation of the kinetics of the RD changes. Illumination with light intensities of 330 μmol photons m^{-2} s^{-1} photon flux density and higher appears to possess an equilibrium RD. We fitted the RD(time) function with an exponential function, for which the characteristic time constants are presented in Table 10. We observed that increasing light intensities result in faster kinetics of the light-induced RD changes. This result is in accordance with the one presented in (Barzda et al. 1996), where the initial rate of the light-induced CD changes (cf. Figure 48) was found to increase with rising light intensity, albeit the experiments of Brazda et al. were performed during the functioning of the linear electron transport (i.e. in the presence of ferricyanide).

Dark adaptation after illumination with light intensities of 650 μmol photons m^{-2} s^{-1} photon flux density and higher appears to induce RD changes with two significantly different time constants as shown in Table 10.

Table 10: Kinetic parameters determined by curve fitting from the time courses of the light-induced RD changes during illumination with different light intensities and in the dark following the preillumination period.

			Illumination intensity [ ]= μmol m^{-2} s^{-1} photon flux density			
			330	650	1200	1700
Illumination	Decay time constant [ ]=s		38 ± 6	35 ± 4	27 ± 2	19 ± 1
Dark adaptation	Rise time constant [ ]=s Relative contribution	fast	-	2.4 ± 0.9 (56 %)	1.9 ± 0.4 (67 %)	0.8 ± 0.4 (63 %)
		slow	41 ± 4	98 ± 39 (44 %)	64 ± 13 (33 %)	155 ± 85 (37 %)

We have to note that, unlike the static structural parameters, the light-induced structural changes of the stroma thylakoids vary significantly between different batches. Therefore in our experiments it was crucial to perform the comparative measurements on the same sample or samples from the same batch. Samples from the same batch investigated with few hours time difference also reveal, that during storage RD tended to increase by several percent. This increase was accelerated when illumination was applied.

6.3 Functional Basis of the Observed Light-induced Structural Changes

We performed comparative experiments on isolated thylakoid membranes in the presence of different reagents, during illumination with fixed (1700 μmol photons m^{-2} s^{-1}) photon flux density in order to reveal the functional origin of the observed structural changes. Light-induced structural changes, presented in paragraphs 6.1 and 6.2 were observed in the presence of 100 μM PMS, i.e. during the functioning of the PSI cycle.

We investigated the influence of 10 μM DCMU (which inhibits the electron transport between Q_A and Q_B) and 1 mM ascorbate (which serves as a reducing agent) on these changes. The results (see Figure 50) show that the RD changes can be elicited

by PSI cyclic electron transport alone. DCMU, however, slightly influences the reversibility of the structural changes. While under the control conditions we observed slight increase in the stroma RD with time and during consecutive illumination cycles, in the presence of DCMU the dark state equilibrium RD decreased with ~ 10 Å as shown in the first (Figure 50 A) and second (Figure 50 B) light dark cycle.

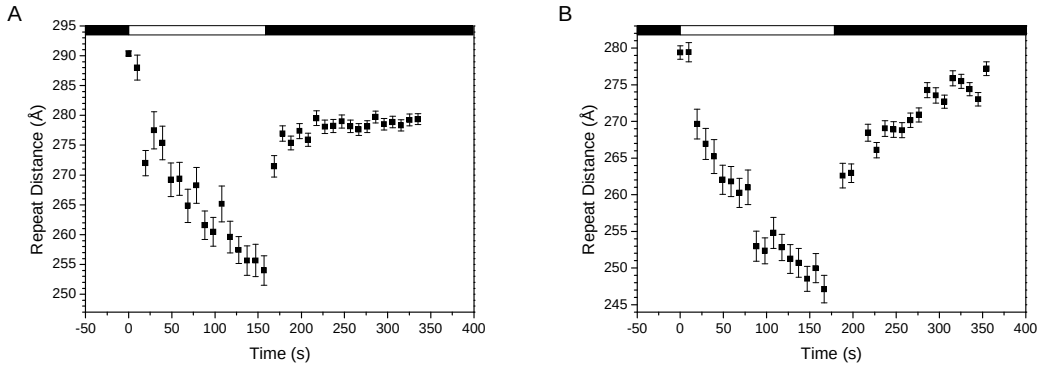

Figure 50: Time courses of calculated stroma thylakoid RD values during illumination with white light of 1700 μmol photons m^{-2} s^{-1} photon flux density or dark adaptation of the isolated spinach thylakoid membranes in the presence of 100 μM PMS, 10 μM DCMU and 1 mM ascorbate during the first (A) and the second (B) light-dark cycle.

As a complementary experiment, we also investigated the influence of far-red illumination (we mounted a long-pass (cut-off) filter with a threshold of 690 nm between the light guide and the sample), where only the PSI is expected to be functioning. The results (see Figure 51) confirm that the RD changes can be elicited by PSI cyclic electron transport alone. In this experiment, unlike in the presence of DCMU, full reversibility was observed, which suggests that in the case of DCMU the shift in the dark equilibrium following illumination was a specific effect of the reagent, independent of the non-functioning PSII.

A correlation between the transmembrane ΔpH and the light-induced shrinkage of granum thylakoids was reported earlier (Murakami and Packer 1970). We repeated the above described experiments (100 μM PMS, 10 μM DCMU and 1 mM ascorbate) in the presence of 2.5 μM nigericin. The influence of this uncoupler on the light-induced changes is clearly visible on the radially averaged scattering curves (Figure 52), and the time course of the calculated stroma repeat distance (Figure 53) confirms that light-

induced structural changes of the stroma thylakoids are negligible when the transmembrane ΔpH is abolished.

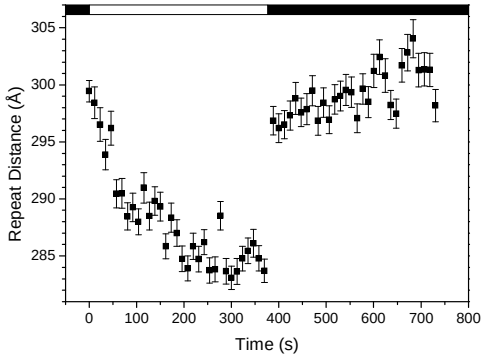

Figure 51: Time course of calculated stroma thylakoid RD values during illumination with far-red light ($\lambda \geq 690\ nm$) or dark adaptation of the isolated spinach thylakoid membranes in the presence of 100 μM PMS.

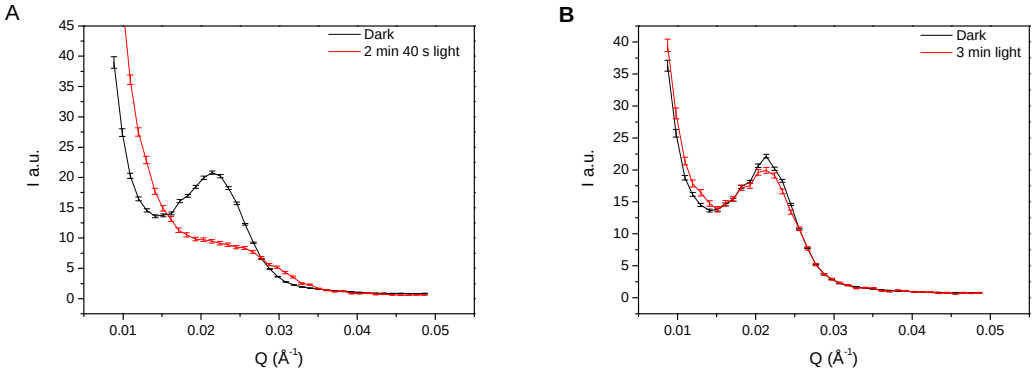

Figure 52: Effect of illumination with white light of 1700 μmol photons m^{-2} s^{-1} photon flux density on the spinach thylakoid membranes in the presence of 100 μM PMS, 10 μM DCMU and 1 mM ascorbate, in the absence (A) and presence (B) of 2.5 μM nigericin.

We also investigated the light-induced changes in the SANS signal arising from the stroma thylakoids – during the operation of the linear electron transport chain, from H_2O to methylviologen or ferricyanide (functioning as terminal electron acceptors at the acceptor side of PSI). In the presence of 1 mM methylviologen we can observe a small shift of the Bragg peak already on the radially averaged scattering curves (Figure 54 A) and the calculated RD values also reveal a shrinkage of the stroma thylakoids (Figure 54 B), during illumination, albeit to a significantly lower extent than in the case of PMS. In the presence of 5 mM ferricyanide we can observe only a small decrease in the Bragg

peak intensity on the radially averaged scattering curves (Figure 55 A) and the calculated RDs do not show any significant change during illumination (Figure 55 B).

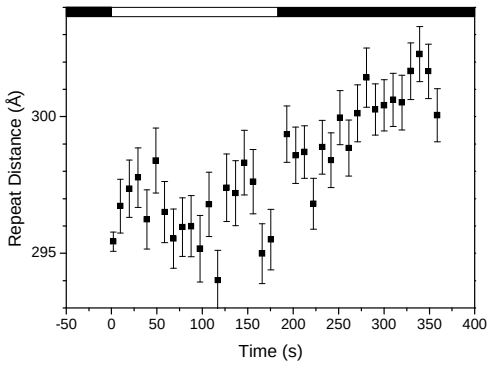

Figure 53: Time course of calculated stroma thylakoid RD values during illumination with white light of 1700 µmol photons m^{-2} s^{-1} photon flux density and in the dark following the preillumination of isolated spinach thylakoid membranes in the presence of 100 µM PMS, 10 µM DCMU, 1 mM ascorbate and 2.5 µM nigericin.

These data show that during the balanced operation of the two photosystems, and despite the generation of the transmembrane ΔpH, the stroma membranes undergo only relatively small (for methylviologen) reorganizations in their multilamellar membrane ultrastructure or the reorganizations are not observable at all (for ferricyanide).

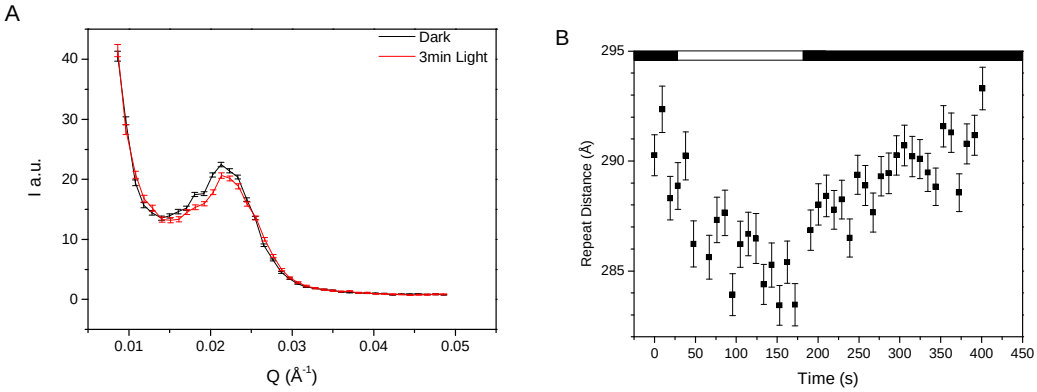

Figure 54: Effect of illumination with white light of 1700 µmol photons m^{-2} s^{-1} photon flux density on the radially averaged scattering curves of spinach thylakoid membranes in the presence of 1 mM methylviologen (A). Time course of calculated stroma thylakoid RD values (B).

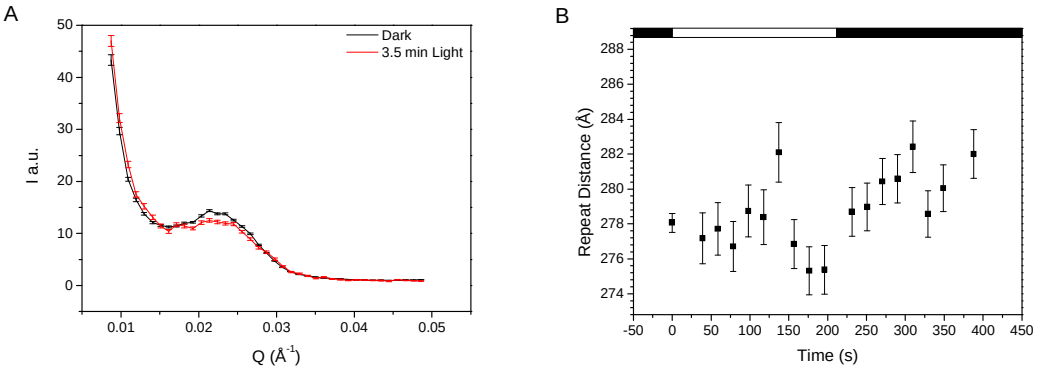

Figure 55: Effect of illumination with white light of 1200 µmol photons m^{-2} s^{-1} photon flux density on the radially averaged scattering curves of spinach thylakoid membranes in the presence of 5 mM ferricyanide (A). Time course of calculated stroma thylakoid RD values (B).

In Chapter 6 we demonstrated that SANS allows the determination of RDs of the stroma thylakoids in intact thylakoid membranes isolated from plants and to monitor their time-resolved reorganization during photosynthesis, an information hitherto not available. Our data provide clear evidence for the occurrence of fully reversible membrane reorganization during the operation of PSI cyclic electron transport, and shows its correlation with the transmembrane ΔpH generated. In the following chapter we show that this technique can also be applied to the investigation of living photosynthetic organisms.

7. Light-induced Reorganizations of Thylakoid Membranes in Lower Organisms

7.1 The Diatom *Phaeodactylum tricornutum*

Diatoms have a dominant role in the energy balance of the biosphere, since they provide ~ 25 % of the primary photosynthetic production on Earth (Lavaud et al. 2007). Their efficient carbon-dioxide sequestration into the deep water layers contributes significantly to the regulation of the atmospheric carbon-dioxide concentration (Falkowski et al. 1998). Furthermore they are widely involved in the biochemical cycles of nitrogen, phosphorus and silicon (Wilhelm et al. 2006).

Intricately patterned, silicified cell walls of diatoms represent one of the most fascinating examples of biominerals (biologically formed inorganic materials) (Poulsen et al. 2003), which on the other hand, render the ambient silicate concentration to be a limiting factor to the growth of diatoms (Egge and Aksnes 1992). In our studies we used *Phaeodactylum tricornutum*, a diatom which lacks the silicon requirement for its growth (Nelson et al. 1984).

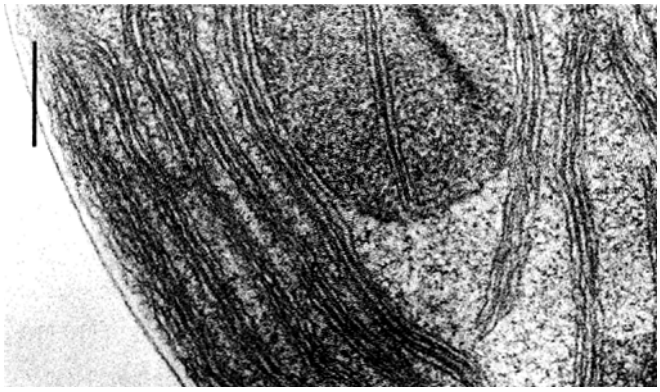

Figure 56: Part of chloroplast cross-section of *Phaeodactylum tricornutum* (copied from (Pyszniak and Gibbs 1992)) with a bar of 0.2 μm. The organization of the thylakoids into bands of three loosely appressed thylakoids is clearly visible.

Diatoms possess a chloroplast envelope (with four membranes) in which the thylakoid membranes, unlike in higher plants, are not differentiated into stroma and grana thylakoids (Lepetit et al. 2007). In *Phaeodactylum tricornutum* the thylakoids are organized into bands of three appressed thylakoids (see Figure 56) (Pyszniak and Gibbs 1992). Each of the thylakoid membranes contains PSII and PSI and fucoxanthin-chlorophyll proteins (FCPs). The latter, the light harvesting antenna complexes of

diatoms show significant homologies to the LHC of plants (Lepetit et al. 2007), however, they possess considerably smaller loop segments (Eppard and Rhiel 1998; Wilhelm et al. 2006) than LHCII.

Diatoms are known to be able to survive large fluctuations in light intensity in mixing waters (Wagner et al. 2006). When a photosynthetic organism experiences extreme and sudden changes in the environmental conditions the structural flexibility is thought to be crucial in the regulation of the photoprotective mechanisms. The investigation of the structural and supramolecular changes is particularly important to obtain a complete picture of the protective mechanisms against surplus light.

Intact *P. tricornutum* cells were shown to exhibit an intense, broad polymer and salt induced (psi)-type CD band with a maximum at around (+)698 nm (see Figure 57), which originates from chirally organized macrodomains of the pigment-protein complexes (Szabó et al. 2008). The results of Szabó and coworkers reveal that these macroassemblies exhibit substantial structural flexibility upon changes in different environmental conditions such as temperature, illumination or osmotic pressure. The psi-type CD in *P. tricornutum* has been proposed to be associated with the multilamellar organization of the thylakoid membrane system. In order to confirm this correlation, and to obtain direct structural information about the organization of thylakoid membranes in living diatoms we performed SANS experiments on *P. tricornutum* cells.

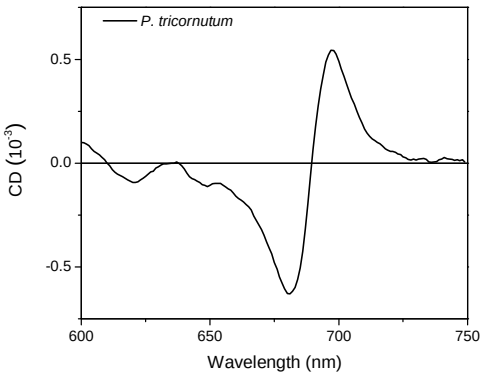

Figure 57: CD spectra of intact *P. tricornutum* cells. The CD measurements were performed as described in (Szabó et al. 2008). Courtesy of Dr. Milán Szabó.

7.1.1 SANS Signals

As pointed out above, the (+)698 nm CD band has been proposed to originate from the multilamellar organization of the membranes. A membrane system with multilamellar organization and well-defined lamellar order can display a SANS profile containing a Bragg peak that is characteristic of the RD of the membranes. Indeed, two dimensional small-angle neutron scattering profiles of suspensions of randomly oriented living *Phaeodactylum tricornutum* cells show two characteristic diffraction rings in the investigated Q range of 0.008 – 0.09 $Å^{-1}$ as shown in Figure 58.

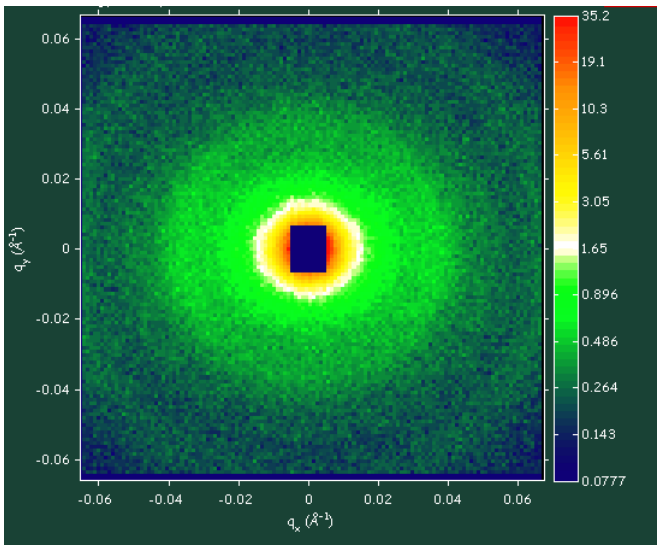

Figure 58: Scattering profile of thylakoid membranes in *Phaeodactylum tricornutum* with two clearly visible diffraction rings, recorded with the 2D detector of the D22 SANS instrument. Sample-to-detector distance, SD = 8 m, collimation, col = 8 m, λ = 6 Å. Corresponding instrumental and buffer background measurements are subtracted, the results are corrected for detector efficiency. Colors are representing the differential scattering cross-section values in cm^{-1} in a logarithmic scale.

Radially averaged SANS curves of *Phaeodactylum tricornutum* cells are shown in Figure 59, revealing two characteristic peaks in the investigated Q-region, for which the interpretation is as follows. The peak at ~ 0.037 $Å^{-1}$ can be considered as a first order Bragg peak. For the second peak at ~ 0.065 $Å^{-1}$ we propose a similar interpretation as discussed for granum thylakoids, i.e. that it originates from paired membranes of adjacent thylakoids. However, in the case of *Phaeodactylum tricornutum* we did not have a model system available to provide experimental proof for this interpretation, such as the BBY for granum thylakoids.

During the extraction of the different peak positions from the experimental scattering curves, we encountered the following problems. A universal fitting method was required which can be applied for all the different batches under different environmental conditions for a proper comparison. We tried to fit the curves corresponding to different samples by the sum of a power function and two Gaussians. As shown in Figure 59 this method was found to be inadequate, probably due to the presence of an ill-defined feature in some of the scattering curves at ~ 0.052 $Å^{-1}$. The involvement of a third peak in the fitting curve, however, rendered the fitting procedure unstable. Therefore, separate fittings of the low and high Q regions were chosen. The low Q region was fitted with the sum of a power function and a Gaussian while the high Q region was fitted with a Gaussian in an interval asymmetrically placed around the peak position as shown in Figure 59. The peak position of the first Gaussian provided the RD values according to equation 4.3.

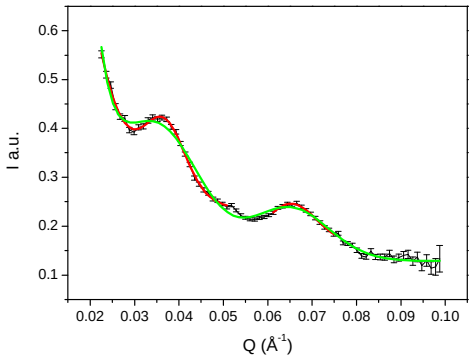

Figure 59: Typical radially averaged SANS scattering curve obtained from suspension of *Phaeodactylum tricornutum* cells. Scattering from the suspending medium and background was subtracted. Measurement was performed on D22 (SD = 8 m, col = 8 m, λ = 6 Å). Fitted functions: sum of a power function and a Gaussian for the low Q-region, and a Gaussian for the high Q-region – in red; the sum of a power function and two Gaussians – in green.

The calculations provided (169 ± 1) Å and (171 ± 1) Å repeat distance values for the thylakoid membranes in a band of three appressed thylakoids for two independent batches. (Variations of RD between independent measurements on the same batch were smaller than 1.5%.) This RD evidently requires a tight packing of membranes, therefore we performed a calculation whether this distance allows the special arrangement of the different protein complexes in the direction perpendicular to the membrane plane. In

plants, such an arrangement of PSII and PSI complexes would require a somewhat larger RD of ~ 185 Å if we consider that PSI protrudes about 40 Å while both PSII and its main light harvesting complexes (LHCII) are extended by about 20 Å into the interthylakoidal space; the membrane thicknesses are ~ 40 Å each, and the lumenal spacing is ~ 45 Å (Dekker and Boekema 2005; Daum et al. 2010). As detailed above FCPs, the light harvesting complexes of diatoms, are significantly smaller than LHCII - thus they allow smaller interthylakoidal space and smaller RD. However, the ATP synthase in diatoms with its estimated large, ~ 140 Å, protrusion (Stock et al. 1999) clearly can only be accommodated in the 'end' membrane, i.e. on the outer surfaces of the groups of three thylakoid membranes (see Figure 60). This implies that the thylakoid in the middle must be energetically coupled, evidently via interconnected lumenal spaces and contiguous bilayer membranes, to the two end membranes.

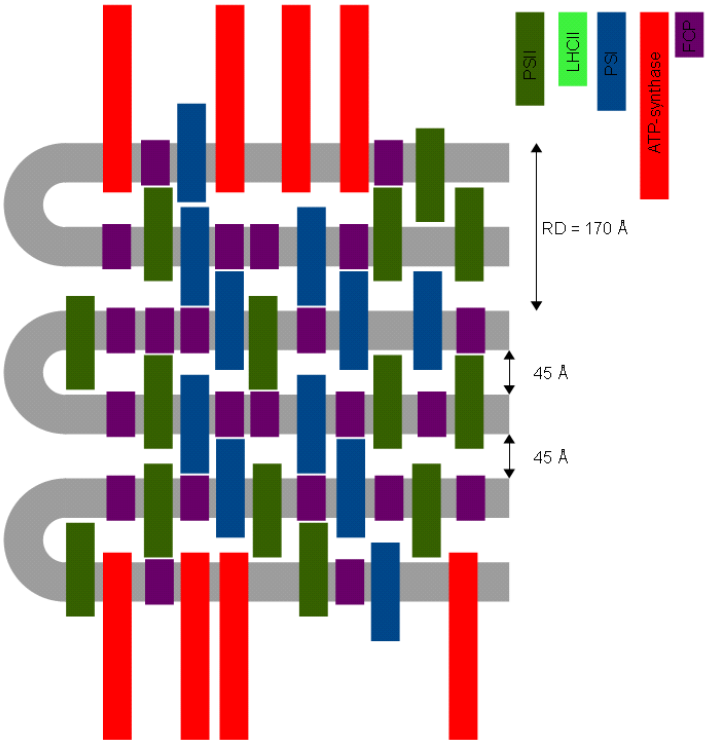

Figure 60: Schematic drawing of the bands of three loosely appressed thylakoids in the *Phaeodactylum tricornutum* showing the approximate size and transmembrane positioning of the main protein complexes in the membrane. The schematic drawing of the LHCII complex is also shown for size comparison.

7.1.2 Light-induced Changes in the Repeat Distances of Thylakoid Membranes

Structural flexibility and the effect of illumination on the photosynthetic complexes in *Phaeodactylum tricornutum* cells were previously investigated by Szabó et al. (2008) by means of circular dichroism. The CD band at 698 nm was observed to increase upon illumination. The changes were reversible but the dark recovery kinetics were relatively slow. The typical time course of the light-induced changes is shown in Figure 61.

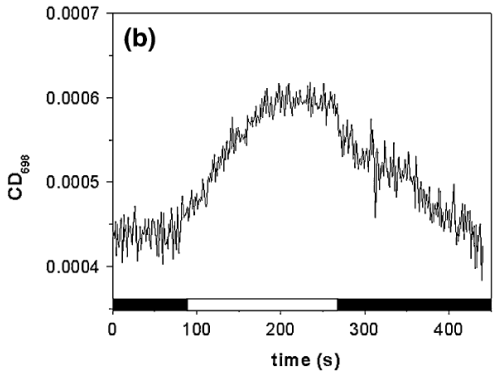

Figure 61: Time course of the light-induced CD changes of *Phaeodactylum tricornutum* cells at 698 nm (copied from (Szabó et al. 2008)). Illumination was provided by blue light of 800 μmol photons m^{-2} s^{-1} (closed bars, dark periods; open bar, illumination).

We investigated the light-induced changes on the periodicity of the thylakoid membranes in these cells. SANS curves of dark adapted and illuminated (with white light of 2000 μmol photons m^{-2} s^{-1} photon flux density for 4 min) diatoms are shown in Figure 62. Upon illumination the center position of the first Gaussian decreased from (0.0369 ± 0.0002) $Å^{-1}$ to (0.0350 ± 0.0003) $Å^{-1}$, revealing an RD increase from (170 ± 1) Å to (180 ± 1) Å. It is interesting to note that the variations in the SANS profile are not confined to the peak at Q ~ 0.037 $Å^{-1}$, but also include the one at Q ~ 0.065 $Å^{-1}$. The center position of the second Gaussian decreased from (0.0653 ± 0.0002) $Å^{-1}$ to (0.0613 ± 0.0004) $Å^{-1}$ which, according to our interpretation, indicates swelling in the paired membranes of adjacent thylakoids.

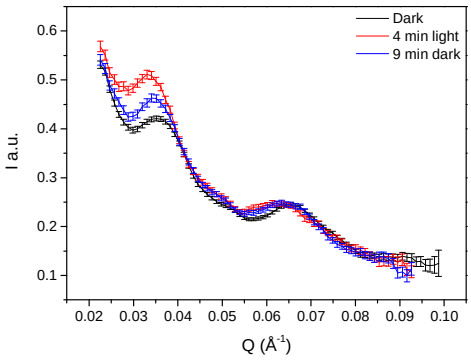

Figure 62: Effect of illumination with white light of 2000 µmol photons m^{-2} s^{-1} photon flux density on the thylakoid membranes in living *Phaeodactylum tricornutum* cells. The curves are smoothed by averaging over three adjacent data points.

In order to understand better the mechanism of the observed light-induced changes we performed complementary measurements in the presence of NH_4Cl and DCMU. Addition of 4 mM NH_4Cl, an uncoupler that abolishes ΔpH, had no significant effect on the light-induced RD changes, as shown in Figure 63. This result and the direction of the light-induced changes suggest that these changes probably originate from variations in the electrostatic interactions due to the presence of local electric fields and/or consequent redistribution of the ions in the electrolyte during photosynthesis (Zimányi and Garab 1982; Zimányi and Garab 1989) or other variations in the surface charges.

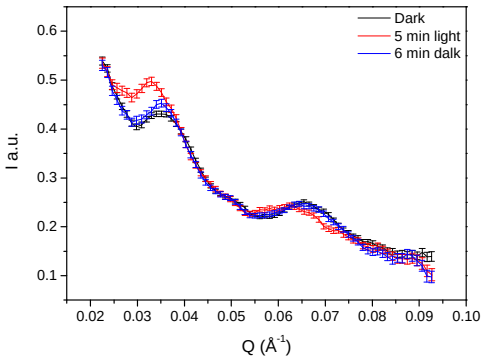

Figure 63: Effect of illumination with white light of 2000 µmol photons m^{-2} s^{-1} photon flux density on the thylakoid membranes in living *Phaeodactylum tricornutum* cells in the presence of 4 mM NH_4Cl. The curves are smoothed by averaging over three adjacent data points.

We also could not observe significant influence of the addition of 10 µM DCMU and sodium dithionite (a reducing agent) on the light-induced changes; however the

changes were not found to be reversible upon dark adaptation, as shown in Figure 64. These results are in accordance with CD measurements of Dr. Milán Szabó, where the full reversibility of light-induced changes in the 698 nm CD band was found to be inhibited or decelerated by the presence of DCMU.

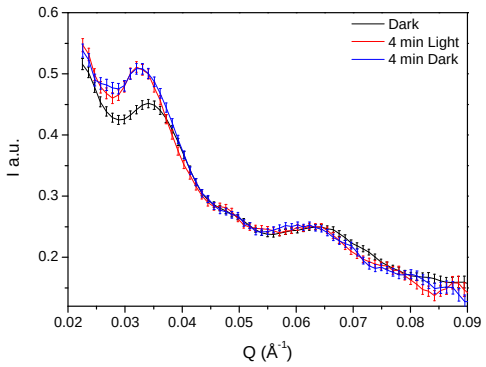

Figure 64: Effect of illumination with white light of 2000 µmol photons m^{-2} s^{-1} photon flux density on the thylakoid membranes in living *Phaeodactylum tricornutum* cells in the presence of 10 µM DCMU and dithionite. The curves are smoothed by averaging over three adjacent data points.

The obtained peak position and calculated repeat distance values for the diatom in the presence or absence of NH_4Cl and DCMU for consecutive dark and light cycles are shown in Table 11.

Table 11: Peak positions of the fitted Gaussians and calculated RD values of thylakoid membranes of *Phaeodactylum tricornutum* cells subjected to consecutive dark/light cycles using white light of 2000 µmol photons m^{-2} s^{-1} photon flux density.

		Dark	Light 1	Dark 2	Light 2	Dark 3
Control	Q_{c1} (10^{-2} Å^{-1})	3.69 ± 0.01	3.50 ± 0.03	3.62 ± 0.02	3.50 ± 0.01	3.53 ± 0.03
	RD (Å)	170 ± 1	180 ± 1	174 ± 1	180 ± 1	178 ± 1
	Q_{c2} (10^{-2} Å^{-1})	6.52 ± 0.02	6.13 ± 0.04	6.35 ± 0.03	6.11 ± 0.03	6.33 ± 0.02
4 mM NH_4Cl	Q_{c1} (10^{-2} Å^{-1})	3.69 ± 0.02	3.50 ± 0.02	3.64 ± 0.02	3.41 ± 0.04	3.64 ± 0.02
	RD (Å)	170 ± 1	180 ± 1	173 ± 1	184 ± 2	173 ± 1
	Q_{c2} (10^{-2} Å^{-1})	6.52 ± 0.02	6.06 ± 0.04	6.50 ± 0.04	6.13 ± 0.04	6.50 ± 0.03
10 µM DCMU	Q_{c1} (10^{-2} Å^{-1})	3.57 ± 0.02	3.41 ± 0.01	3.45 ± 0.02	3.35 ± 0.02	3.43 ± 0.01
	RD (Å)	176 ± 1	184 ± 1	182 ± 1	188 ± 1	183 ± 1
	Q_{c2} (10^{-2} Å^{-1})	6.37 ± 0.04	6.05 ± 0.04	6.00 ± 0.03	6.00 ± 0.05	6.11 ± 0.04

We also performed SANS measurements on diatoms in the presence of 0.5 mM *p*-benzoquinone, which serves as an electron acceptor predominantly for Q_B and, with a smaller rate for Q_A (Tanaka-Kitatani et al. 1990). We could not observe any significant light-induced structural changes of the thylakoid membranes on the radially averaged SANS curves, as shown in Figure 65. Taking into account that these externally added molecules accept electrons originating from the primary charge separation, this observation can most probably be reconciled with the above notion on the role of electrostatic interactions. However, this question evidently requires further investigations.

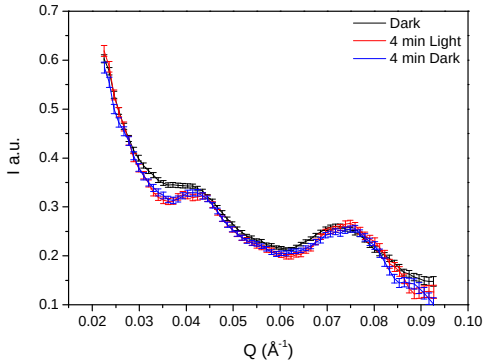

Figure 65: Effect of illumination with white light of 2000 µmol photons m^{-2} s^{-1} photon flux density on the thylakoid membranes in living *Phaeodactylum tricornutum* cells in the presence of 0.5 mM *p*-benzoquinone. The measurements were performed on D22 (SD = 8 m, col = 8 m, λ = 6 Å). The curves are smoothed by averaging over three adjacent data points.

Furthermore upon the addition of the 0.5 mM *p*-benzoquinone the observed RD for the thylakoids was found to be significantly decreased to (148 ± 1) Å. This result suggests major reorganizations in the thylakoid membrane upon this treatment. The nature of these reorganizations, however, remains yet to be explored. In *Chlamydomonas reinhardtii* *p*-benzoquinone was found to block the thylakoid membranes in their original state of either state I or state II by rendering the LHC phosphorylation state invariant, most probably through intramolecular cross-linking in the kinase/phosphatase system (Bulté and Wollman 1990), providing a possible explanation for the inactivation of the light-induced structural changes in thylakoids of diatoms, in the presence of *p*-benzoquinone. We have to note, however, that the results presented here on the effect of *p*-benzoquinone are preliminary and will be completed in further experiments.

7.1.3 Light-intensity Dependent Kinetics and Reversibility of the Light-induced Changes in the Repeat Distances of Thylakoids

The light-induced increase in the amplitude of the psi type CD became larger when 800 µmol photons m^{-2} s^{-1} illumination intensity was used instead of 100 µmol photons m^{-2} s^{-1} (Nagy et al. 2011c). We investigated the influence of illumination with similar light intensities on the RD of thylakoid membranes in *Phaeodactylum tricornutum* cells. The effect of illumination with white light of 150 and 1200 µmol photons m^{-2} s^{-1} photon flux density on the radially averaged scattering curves is presented in Figure 66 revealing that similar to the light-induced CD changes, higher illumination results in more pronounced alteration of the SANS signal. Calculated RD changes in the two cases are presented in Table 12.

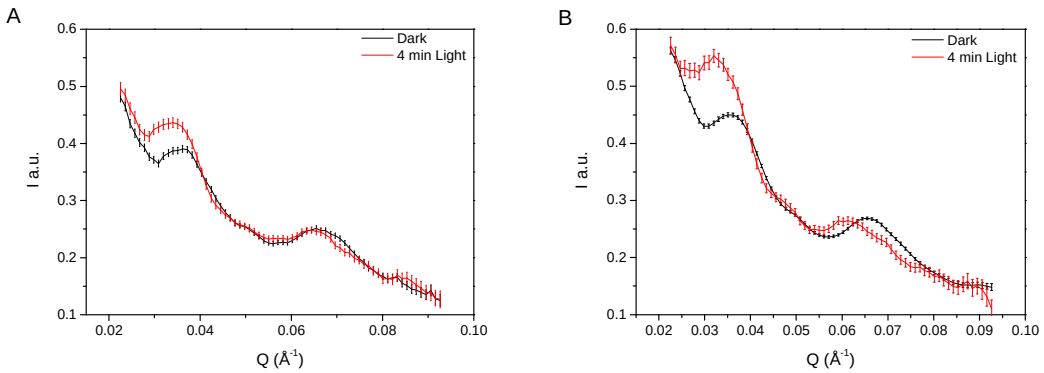

Figure 66: Effect of illumination with white light of 150 µmol photons m^{-2} s^{-1} (A) and 1200 µmol photons m^{-2} s^{-1} (B) photon flux density on the thylakoid membranes in living *Phaeodactylum tricornutum* cells. The curves are smoothed by averaging over three adjacent data points.

Table 12: Effect of illumination on the magnitude of psi-type CD at (+)698 nm, on the Q values of the two peaks in the scattering curves and on the calculated RD changes of thylakoid membranes in *P. tricornutum* cells. In CD measurements the photon flux densities of the blue light, at low light (LL) and high light (HL) were 100 and 800 µmol photons m^{-2} s^{-1}, respectively. In SANS experiments, white light of 150 (LL) and 1200 (HL) µmol photons m^{-2} s^{-1} were used. Results for the CD measurements are courtesy of Dr. Milán Szabó.

	ΔCD/CD at 698 nm	ΔQ^*_1 [10^{-3} Å^{-1}]	ΔRD [Å]	ΔQ^*_2 [10^{-3} Å^{-1}]
LL illuminated	0.18±0.03	-1.8 ± 0.5	+9 ± 2	- 3.2 ± 0.6
HL illuminated	0.36±0.045	- 3.2 ± 0.2	+15 ± 1	- 4.7 ± 0.2

We have to note that when the illumination level is further increased from 1200 to 2000 μmol photons m^{-2} s^{-1} photon flux density, we cannot observe further increase in the light-induced RD changes, they rather decline. We do not have information about comparative CD measurements; but based on (Ting and Owens 1994) 2000 μmol photons m^{-2} s^{-1} photon flux density can be considered as a photoinhibitory condition, which provides a possible explanation for the decreased light-induced RD changes.

In the case of the measurements with illumination with 1200 μmol photons m^{-2} s^{-1} photon flux density we could also follow the evolution of the calculated RD values during the illumination and dark adaptation periods (Figure 67).

An apparent feature of the curve presented in Figure 67 is the significantly slower kinetics of the RD recovery during dark adaptation, compared to the kinetics of the light-induced changes. The timescale of the full reversibility (30-60 min) is similar to the time required for the recovery of the non-photochemical quenching of chlorophyll fluorescence (NPQ) of *Phaeodactylum tricornutum* cells in dark after illumination with 800 μmol photons m^{-2} s^{-1} photon flux density for 15 min as shown in (Goss et al. 2006).

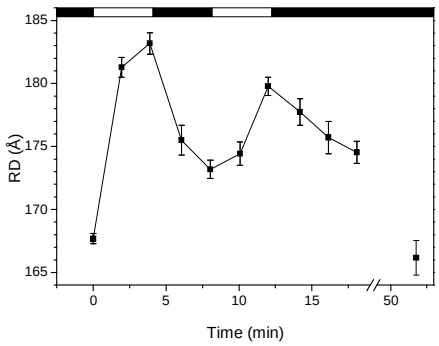

Figure 67: Time course of the light-induced variations in the RDs of thylakoid membranes in living *Phaeodactylum tricornutum* cells illuminated with white light of 1200 μmol photons m^{-2} s^{-1} photon flux density (closed bars, dark periods; open bar, illumination).

The above presented data provide clear evidence that small but well discernible membrane reorganizations occur in diatoms during photosynthesis. This structural flexibility of diatoms might be related to their well known ability to adapt to fluctuating light conditions (Wagner et al. 2006; Lavaud et al. 2007), which renders the diatom to be a dominant phytoplankton in turbulent mixing waters (Huisman et al. 2004).

7.2 Thylakoid Membranes of the Cyanobacterium *Synechocystis* sp. PCC 6803

The cyanobacteria, earlier known as blue-green algae, are photosynthetic prokaryotes, having a photosynthetic mechanism very similar to that present in photosynthetic eukaryotes. Cyanobacteria have a high tolerance for different environmental conditions such as high and low temperature extremities or a low amount of available water or nutrients (Blankenship 2002). Cyanobacteria possess a thylakoid membrane system which accommodates photosystems I and II. Cyanobacterial thylakoids are not differentiated to stacked and unstacked regions, as chloroplast thylakoids (Olive et al. 1997). However, different protein complexes were found to be unevenly distributed, for example, in *Synechococcus* PCC 7942 (Sherman et al. 1994), while in *Synechocystis* PCC 6803 no such heterogeneity was observed (Olive et al. 1997). The EM image of *Synechocystis* PCC 6803 cells (see Figure 68) reveals a regular arrangement of the thylakoid membranes.

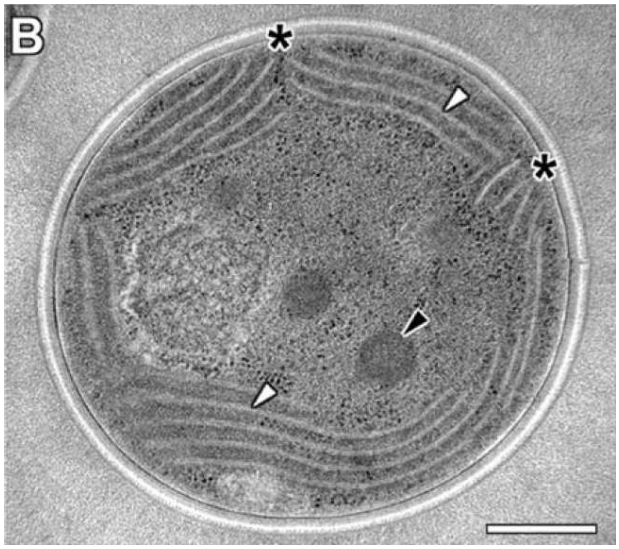

Figure 68: Transmission electron microscopy image of *Synechocystis* sp. PCC 6803 (copied from (van de Meene et al. 2006)) with a bar of 0.2 μm. Contoured arrays of thylakoid membranes are marked with white arrowheads.

The typical repeat distance of the thylakoid membranes is expected to be significantly different from that of diatoms or higher plants because the packing density of membranes in cyanobacteria is determined by their light-harvesting antennae, the phycobilisomes (PBSs). The distance between two adjacent membranes (the

interthylakoidal space) was found to be 460 and 40 Å, in the presence and absence of phycobilisomes, respectively - determined by electron microscopy on the wild type and a mutant unicellular cyanobacterium *Synechocystis* PCC 6803 (Olive et al. 1997). Arrangement of the PBS in the multilamellar thylakoid membrane system is shown in Figure 69.

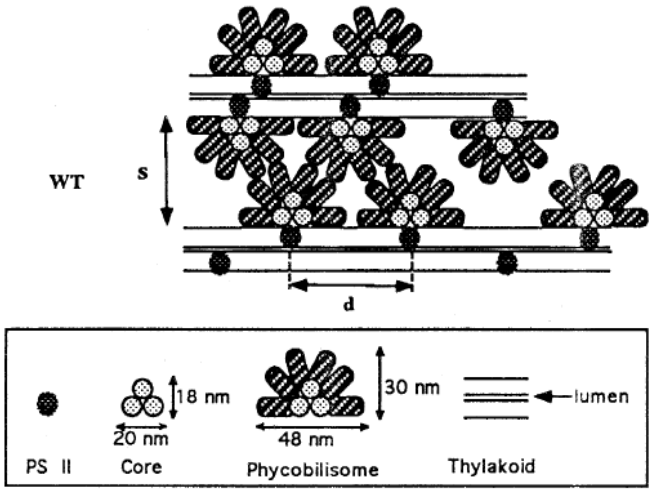

Figure 69: Schematic representation of the phycobilisomes organization in *Synechocystis* sp. PCC 6803 copied from (Olive et al. 1997).

In the present study we investigated wild type (WT) and PAL mutant cells of *Synechocystis* PCC 6803. PAL mutant cells are completely devoid of PBS (Ajlani and Vernotte 1998).

7.2.1 SANS Signals Arising from the Wild Type and the PAL Mutant *Synechocystis* sp. PCC 6803 and their Light-induced Changes

As shown in Figure 70 well-defined characteristic peaks could not be observed on radially averaged SANS curves of WT *Synechocystis* PCC 6803 cells. Considering the above cited interthylakoidal space and the contribution of two thylakoid membranes and the lumenal space as discussed in Paragraph 7.1.1, we would expect an RD between 550 and 600 Å in the wild type cells, i.e. a peak between 0.0105 $Å^{-1}$ and 0.0114 $Å^{-1}$. On the SANS curves no Bragg peak could be discerned in the corresponding Q-range, most probably because of strong forward scattering of the whole cells and the smearing effect of the hemispherically shaped membrane-anchored phycobilisomes. In order to reveal

the possible existence of the peak, corresponding to an RD of ~ 600 Å, further experiments are needed to be performed with a different instrument setting.

In a pilot experiment we investigated the effect of illumination with white light of 2000 μmol photons m^{-2} s^{-1} photon flux density for up to 10 min with a 1 min time resolution on the WT cells, but we could not a observe significant changes in the radially averaged SANS curves, an experimental finding which requires confirmation.

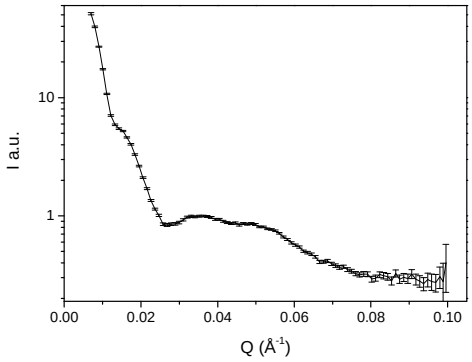

Figure 70: Radially averaged SANS scattering curve obtained from suspension of WT *Synechocystis* sp. PCC 6803 cells. Scattering from the suspending medium and background was subtracted. Measurement was performed on D22 (SD = 8 m, col = 8 m, λ = 6 Å).

The two dimensional small-angle neutron scattering profiles of suspensions of randomly oriented living PAL mutant *Synechocystis* PCC 6803 cells show two characteristic diffraction rings (Figure 71).

Radially averaged SANS curves of PAL mutant *Synechocystis* PCC 6803 cells are shown in Figure 72, revealing two characteristic peaks in the investigated Q-region. In our interpretation the peak at Q ~ 0.032 $Å^{-1}$ is considered as a first order Bragg peak. The interpretation of the second peak at Q ~ 0.048 $Å^{-1}$ is not clear at the moment. Tentatively, the second peak is assigned to adjacent membrane pairs in the multilamellar system, as in the case of granum and BBY.

For the extraction of the different peak positions from the experimental scattering curves, we fitted the curves corresponding to different samples by the sum of a power function and two Gaussians. The peak position of the first Gaussian provided the RD values according to equation 4.3. We obtained (195 ± 1) Å and (180 ± 1) Å repeat

distance values for two different batches of cells. However, variations of RD between independent measurements on the same batch were smaller than 1.5%.

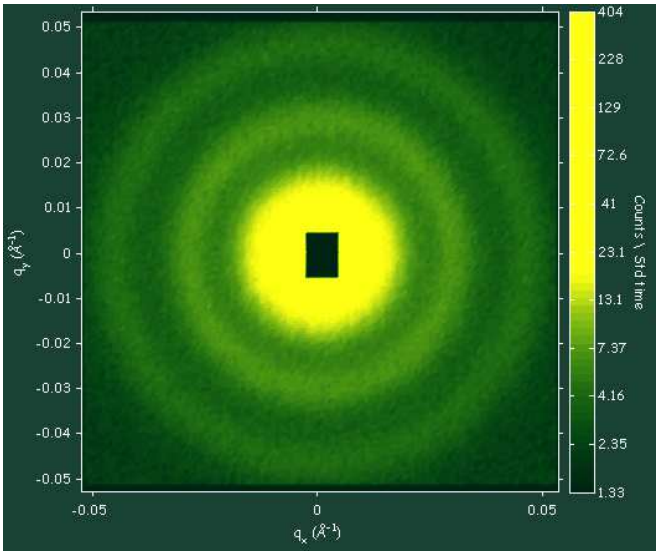

Figure 71: SANS detector image of thylakoid membranes in PAL mutant of *Synechocystis* sp. PCC 6803 with two clearly visible diffraction rings, recorded with the 2D detector of the D22 SANS instrument. SD = 10 m, collimation, col = 11.2 m, λ = 6 Å. Colors are representing the counts in the pixels per 100 s in a logarithmic scale.

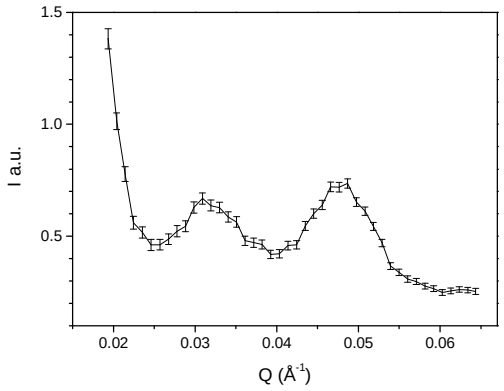

Figure 72: Typical radially averaged SANS scattering curve obtained from suspension of PAL mutant cells of *Synechocystis* sp. PCC 6803. Scattering from the suspending medium and background was subtracted. Measurement was performed on D22 (SD = 8 m, col = 8 m, λ = 6 Å).

We also investigated the light-induced changes on the periodicity of the thylakoid membranes in PAL mutant *Synechocystis* PCC 6803 cells. SANS curves of dark adapted, illuminated (with white light of 2000 μmol photons m^{-2} s^{-1} photon flux density for 6 min) and subsequently dark adapted (for 60 min) cells are shown in Figure 73.

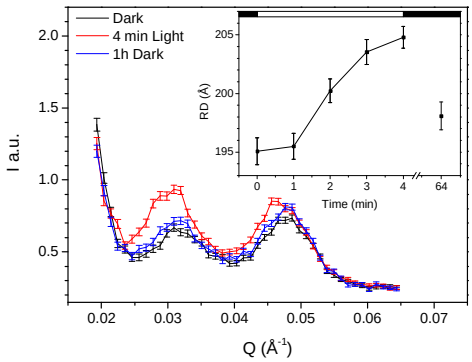

Figure 73: Effect of illumination with white light of 2000 µmol photons m^{-2} s^{-1} photon flux density on the thylakoid membranes in living *Synechocystis* sp. PCC 6803 cells. Inset shows the time course of the light-induced variations in the RD and its dark recovery phase, calculated from the first order Bragg peak.

Upon illumination the center position of the first Gaussian decreased from (0.0322 ± 0.0002) $Å^{-1}$ to (0.0307 ± 0.0001) $Å^{-1}$, revealing an RD increase from (195 ± 1) Å to (205 ± 1) Å. The center position of the second Gaussian decreased from (0.0477 ± 0.0001) $Å^{-1}$ to (0.0467 ± 0.0001) $Å^{-1}$, which, according to our interpretation, indicates swelling in the paired membranes of adjacent thylakoids. The time evolution of the RD upon illumination and its dark-recovery is shown in Figure 73. Further experiments are required in order to obtain more detailed kinetics of the observed light-induced changes and their sensitivity to different agents.

In Chapter 7 the typical SANS signals of some living cyanobacterial and algal cells were presented. With the aid of SANS – which we previously applied for determining the RDs of thylakoid membranes and their variations induced by light or by variations in the physicochemical environment of the membranes – we determined the characteristic repeat distances of thylakoid membranes in the diatom *Phaeodactylum tricornutum* and in the PAL mutant of the cyanobacterium *Synechocystis* PCC 6803. For the first time, we also observed fully reversible reorganizations – changes in the RDs – during photosynthesis in intact cells, which, as shown for *P. tricornutum*, also affected the long range chiral order of chromophores in the thylakoid membranes. These data, together with the data obtained for isolated plant thylakoid membranes show that the periodic membrane ultrastructure in a variety of different organisms performing oxygenic photosynthesis are all capable of undergoing reversible changes, small but well discernible reorganizations. Thus, it appears that the mesoscale membrane ultrastructure

of the thylakoid membranes possess a substantial structural flexibility, a dynamic property of the membrane system, a capability which probably plays an important role in the energy conversion of membranes and/or in different regulatory mechanisms.

In the following chapter, I investigate the dynamical properties of photosystem II membrane fragments (BBY) with the technique of elastic incoherent neutron scattering, which carries information mainly on the averaged movement of individual hydrogen atoms and thus on the dynamic characteristics of the lipid-protein assembly.

8. Dynamical Studies on Photosystem II Membrane Fragments and Thylakoid Membranes

Incoherent neutron scattering has been used for characterizing the dynamic properties of many different biological samples, such as myoglobin, bacteriorhodopsin, hemoglobin and lysozyme (Doster et al. 1989; Ferrand et al. 1993; Stadler et al. 2009; Magazù et al. 2010). However, the use of this technique in photosynthesis research is still uncommon. The first elastic and quasi-elastic neutron scattering measurements on photosystem II (PSII) membrane fragments (BBY) in the temperature range between 5 and 300 K, have only recently been published (Pieper et al. 2007; Pieper et al. 2008). These studies revealed clear correlations between the dynamic properties of proteins and the photochemical activity of PSII, in particular with the efficiency of the $Q_A \rightarrow Q_B$ electron transfer. The major aim of our study was to extend these investigations to the physiological range of temperatures, where photosynthetic membranes are frequently exposed to environmental stress effects and thus are subject of substantial reorganizations as part of their multilevel regulatory mechanisms.

As we discussed in detail in paragraph 5.1.2 several processes are participating in the adaptation of plants to different light conditions. Specific reorganizations of the membrane ultrastructure can be induced also by elevated temperatures, either in the dark or in combination with strong illumination (Anderson and Andersson 1988; Dobrikova et al. 2003; Páli et al. 2003). The most heat sensitive component of the photosynthetic electron transport chain is the oxygen evolving complex (presented in detail in paragraph 3.1.4). Upon heat stress the OEC is damaged due to the dissociation of the 33 kDa protein from the lumenal side of PSII around 40 ºC (Enami et al. 1994), while the activity of the reaction centers and the membrane energization can be retained (Tóth et al. 2009; Tóth et al. 2011).

8.1 Effect of Hydration on the Dynamics of PSII Membranes

We investigated PSII membranes with hydration levels of 57 and 75 % r.h. Figure 74 shows the logarithm of the scattering intensities as a function of Q^2 for the control, i.e. for the 75 % r.h. sample. The region, where they depend linearly on Q^2, is indicated by

the superimposed thick lines in Figure 74; the deviation from the Gaussian behavior at higher Q^2 values is clearly visible.

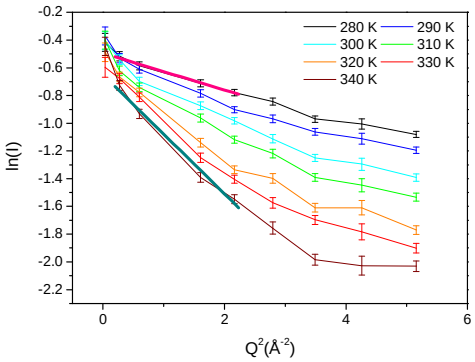

Figure 74: Logarithm of the scattered intensity from 75 % r.h. PSII (BBY) membranes at different temperatures as a function of Q^2. The linear section in the curves for low Q^2 values is clearly visible; fits are shown for the lowest and highest temperatures.

MSD values for different samples were extracted from the slope of the corresponding curves as described in equation 2.42. The MSD values for the 57 and 75 % r.h. sample are shown in Figure 75. The slope of the MSD curve for the 75 % r.h. sample is similar in the 280-310 K and the 320-340 K temperature regions, whereas in the range of 310-320 K two consecutive changes of slope can be observed. The relatively large increase of the slope (hereafter called transition) is evidently a signature of a structural reorganization in the sample, which gives rise to a release of the resilience. Our data reveal a transition only in the sample with the higher hydration level (Figure 75), while the MSD of the less hydrated sample (of 57 % r.h.) increases almost linearly with temperature, and does not display a clearly discernible transition.

Hydration is known to have a crucial function in protein dynamics. The influence of hydration on the dynamics of BBY has earlier been investigated (Pieper et al. 2008), and the dynamical transition at 240 K, associated with the glass transition in the protein hydration shell (Doster et al. 1989; Doster 2008), has been found to be missing in dry samples (Pieper et al. 2007).

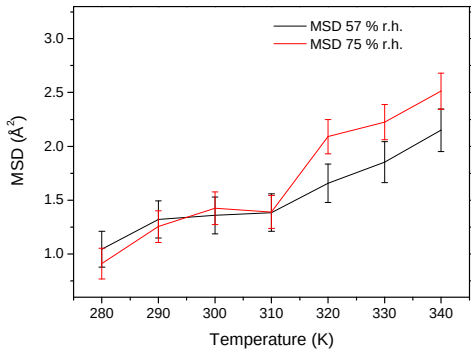

Figure 75: Comparison of the temperature dependence of MSD of PSII (BBY) membranes with 57% and 75% relative humidity.

It is also worth noting that the hydration level of lipid bilayers strongly influences their periodicity (Kucerka et al. 2005; Trapp et al. 2010) and also the phase behavior of lipids (Smith et al. 1988). This poses the possibility of involvement of lipids in the transition, which will be discussed in a later paragraph.

It is to be noted that the error bars of the curves presented in Figure 75 are relatively high for two reasons: (i) in this temperature range the scattering intensities are relatively low and thus relatively long counting times are required to obtain good statistics, and (ii) the functions, presented in Figure 74, can be considered to be linear only for a few data points, resulting in high errors for the slope of the fitted curves. However, we repeated the experiment on the 75% r.h. sample twice and the results were found to be exactly reproducible.

8.2 Effect of Heat- and TRIS-treatments on the Dynamics of PSII Membranes

In order to clarify the structural basis of the dynamical changes we investigated the effects of heat treatments at 323 and 333 K and of TRIS-washing of the membranes. Upon heat treatment at 323 K OEC loses its activity, mainly because of the detachment of the extrinsic proteins surrounding the Mn-complex (Nash et al. 1985; Enami et al. 1994; Yamane et al. 1998; Barra et al. 2005; Tóth et al. 2009). The heat treatment at 333 K leads to the denaturation of other protein components that are crucial for the rest of the electron transport chain (see (Thompson et al. 1986; Thompson et al. 1989)). TRIS

washing is also known to remove the 17, 23, and 33 kDa polypeptides of OEC (Kuwabara and Murata 1983). The removal of the 33 kDa protein has been proposed to result in the destabilization of the core-core interactions in the PSII dimer in BBY membranes isolated from spinach (Boekema et al. 2000). The stabilization effect of the presence of the 33 kDa protein has also been shown on PSII dimers of cyanobacterium *Synechococcus* sp. (Dekker et al. 1988). The effect of TRIS treatment was investigated by AFM on PSII supercomplexes isolated from spinach, and revealed the disintegration of the supercomplexes into subparticles (Kirchhoff et al. 2008), confirming the importance of the extrinsic subunits in PSII organization. Hence, upon heat-treatment and TRIS-washing, in addition to the detachment of OEC from the membranes PSII supercomplexes are expected to be found in monomeric form, while in the control sample the removal of OEC and monomerization of PSII is expected to occur upon heating during the EINS experiment. In these samples MSD values differed significantly from those in the control sample and also from each other (Figure 76).

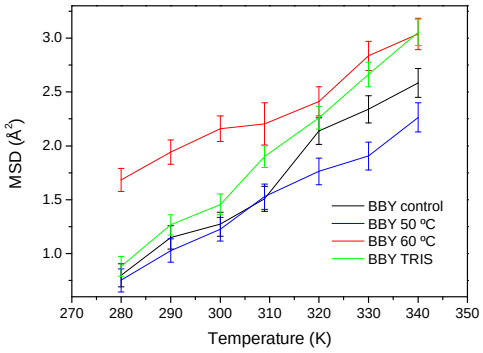

Figure 76: Comparison of the temperature dependence of MSD of control, heat treated (50 ºC and 60 ºC) and TRIS-washed PSII (BBY) membranes

Pseudo force constant values, calculated according to equation 2.43, were associated with specific temperature regions in the 4 different samples (Table 13).

There are three distinct temperature regions concerning the dynamical behavior of the control sample. The upper value of the first temperature range (280 – 310 K) approximately coincides with the highest temperature where the photosynthetic apparatus is fully functional. Our results show that in this temperature range the resilience of BBY does not change significantly. We observed similar resilience in the

320 – 340 K range. However, in the 310 – 320 K temperature range the resilience of the control sample significantly decreases, a transition which cannot be seen in the heat- and TRIS-treated samples. The calculated pseudo force constant values for the heat treated samples in the whole investigated temperature range are similar to the ones of the control sample for the low (< 310 K) and high (> 320 K) temperature values. The TRIS-treated sample appears to be softer in the whole temperature range than the heat-treated samples.

Table 13: Pseudo force constant values of the control, heat-treated (50 and 60 ºC) and TRIS-washed PSII (BBY) membranes in different temperature intervals, calculated according to equation 2.43. In the $310K \le T \le 320K$ temperature range $\langle k' \rangle$ was obtained by considering two temperature points, therefore no errorbar is given.

Sample	Temperature range	Pseudo force constant $\langle k' \rangle [N/m]$
Control	$280K \le T \le 310K$	0.12 ± 0.03
	$310K \le T \le 320K$	≈ 0.05
	$320K \le T \le 340K$	0.12 ± 0.05
50 ºC treated	$280K \le T \le 340K$	0.11 ± 0.01
60 ºC treated	$280K \le T \le 340K$	0.13 ± 0.01
TRIS-washed	$280K \le T \le 340K$	0.08 ± 0.01

The increased flexibility of the membranes in the 310 – 320 K interval can be correlated with the loss of the oxygen evolution activity; it starts to decrease at ~ 313 K and half inactivation occurs at 320 K (Nash et al. 1985). Hence we propose that the decreased resilience of the sample in this temperature interval is the consequence of the reorganization of the PSII complexes, the detachment of OEC and the destabilization of the PSII dimers.

A surprising characteristic of the MSD curves of the heat treated samples is the significantly higher MSD absolute values for the 333 K treated sample compared to the ones of the 323 K treated, which might be related to monomerization of LHCII trimers at this temperature as shown on isolated trimers (Garab et al. 2002) and on thylakoid membranes, isolated from barley (Dobrikova et al. 2003).

8.3 Comparative Circular Dichroism and Differential Scanning Calorimetry Measurements

In order to investigate the effect of the heat-treatments and the TRIS-washing on PSII membranes and to provide explanation for the observed transition in the MSD curves, Dr. Sashka B. Krumova carried out CD measurements as a function of temperature and also performed DSC experiments. These measurements provide further information about the nature of temperature-dependent reorganizations in the membranes.

The largest heat-susceptibility of the CD signals was exhibited by the (-)457 nm band; a heat treatment at 50 °C led to a substantial loss of this minor excitonic band (marked by orange arrow in Figure 77). This temperature appears to correlate with the temperature corresponding to the transition in the MSD curve of control BBY. However, temperature dependent CD measurements did not show any significant difference between the control and TRIS-treated BBY in the 4 – 75 ºC temperature range. Therefore, the transition affecting the 457-465 nm CD band-pair is unlikely to originate from monomerization of the PSII dimer.

DSC measurements were used in order to investigate the changes in the thermal stability of BBY membranes after TRIS-washing. Transitions occurring at temperatures at which a change in the dynamics of BBY was observed by EINS measurements (around 40 – 50 ºC) were of particular interest. As can be seen in Figure 78 the enthalpy of the transitions below 60 ºC is largely decreased in the TRIS-washed sample.

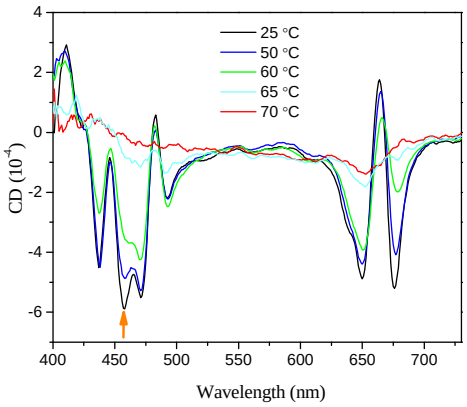

Figure 77: CD spectra of PSII membranes recorded at different temperatures. The *chl* concentration of the samples is 20 µg/ml. (courtesy of Dr. Sashka B. Krumova)

The DSC transition at around 49 °C has been shown to be associated with the oxidation of cytochrome b_{559}, the inactivation of OEC and the monomerization of the PSII core (Thompson et al. 1986; Thompson et al. 1989). It is evident that the TRIS-washing has a major effect on this transition and gives further evidence that the transition observed by EINS at 47 ºC is associated with the OEC inactivation and monomerization of the PSII core.

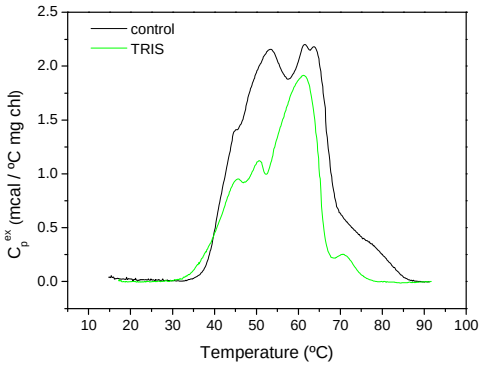

Figure 78: DSC thermogram of control and TRIS-washed PSII (BBY) membranes. (courtesy of Dr. Sashka B. Krumova)

8.4 Possible Involvement of Lipids in the Observed Transition

As we estimated in Paragraph 4.2 ~ 63 % of the EINS signal of BBY originates from proteins, while the contribution of the lipid part is ~ 37 %. Therefore we need to discuss the possible involvement of the lipids in the transition, observed by EINS.

Unpublished EINS experiments, performed by J. Peters and M. Trapp, on model lipid systems of 1,2-dimyristoyl-sn-glycero-3-phosphocholine (DMPC) revealed a transition in the MSD of lipid vesicles around 297 K which resembled the one observed in BBY - suggesting that at least part of the flexibility changes in BBY can originate from changes in the lipid phases. In the case of fully saturated DMPC samples the observed transition can be connected to the well known $L_\beta - L_\alpha$ (gel-to-liquid phase transition) which occurs around 296 K, as determined with the aid of DSC measurements (Keough and Davis 1979). The lipid phase behavior in thylakoid membranes has been extensively studied for decades (see (Williams 1998) and refs. therein). The gel-to-liquid phase transition of lipids is strongly influenced by the number

and position of the cis unsaturated double bonds in the lipid hydrocarbon chains. In accordance with the high ratio of unsaturated fatty acid chains in plant photosynthetic membrane lipids, there is little or no evidence showing the existence of a gel phase of lipids in these membranes above 273 K (Williams and Quinn 1987). Hence, the phase transition, observed by EINS in the temperature range of 310 – 320 K cannot be connected to $L_\beta - L_\alpha$ phase transition. It is also important to note, that the phase behavior of lipids in plant thylakoid membranes under physiological conditions cannot be described simply by liquid crystalline lipid phase. Spectroscopic data analysis of the lipophilic fluorescent probe Merocyanine 540 (Krumova et al. 2008b) and ^{31}P-NMR studies (Krumova et al. 2008a) have shown that at elevated temperatures, between 25 and 45 ºC, significant parts of the bulk lipids of the thylakoid membranes are gradually excluded from the lamellar phase. Above 45 ºC, phase separation of non-bilayer forming lipids has been observed in thylakoid membranes (Williams and Quinn 1987; Kóta et al. 2002). The phase behavior of thylakoid membrane lipids can exert a strong influence on the function and organization of the incorporated membrane proteins (cf (Garab et al. 2000; Simidjiev et al. 2000; Páli et al. 2003; Yang et al. 2006; Schaller et al. 2011), which might contribute to the observed EINS transition. Currently there is no satisfactory information about lipid phase transitions in BBY. Therefore the question concerning the role of lipids in the observed EINS transitions remains open.

8.5 The Lack of the Transition in Thylakoid Membranes

We performed similar experiments, as presented above, on an aqueous suspension of control and heat treated intact thylakoid membranes. These samples, although built partly of the same components which can be found in BBY samples, contain multiple other components, especially in their stroma thylakoids (e.g. ATP synthase, photosystem I); they also contain additional compounds in the lumenal aqueous phase (water soluble proteins), which are absent in BBY.

Thylakoid membrane samples, measured in the form of dense solutions, contain significant amounts of buffer, unlike BBY samples. Thus during the data treatment, scattering from the buffer, measured independently, is also needed to be subtracted from sample scattering. Due to practical reasons (as various possible choices for the sample

volume, the time needed for the determination of the buffer content) the amount of the buffer, contained in the measured sample and the amount of buffer measured separately were not identical. For proper background subtraction, the buffer content needs to be corrected.

The amount of buffer in the thylakoid membrane samples was defined in the following way: A minor portion of the sample prepared for the measurement was separated and used for determination of the D_2O content. These portions of each sample were lyophilized and the masses of the samples before and after lyophilization were compared, providing information about the D_2O content and thus the buffer content of the measured sample. Experimental scattering from the empty cell filled with an arbitrary amount of buffer can be modified to simulate scattering from the empty cell and the appropriate amount of buffer. Further data treatment is identical to that mentioned before.

We compared the MSD values calculated for the control and heat treated thylakoid samples (Figure 79). In the temperature range of 280-340 K neither one of the samples showed distinguishable transitions. We also could not see any sign of the transition which was present in BBY, which does not, however, allow us to conclude that the transition is completely absent in thylakoid membranes. As explained above, thylakoid membranes have a more complex composition compared to BBY, which can be one of the reasons for the error bars being significantly higher in Figure 79 then in Figure 76. The complex composition may hinder the transition to be observed by the method presented in this work.

We also have to consider the somewhat lower protein content in the thylakoid compared to BBY. Since, as we detailed above, the transition, observed by EINS on BBY can be associated with the OEC inactivation and monomerization of PSII core, the lower protein content of the thylakoid membrane further hinders the protein related phase transition even if it exists in thylakoid membranes.

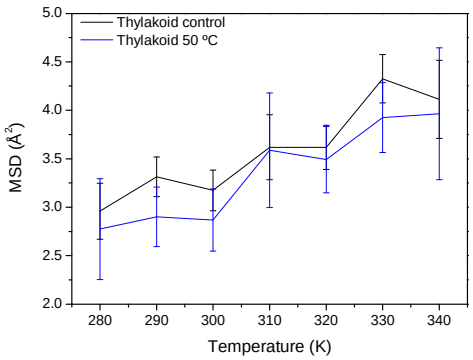

Figure 79: Comparison of the temperature dependence of MSD of control and 50 ºC treated thylakoid membranes.

In this chapter we presented how elastic incoherent neutron scattering can be applied for the dynamical investigation of the photosystem II membrane fragments at physiological and relevant superphysiological temperatures. The obtained results show the presence of a hydration dependent transition in the sample between 37 and 47 °C. Comparative measurements of photosystem II membrane fragments subjected to different treatments prior the experiments revealed a correlation between the observed transition and the detachment of the oxygen evolving complex from the membrane.

9. Conclusions and Future Perspectives

In my PhD work I investigated the structure and structural flexibility of thylakoid membranes isolated from spinach leaves as well as in intact algal cells of *Phaeodactylum tricornutum* and in intact cyanobacterial cells of *Syncechocystis* sp. PCC 6803 by small-angle neutron scattering. I also studied the dynamic properties of photosystem II membranes at physiological temperatures by elastic incoherent neutron scattering. My results can be summarized as follows:

1. Small-angle neutron scattering is a suitable technique for the accurate determination of stroma thylakoid repeat distances (RD) in isolated plant thylakoid membranes via a related Bragg peak present in the radially averaged scattering curves collected at the high flux instrument, D22. The repeat distance depends on the osmolarity and the ionic strength of the suspending medium [Posselt, D., Nagy, G., Kirkensgaard, J. J. K., Holm, J. K., AAgaard, T. H., Timmins, P., Retfalvi, E., Rosta, L., Kovacs, L. and Garab, G. (2011) Small-angle neutron scattering study of the ultrastructure of chloroplast thylakoid membranes - periodicity and structural flexibility of the stroma lamellae. submitted to Biochim Biophys Acta Bioenerg].
2. SANS studies revealed that the chemical reduction of the PQ-pool by duroquinol induces swelling of the stroma thylakoid membranes of plants, while the consecutive phosphorylation of the main light harvesting antenna (LHCII) and some other phosphoproteins does not exert a significant effect on the periodicity of the stroma thylakoid membranes (Várkonyi et al. 2009).
3. SANS curves of plant thylakoid membranes do not show the presence of a first order Bragg peak corresponding to the expected periodicity of the granum thylakoid membranes. A characteristic peak observed at 0.07 $Å^{-1}$ in the scattering curves of isolated plant thylakoid membranes and of photosystem II enriched (BBY) membranes, are proposed to originate from the form factor of stacked membrane pairs and their variations carry information about changes in the distance between these membranes [Nagy, G., Kovács, L., Peters, J., Garab, G. and Posselt, D. Small-angle neutron scattering of isolated plant thylakoid and photosystem II enriched membranes. The signature of grana (in preparation)].

4. SANS was used to obtain information on the ultrastructure of multilamellar photosynthetic membranes isolated from higher plants and in living cyanobacterial and algal cells. We determined the characteristic repeat distances of the thylakoid membranes in the PAL mutant *Synechocystis* PCC 6803 cells, in the diatom *Phaeodactylum tricornutum* and in intact thylakoid membranes isolated from spinach leaves and these repeat distances could be correlated with the size and the arrangement of the different protein complexes in the thylakoid membranes (Nagy et al. 2011b).
5. We discovered an unexpectedly high structural flexibility of the plant thylakoid membranes during photosynthesis and recorded the light-induced reorganization kinetics with an unprecedented time resolution of several seconds. We showed that these reorganizations in the stroma thylakoid membranes were driven by the transmembrane ΔpH, and could be enhanced by the operation of the cyclic electron transport around photosystem I (Nagy et al. 2011b).
6. Rapid light-induced, dark-reversible reorganizations in the ultrastructure of the thylakoid membranes, on a timescale of minutes, were shown to occur – to our knowledge, for the first time – in living cyanobacterial and algal cells, which appeared to be associated with regulatory functions. The observed changes in the membrane repeat distances are small, at most 2 nm, and thus their detection, especially under physiologically relevant conditions, requires the use of a non-invasive structure-investigation technique, such as SANS, offering high accuracy combined with statistical averaging for the entire, inherently heterogeneous populations of cells and membranes (Nagy et al. 2011b).
7. We found correlation between the light-induced variations in the repeat distances, determined by SANS measurements, and in the long-range chiral order of the chromophores, revealed by circular dichroism spectroscopy, in *Phaeodactylum tricornutum* cells and propose that the RD changes are driven by variations in the electrostatic interactions between the adjacent membranes (Nagy et al. 2011c).
8. By temperature-dependent EINS we revealed a hydration-dependent transition - a significantly increased flexibility between 37 and 47 ºC – in photosystem II

membrane fragments (BBY). We have shown that the transition is correlated with the detachment of the oxygen evolving complex from the membrane. The results also demonstrate that elastic incoherent neutron scattering is a suitable experimental tool for the investigation of the dynamic properties of photosynthetic membranes at physiological temperatures (Nagy et al. 2011a).

In the following section I would like to address a few questions, work in progress and plans for the near future, which are not discussed or only marginally treated in the dissertation but nevertheless constitute important parts of my work on this field:

1. In our neutron scattering experiments on thylakoid membranes isolated from higher plants we could obtain information mostly about the periodicity of the stroma thylakoid membranes under a variety of conditions. As shown in Figure 9, the stroma membranes are wound around the granum 'pillars' and are joined to the stacked thylakoid membranes, i.e. to the grana. In order to have a better understanding of the different structural changes in the thylakoid membrane assembly, the structural parameters of the granum thylakoids and their reorganizations should also be revealed – for these, SANS appeared not to be a suitable technique. Hence, we plan to perform complementary experiments with small-angle X-ray scattering (SAXS) at synchrotron radiation facilities. In these experiments we can capitalize on the different scattering length density profiles of the thylakoid membranes for X-rays and neutrons. Further, the contrast between the lipid and the aqueous phase in the thylakoid membrane is also planned to be varied by the application of OsO_4 staining, widely used for electronmicroscopy. On the same instrument we will also have the possibility to investigate the occurrence of the non-lamellar lipid phase in the thylakoid membranes, the existence of which has recently been indicated by P-NMR measurements – a question related to our EINS measurements. (Experiments to elucidate these questions are to be carried out at the SAXS Beamline of ELETTRA, Italy, in August 2011). We also plan to elucidate the exact structural basis of different characteristics of SANS curves of the thylakoid membranes of different organisms, especially of the characteristic peak at 0.07 $Å^{-1}$ on the

scattering curve of thylakoid membranes of higher plants, by taking aliquots from the samples during our SANS experiments, and fixing them for electronmicroscopy measurements (an experiment, partly dedicated to address these questions, is scheduled for November 2011 at the D11 instrument of ILL, France).

2. We have shown that the thylakoid membranes in the PAL mutant of *Syncechocystis* sp. PCC 6803 cells are also capable of undergoing light-induced changes, i.e. an increase in the repeat distances. We have not investigated, however, the mechanism of these reorganizations. Hence, we plan to determine the light intensity dependence of these reorganizations in the presence or absence of different inhibitors and other chemical agents (an experiment partly dedicated to address these questions, is scheduled for November 2011 at the D11 instrument of ILL, France).
3. In order to extend our investigations on the effect of phosphorylation-induced state transitions on the membrane ultrastructure, in collaboration with Prof. Jun Minagawa (National Institute for Basic Biology, Okazaki, Japan), Dr. Giovanni Finazzi (CNRS, Grenoble, France) and Dr. Michael Haertlein (ILL, Grenoble, France), we have performed experiments on wild type and different mutant algal cells. We found that in these living cells phosphorylation and dephosphorylation of membranes lead to well discernible SANS profiles (experiment conducted on D22 SANS instrument at the ILL; the data treatment is in progress).
4. During our SANS experiments investigating the mechanism of the light-induced RD changes in isolated plant thylakoid membranes we wanted to carry out our measurements at different temperatures in order to determine the activation energy(ies) of the process(es) participating in the reorganizations. We encountered, however, difficulties in controlling the temperature. Currently we are planning to design a sample holder, which allows proper illumination, magnetic orientation and efficient temperature control for these SANS measurements.
5. In order to find correlation between the Hofmeister effects and dynamical properties of proteins subjected to different salt solutions we performed elastic

incoherent neutron scattering experiments on bacteriorhodopsin containing purple membranes in collaboration with Dr. Andás Dér (Biological Research Center, Szeged, Hungary). The experimental results revealed a transition in the investigated samples at a temperature depending on the type of the salts present in the buffer. The shift in transition temperature is in good accordance with DSC measurements showing how the temperature for the α_{II}-α_{I} conformation change of the bacteriorhodopsin depends on the type of salt present in the buffer. (Experiment conducted on IN13 and IN16 EINS instruments at the ILL; complementary spectroscopic measurements are in progress.)

References

Adams, J. R. and Merz, A. R. (1929) Hygroscopicity of fertilizer materials and mixtures. Industrial and Engineering Chemistry 21: 305-307

Adams, P. D., Afonine, P. V., Bunkóczi, G., Chen, V. B., Davis, I. W., Echols, N., Headd, J. J., Hung, L.-W., Kapral, G. J., Grosse-Kunstleve, R. W., McCoy, A. J., Moriarty, N. W., Oeffner, R., Read, R. J., Richardson, D. C., Richardson, J. S., Terwilliger, T. C. and Zwart, P. H. (2010) PHENIX: a comprehensive Python-based system for macromolecular structure solution. Acta Crystallographica Section D-Biological Crystallography 66: 213-221

Ajlani, G. and Vernotte, C. (1998) Construction and characterization of a phycobiliprotein-less mutant of *Synechocystis* sp. PCC 6803. Plant Molecular Biology 37: 577-580

Albertsson, P. (2001) A quantitative model of the domain structure of the photosynthetic membrane. Trends Plant Sci 6: 349-354

Alefeld, B. (1966) Rückstreuversuche hoher Auflösung mit Neutronen. Bayer Akad Wiss 11: 109

Alina, G., Cortes Hernandez, R., Butler, P., Doucet, M., Jackson, A., Kienzle, P., Kline, S. and Zhou, J. (2011). "http://danse.chem.utk.edu/index.html." Retrieved 28 Jul, 2011.

Allen, J. F. and Holmes, N. G. (1986). Electron Transport and Redox Titration. Photosynthesis: Energy transduction — A practical approach. M. F. Hipkins and N. R. Baker. Oxford, IRL Press**:** 199.

Allen, J. F. (1992) How does protein phosphorylation regulate photosynthesis? Trends Biochem Sci 17: 12-17

Allen, J. F. and Forsberg, J. (2001) Molecular recognition in thylakoid structure and function. Trends Plant Sci 6: 317-326

Allen, J. F. (2003) State transitions - a question of balance. Science 299: 1530-1532

Amunts, A., Toporik, H., Borovikova, A. and Nelson, N. (2010) Structure determination and improved model of plant photosystem I. J Biol Chem 285: 3478-86

Anderson, J. M. and Andersson, B. (1988) The dynamic photosynthetic membrane and regulation of solar energy conversion. Trends Biochem Sci 13: 351-355

Anderson, J. M. (1999) Insights into the consequences of grana stacking of thylakoid membranes in vascular plants: a personal perspective. Aust J Plant Physiol 26: 625-639

Aro, E. M., Virgin, I. and Andersson, B. (1993) Photoinhibition of photosystem II. Inactivation, protein damage and turnover. Biochim Biophys Acta 1143: 113-134

Aro, E. M. and Ohad, I. (2003) Redox regulation of thylakoid protein phosphorylation. Antioxidants & Redox Signaling 5: 55-67

Austin, J. R. n. and Staehelin, L. A. (2011) Three-dimensional architecture of grana and stroma thylakoids of higher plants as determined by electron tomography. Plant Physiol 155: 1601-1611

Barber, J. and Chow, W. S. (1979) A mechanism for controlling the stacking and unstacking of chloroplast thylakoid membranes. FEBS Lett 105: 5-10

Barber, J. (1982) Influence of surface charges on thylakoid structure and function. Annu Rev Plant Physiol 33: 261-295

Barra, M., Haumann, M. and Dau, H. (2005) Specific loss of the extrinsic 18 KDa protein from photosystem II upon heating to 47 degrees C causes inactivation of oxygen evolution likely due to Ca release from the Mn-complex. Photosynth Res 84: 231-237

Barzda, V., Istokovics, A., Simidjiev, I. and Garab, G. (1996) Structural flexibility of chiral macroaggregates of light-harvesting chlorophyll a/b pigment-protein complexes. Light-induced reversible structural changes associated with energy dissipation. Biochemistry 35: 8981-8985

Bee, M. J. Y. (1988). Quasielastic Neutron Scattering: Principles and Applications in Solid State Chemistry, Biology and Materials Science, Institute of Physics Publishing.

Berthold, D. A., Babcock, G. T. and Yocum, C. F. (1981) A highly resolved, oxygen-evolving photosystem II preparation from spinach thylakoid membranes. FEBS Lett 134

Blankenship, R. E. (2002). Molecular Mechanisms of Photosynthesis. Malden, USA, Blackwell Science Ltd.

Boekema, E. J., Breemen, J. F., van Roon, H. and Dekker, J. P. (2000) Conformational changes in photosystem II supercomplexes upon removal of extrinsic subunits. Biochemistry 39: 12907-15

Boltzmann, L. E. (1872) Weitere Studien über das Wärmegleichgewicht unter Gasmolekülen. Sitzungsberichte Akademie der Wissenschaften 66: 275-370

Brangeon, J. and Mustárdy, L. (1979) The ontogenetic assembly of intra-chloroplastic lamellae viewed in 3-dimension. Biol Cell 36 71–80

Bulté, L. and Wollman, F. A. (1990) Stabilization of states I and II by *p*-benzoquinone treatment of intact cells of *Chlamydomonas reinhardtii*. Biochim Biophys Acta Bioenerg 1016: 253-258

Buschmann, C. (2001) Photosynthetic activity from different depths of a leaf by measuring the *in vivo* photoacoustic signal with light of different color, intensity and modulation frequency. Anal Sci 17: s334-s337

Buttaro, V. (2005). "The High energy Inelastic Neutron Scattering (HINS) regime." Retrieved 28 Jul, 2011, from http://www.fisica.uniroma2.it/~vesuvio/dins/html/hins.html.

Cantor, C. R. and Schimmel, P. R. (1980). Biophysical Chemistry, Part II Techniques for the Study of Biological Structure and Function. San Francisco, W. H. Freeman and Company.

Chadwick, J. (1932) Possible existence of a neutron. Nature 129: 312-312

Chow, W. S., Thorne, S. W., Duniec, J. T., Sculley, M. J. and Boardman, N. K. (1980) The stacking of chloroplast thylakoids : Effects of cation screening and binding, studied by the digitonin method Arch Biochem Biophys 201: 347-355

Chow, W. S., Melis, A. and Anderson, J. M. (1990) Adjustments of photosystem stoichiometry in chloroplasts improve the quantum efficiency of photosynthesis. Proc Natl Acad Sci USA 87: 7502-7506

Chow, W. S., Kim, E. H., Horton, P. and Anderson, J. M. (2005) Granal stacking of thylakoid membranes in higher plant chloroplasts: the physicochemical forces at work and the functional consequences that ensue. Photochemical & Photobiological Sciences 4: 1081-1090

Chuartzman, S. G., Nevo, R., Shimoni, E., Charuvi, D., Kiss, V., Ohad, I., Brumfeld, V. and Reich, Z. (2008) Thylakoid membrane remodeling during state transitions in *Arabidopsis*. Plant Cell 20: 1029–1039

Conrad, H. (2005). Neutron Sources. Neutron Scattering. T. Brückel, G. Heger, D. Richter and R. Zorn. Jülich, Forschungszentrum Jülich GmbH.

Cseh, Z., Vianelli, A., Rajagopal, S., Krumova, S., Kovács, L., Papp, E., Barzda, V., Jennings, R. and Garab, G. (2005) Thermo-optically induced reorganizations in the main light harvesting antenna of plants. I. Non-Arrhenius type of temperature dependence and linear light-intensity dependencies. Photosynth Res 86: 263-273

Cser, L. (2010). Kondenzált Közegek Vizsgálata Neutronszórással. Budapest, Typotex.

Daum, B., Nicastro, D., Austin, J. R. n., McIntosh, J. R. and Kuhlbrandt, W. (2010) Arrangement of photosystem-II and ATP synthase in chloroplast membranes of spinach and pea. Plant Cell 22: 1299-312

Deamer, D. W., Crofts, A. R. and Packer, L. (1967) Mechanisms of light-induced structural changes in chloroplasts I. Light-scattering increments and ultrastructural changes mediated by proton transport Biochim Biophys Acta Bioenerg 131: 81-96

Dekker, J. P., Boekema, E. J., Witt, H. T. and Rogner, M. (1988) Refined purification and further characterization of oxygen-evolving and Tris-treated Photosystem II particles from the thermophilic *Cyanobacterium synechococcus* sp. Biochim Biophys Acta Bioenerg 936: 307-318

Dekker, J. P. and Boekema, E. J. (2005) Supramolecular organization of thylakoid membrane proteins in green plants. Biochim Biophys Acta Bioenerg 1706: 12-39

Demé, B., Dubois, M. and Zemb, T. (2002) Swelling of a lecithin lamellar phase induced by small carbohydrate solutes. Biophys J 82: 215-225

Dianoux, A. L. and Lander, G., Eds. (2003). Neutron Data Booklet. Grenoble, Institut Laue-Langevin.

Dobrikova, A. G., Varkonyi, Z., Krumova, S. B., Kovacs, L., Kostov, G. K., Todinova, S. J., Busheva, M. C., Taneva, S. G. and Garab, G. (2003) Structural rearrangements in chloroplast thylakoid membranes revealed by differential scanning calorimetry and circular dichroism spectroscopy. Thermo-optic effect. Biochemistry 42: 11272-11280

Dorne, A. J., Joyard, J. and Douce, R. (1990) Do thylakoids really contain phosphatidylcholine? Proc Natl Acad Sci USA 87: 71-74

Doster, W., Cusack, S. and Petry, W. (1989) Dynamical transition of myoglobin revealed by inelastic neutron scattering. Nature 337: 754-756

Doster, W. (2008) The dynamical transition of proteins, concepts and misconceptions. Eur Biophys J 37: 591-602

Douce, R. and Joyard, J. (1996). Biosynthesis of thylakoid membrane lipids. Advances in Photosynthesis/Oxygenic Photosynthesis: The Light Reactions. D. R. Ort and C. F. Yocum. The Netherlands, Kluwer Academic Publishers.

Duchene, S. and Siegenthaler, P. (2000) Do glycerolipids display lateral heterogeneity in the thylakoid membrane. Lipids 35: 739-744

Egelstaff, P. A. (1965). Thermal Neutron Scattering. London, Academic Press.

Egge, J. K. and Aksnes, D. L. (1992) Silicate as regulating nutrient in phytoplankton competition. Marine Ecology Progress Series 83: 281-289

Enami, I., Kitamura, M., Tomo, T., Isokawa, Y., Ohta, H. and Katoh, S. (1994) Is the primary cause of thermal inactivation of oxygen evolution in spinach PS II membranes release of the extrinsic 33 kDa protein or of Mn? . Biochim Biophys Acta 1186: 52-58

Eppard, M. and Rhiel, E. (1998) The genes encoding light-harvesting subunits of Cyclotella cryptica (Bacillariophyceae) constitute a complex and heterogeneous family. Molecular and General Genetics 260: 335-345

ESRF. (2011). "Brilliance." Retrieved 28 Jul, 2011, from http://www.esrf.eu/Accelerators/Performance/Brilliance.

Falkowski, P. G., Barber, R. T. and Smetacek, V. (1998) Biogeochemical controls and feedbacks on ocean primary production : Chemistry and biology of the oceans. Science 281: 200-206

Ferrand, M., Dianoux, A. J., Petry, W. and Zaccai, G. (1993) Thermal motions and function of bacteriorhodopsin in purple membranes: Effects of temperature and hydration studied by neutron scattering. Proc Natl Acad Sci USA 90: 9668-9672

Ferreira, K. N., Iverson, T. M., Maghlaoui, K., Barber, J. and Iwata, S. (2004) Architecture of the Photosynthetic Oxygen-Evolving Center Science 303: 1831 - 1838

Gahler, R. (2010). Personal communication. Grenoble, Institut Laue-Langevin.

Garab, G. and Mustárdy, L. (1999) Role of LHCII-containing macrodomains in the structure, function and dynamics of grana. Aust J Plant Physiol 26: 649-658

Garab, G., Lohner, K., Laggner, P. and Farkas, T. (2000) Self-regulation of the lipid content of membranes by non-bilayer lipids: a hypothesis. Trends Plant Sci 5: 489-494

Garab, G., Cseh, Z., Kovács, L., Rajagopal, S., Várkonyi, Z., Wentworth, M., Mustárdy, L., Dér, A., Ruban, A. V., Papp, E., Holzenburg, A. and Horton, P. (2002) Light-induced trimer to monomer transition in the main light-harvesting antenna complex of plants: thermo-optic mechanism. Biochemistry 41: 15121-15129

Garab, G. and van Amerongen, H. (2009) Linear dichroism and circular dichroism in photosynthesis research. Photosynth Res 101: 135-146

Geacintov, N. E., Nostrand, F. V., Becker, J. F. and Tinkel, J. B. (1972) Magnetic field induced orientation of photosynthetic systems. Biochim Biophys Acta 267: 65-79

Goss, R., Pinto, E. A., Wilhelm, C. and Richter, M. (2006) The importance of a highly active and ΔpH-regulated diatoxanthin epoxidase for the regulation of the PS II antenna function in diadinoxanthin cycle containing algae. J Plant Physiol 163: 1008-1021

Govindjee, Kern, J. F., Messinger, J. and Whitmarsh, J. (2010). Photosystem II. Encyclopedia of Life Sciences. Chichester, John Wiley & Sons, Ltd.

Grillo, I. (2008). Small-angle neutron scattering and applications in soft condensed matter Soft-Matter Characterisation. R. Borsali and R. Pecora, Springer 723.

Guinier, A. and Fournet, G. (1955). Small-Angle Scattering of X-rays New York, John Wiley.

Gunning, B. E. S. and Steer, M. W. (1975). Ultrastructure and the Biology of Plant Cells. London, Edward Arnold.

Guskov, A., Kern, J., Gabdulkhakov, A., Broser, M., Zouni, A. and Saenger, W. (2009) Cyanobacterial photosystem II at 2.9-Å resolution and the role of quinones,

lipids, channels and chloride. Nature Structural & Molecular Biology 16: 334-342

Haferkamp, S. and Kirchhoff, H. (2008) Significance of molecular crowding in grana membranes of higher plants for light harvesting by photosystem II. Photosynth Res 95: 129-134

Harroun, T. A., Wignall, G. D. and Katsaras, J. (2006). Neutron Scattering for Biology. Neutron Scatering in Biology. J. Fitter, T. Gutberlet and J. Katsaras. Berlin Heidelberg Springer**:** 1-18.

Holm, J. K. (2004). Structure and Structural Flexibility of Chloroplast Thylakoid Membranes. IMFUFA - Institute of Mathematics and Physics. Roskilde, Roskilde University. Ph.D.: 249.

Holt, N. E., Fleming, G. R. and Niyogi, K. K. (2004) Toward an understanding of the mechanism of nonphotochemical quenching in green plants. Biochemistry 43: 8281-8289

Huisman, J., Sharples, J., Stroom, J. M., Visser, P. M., Kardinaal, W. E. A., Verspagen, J. M. H. and Sommeijer, B. (2004) Changes in turbulent mixing shift competition for light between phytoplankton species. Ecology 85: 2960-2970

ILL. (2011). "Large dynamic range small-angle diffractometer D22." Retrieved 28 Jul, 2011, from http://www.ill.eu/instruments-support/instruments-groups/instruments/d22/.

Iwai, M., Takahashi, Y. and Minagawa, J. (2008) Molecular remodeling of photosystem II during state transitions in Chlamydomonas reinhardtii. Plant Cell 20: 2177-2189

Iwai, M., Yokono, M., Inada, N. and Minagawa, J. (2010) Live-cell imaging of photosystem II antenna dissociation during state transitions. Proc Natl Acad Sci USA 107: 2337-2342

Izawa, S. and Good, E. (1966) Effect of salts and electron transport on the conformation of isolated chloroplasts. II. Electron microscopy. Plant Physiol 41: 544-552

Kanervo, E., Suorsa, M. and Aro, E. M. (2005) Functional flexibility and acclimation of the thylakoid membrane. Photochemical & Photobiological Sciences 4: 1072-1080

Kausche, G. A. and Ruska, H. (1940) Zur Frage der Chloroplastenstruktur. Naturwissenschaften 28: 303-304

Keough, K. M. W. and Davis, P. J. (1979) Gel to liquid-crystalline phase transitions in water dispersions of saturated mixed-acid phosphatidylcholines. Biochemistry 18: 1453-9

Kirchhoff, H., Mukherjee, U. and Galla, H. J. (2002) Molecular architecture of the thylakoid membrane: lipid diffusion space for plastoquinone. Biochemistry 41: 4872-82

Kirchhoff, H., Tremmel, I., Haase, W. and Kubitscheck, U. (2004) Supramolecular photosystem II organization in grana thylakoid membranes: evidence for a structured arrangement. Biochemistry 43: 9204-13

Kirchhoff, H., Lenhert, S., Buchel, C., Chi, L. and Nield, J. (2008) Probing the organization of photosystem II in photosynthetic membranes by atomic force microscopy. Biochemistry 47: 431-40

Kiss, J. G., Garab, G., Toth, Z. M. and Faludi-Danie, A. (1986) The light-harvesting chlorophyll a/b protein acts as a torque aligning chloroplast in a magnetic field. Photosynth Res 10: 217-222

Kittel, C. (1967). Introduction to Solid State Physics. New York, John Wiley & Sons.

Knox, P. P. and Garab, G. (1982) The effect of a permanent electric field on thermoluminescence of chloroplasts. Photochem Photobiol 35: 733-736

Knox, R. S. and Davidovich, M. A. (1978) Theory of fluorescence polarization in magnetically oriented photosynthetic systems. Biophys J 24: 689-712

Kóta, Z., Szalontai, B., Droppa, M., Horváth, G. and Páli, T. (2002) The formation of an inverted hexagonal phase from thylakoid membranes upon heating. Cell Mol Biol Lett 7: 126-128

Krueger, S., Perez-Salas, U. A., Gregurick, S. K. and Kuzmanovic, D. (2006). Small Angle Neutron Scattering from Proteins, Nucleic Acids, and Viruses. Neutron Scatering in Biology. J. Fitter, T. Gutberlet and J. Katsaras. Berlin Heidelberg, Springer**:** 161-185.

Krumova, S. B., Dijkema, C., de Waard, P., Van As, H., Garab, G. and van Amerongen, H. (2008a) Phase behavior of phosphatidylglycerol in spinach thylakoid membranes as revealed by ^{31}P-NMR. Biochim Biophys Acta 1778: 997-1003

Krumova, S. B., Koehorst, R. B. M., Bóta, A., Páli, T., van Hoek, A., Garab, G. and van Amerongen, H. (2008b) Temperature dependence of the lipid packing in thylakoid membranes studied by time- and spectrally resolved fluorescence of Merocyanine 540. Biochim Biophys Acta 1778: 2823-2833

Kucerka, N., Nagle, J. F., Feller, S. E. and Balgavy, P. (2004) Models to analyze small-angle neutron scattering from unilamellar lipid vesicles. Phys Rev E 69: 051903

Kucerka, N., Liu, Y., Chu, N., Petrache, H. I., Tristram-Nagle, S. and Nagle, J. F. (2005) Structure of fully hydrated fluid phase DMPC and DLPC lipid bilayers using X-ray scattering from oriented multilamellar arrays and from unilamellar vesicles. Biophys J 88: 2626-2637

Kuwabara, T. and Murata, N. (1983) Quantitative analysis of the inactivation of photosynthetic oxygen evolution and the release of polypeptides and manganese in the photosystem II particles of spinach chloroplasts. Plant Cell Physiol 24: 741-747

Lavaud, J., Strzepek, R. F. and Kroth, P. G. (2007) Photoprotection capacity differs among diatoms: Possible consequences on the spatial distribution of diatoms related to fluctuations in the underwater light climate. Limnol Oceanogr 52: 1188-1194

Lechner, R. E. and Longeville, S. (2006). Quasielastic Neutron Scattering in Biology, Part I: Methods. Neutron Scatering in Biology. J. Fitter, T. Gutberlet and J. Katsaras. Berlin Heidelberg Springer**:** 309-354.

Lee, H. Y., Hong, Y. N. and Chow, W. S. (2001) Photoinactivation of photosystem II complexes and photoprotection by non-functional neighbours in *Capsicum annuum* L. leaves. Planta 212: 332-342

Lepetit, B., Volke, D., Szabó, M., Hoffmann, R., Garab, G., Wilhelm, C. and Goss, R. (2007) Spectroscopic and molecular characterization of the oligomeric antenna of the diatom *Phaeodactylum tricornutum*. Biochemistry 46: 9813-9822

Leyon, H. (1956) The structure of chloroplasts. Svensk Kem. Tidskr. 68: 70-88

Lodish, H., Baltimore, D., Berk, A., Zipursky, S. L., Matsudaira, P. and Darnell, J. (1995). Molecular Cell Biology. New York, Scientific American Books.

Loong, C. K., Ikeda, S. and Carpenter, J. M. (1987) The resolution function of a pulsed-source neutron chopper spectrometer Nuclear Instruments and Methods in Physics Research Section A: Accelerators, Spectrometers, Detectors and Associated Equipment 260: 381-402

Lovesey, S. W. (1984). Theory of Neutron Scattering from Condensed Matter. Oxford, Clarendon Press.

Magazù, S., Migliardo, F. and Benedetto, A. (2010) Mean square displacements from elastic incoherent neutron scattering evaluated by spectrometers working with different energy resolution on dry and hydrated (H2O and D2O) lysozyme. J Phys Chem B 114: 9268-9274

Martin, B. R. (2006). Nuclear and Particle Physics. Chichester, England, John Wiley & Sons, Ltd.

McDaniel, R. V. (1988) Neutron diffraction studies of digalactosyldiacyiglycerol. Biochim Biophys Acta Biomemr 940: 158-164

Mills, J. D. (1986). Photophosphorylation. Photosynthesis: Energy transduction — A practical approach. M. F. Hipkins and N. R. Baker. Oxford, IRL Press**:** 199.

Mullineaux, C. W. (2005) Function and evolution of grana. Trends Plant Sci 10: 521-525

Murakami, S. and Packer, L. (1970) Protonation and chloroplast membrane structure. The Journal of Cell Biology 47: 332-351

Murakami, S. and Packer, L. (1971) The role of cations in the organization of chloroplast membranes. Arch Biochem Biophys 146: 337-347

Mustárdy, L. and Garab, G. (2003) Granum revisited. A three-dimensional model – where things fall into place. Trends Plant Sci 8: 117-122

Mustárdy, L., Buttle, K., Steinbach, G. and Garab, G. (2008) The three-dimensional network of the thylakoid membranes in plants: quasihelical model of the granum-stroma assembly. Plant Cell 20: 2552-2557

Nagy, G., Pieper, J., Krumova, S. B., Kovács, L., Trapp, M., Garab, G. and Peters, J. (2011a) Dynamic properties of photosystem II membranes at physiological temperatures characterized by elastic incoherent neutron scattering. Increased flexibility associated with the inactivation of the oxygen evolving complex. Photosynth Res doi: 10.1007/s11120-011-9701-x

Nagy, G., Posselt, D., Kovács, L., Holm, J. K., Szabó, M., Ughy, B., Rosta, L., Peters, J., Timmins, P. and Garab, G. (2011b) Reversible membrane reorganizations during photosynthesis in vivo: revealed by small-angle neutron scattering. Biochem J 436: 225-230

Nagy, G., Szabó, M., Ünnep, R., Káli, G., Miloslavina, Y., Lambrev, P. H., Zsiros, O., Porcar, L., Rosta, L. and Garab, G. (2011c) Modulation of the multilamellar membrane organization and of the chiral macrodomains in the diatom *Phaeodactylum tricornutum* revealed by small-angle neutron scattering and circular dichroism spectroscopy. Photosynth Res doi: 10.1007/s11120-011-9693-6

Nash, D., Miyao, M. and Murata, N. (1985) Heat inactivation of oxygen evolution in Photosystem II particles and its acceleration by chloride depletion and exogenous manganese. Biochim Biophys Acta Bioenerg 807: 127-133

Natali, F., Peters, J., Russo, D., Barbieri, S., Chiapponi, C., Cupane, A., Deriu, A., Di Bari, M. T., Farhi, E., Gerelli, Y., Mariani, P., Paciarioni, A., Rivasseau, C., Schiro, G. and Sonvico, F. (2008) IN13 backscattering spectrometer at ILL: looking for motions in biological macromolecules and organisms. Neutron News 19: 14-18

Nelson, D. M., Riedel, G. F., Millan-Nunez, R. and LAra-Lara, J. R. (1984) Silicon uptake by algae with no known Si requirement. I: True cellular uptake and pH-induced precipitation by *Phaeodactylum tricornutum* (Bacillariophyceae) and *Platymonas* sp. (Prasinophyceae). Journal of Phycology 20: 141-147

Nield, J. (2010). "Schematic model of the major protein complexes involved in photosynthesis." Retrieved 28 Jul, 2011, from http://photosynthesis.sbcs.qmul.ac.uk/nield/psIIimages/oxygenicphotosynthmodel.html.

NIST. (2011). "Scattering Length Density Calculator." Retrieved 28 Jul, 2011, from http://www.ncnr.nist.gov/resources/sldcalc.html.

O'Brien, F. E. M. (1948) The control of humidity by saturated salt solutions J Sci Instrum 25: 73-76

Olive, J., Ajlani, G., Astier, C., Recouvreur, M. and Vernotte, C. (1997) Ultrastructure and light adaptation of phycobilisome mutants of *Synechocystis* PCC 6803. Biochim Biophys Acta Bioenerg 1319: 275-282

Pabst, G., Rappolt, M., Amenitsch, H. and Laggner, P. (2000) Structural information from multilamellar liposomes at full hydration: Full q-range fitting with high quality x-ray data. Phys. Rev. E. 62: 4000-4009

Páli, T., Garab, G., Horváth, L. I. and Kóta, Z. (2003) Functional significance of the lipid-protein interface in photosynthetic membranes. Cell Mol Life Sci 60: 1591-1606

Paolillo, D. J. and MacKay, N. C. (1969) The structure of grana in flowering plants. American Journal of Botany 56: 344-347

Peters, J., Champion, J. D. M., Zsigmond, G., Bordallo, H. N. and Mezei, F. (2006) Using Fermi choppers to shape the neutron pulse. Nuclear Instruments and Methods in Physics Research Section A: Accelerators, Spectrometers, Detectors and Associated Equipment 557: 580-584

Pieper, J., Hauss, T., Buchsteiner, A., Baczyn´ski, K., Adamiak, K., Lechner, R. E. and Renger, G. (2007) Temperature- and hydration-dependent protein dynamics in photosystem II of green plants studied by quasielastic neutron scattering. Biochemistry 46: 11398-11409

Pieper, J., Hauß, T., Buchsteiner, A. and Renger, G. (2008) The effect of hydration on protein flexibility in photosystem II of green plants studied by quasielastic neutron scattering. Eur Biophys J 37: 657-663

Posch, M. G., Perrot, A., Geier, C., Boldt, L. H., Schmidt, G., Lehmkuhl, H. B., Hetzer, R., Dietz, R., Gutberlet, M., Haverkamp, W. and Ozcelik, C. (2009) Genetic deletion of arginine 14 in phospholamban causes dilated cardiomyopathy with attenuated electrocardiographic R amplitudes. Heart Rhythm 6: 480-6

Poulsen, N., Sumper, M. and Kröger, N. (2003) Biosilica formation in diatoms: Characterization of native silaffin-2 and its role in silica morphogenesis. Proc Natl Acad Sci USA 100: 12075-12080

Profio, A. E. (1976). Experimental Reactor Physics. New York, John Wiley & Sons.

Pyszniak, A. M. and Gibbs, S. P. (1992) Immunocytochemical localization of photosystem I and the fucoxanthin-chlorophyll a/c light-harvesting complex in the diatom *Phaeodactylum tricornutum*. Protoplasma 166: 208-217

Reat, V., Zaccai, G., Ferrand, M. and Pfister, C. (1997). Functional dynamics in purple membrane. Biological Macromolecular Dynamics. S. Cusack, H. Buuttner, M. Ferrand, P. Langan and P. Timmins. Schenectady, Adeline Press**:** 117-122.

Rhee, K., Morris, E. P., Barber, J. and Kuhlbrandt, W. (1998) Three-dimensional structure of the plant photosystem II reaction centre at 8 Å resolution. Nature 396: 283-286

Richter, D. (2005). Properties of the Neutron, Elementary Scattering Processes. Neutron Scattering. T. Brückel, G. Heger, D. Richter and R. Zorn. Jülich, Forschungszentrum Jülich GmbH.

Rochaix, J. (2007) Role of thylakoid protein kinases in photosynthetic acclimation. FEBS Lett 581: 2768-2775

Rosta, L. (2002) Cold neutron research facility at the Budapest Neutron Centre. Appl Phys A 74: s52-s54

Sadler, D. M. and Worcester, D. L. (1982) Neutron diffraction studies of oriented photosynthetic membranes. Journal of Molecular Biology 159: 467-482

Schaller, S., Latowski, D., Jemioła-Rzemińska, M., Dawood, A., Wilhelm, C., Strzałka, K. and Goss, R. (2011) Regulation of LHCII aggregation by different thylakoid membrane lipids. Biochim Biophys Acta 1807: 326-335

Schober, H. (2010) Diffusion des neutrons par la matiere cristalline ou amorphe non-magnetique. Collection SFN 10: 159-336

Schwahn, D. (2005). Soft Matter: Structure. Neutron Scattering. T. Brückel, G. Heger, D. Richter and R. Zorn. Jülich, Forschungszentrum Jülich GmbH.

Sears, V. F. (1989). Neutron Optics: An Introduction to the Theory of Neutron Optical Phenomena and their Applications. Oxford, Oxford University Press.

Sears, V. F. (1992) Neutron scattering lengths and cross sections. Neutron News 3: 26-37

Serdyuk, I. N., Zaccai, N. R. and Zaccai, J. (2007). Methods in Molecular Biophysics: Structure, Dynamics, Function. Cambridge, Cambridge University Press.

Sherman, D. M., Troyan, T. A. and Sherman, L. A. (1994) Localization of membrane proteins in the cyanobacterium *Synechococcus* sp. PCC7942 (radial asymmetry in the photosynthetic complexes). Plant Physiol 106: 251-262

Simidjiev, I., Stoylova, S., Amenitsch, H., Jávorfi, T., Mustárdy, L., Laggner, P., Holzenburg, A. and Garab, G. (2000) Self-assembly of large, ordered lamellae from non-bilayer lipids and integral membrane proteins *in vitro*. Proc Natl Acad Sci USA 97: 1473-1476

Smith, G. S., Sirota, E. B., Safinya, C. R. and Clark, N. A. (1988) Structure of the L_β phases in a hydrated phosphatidylcholine multimembrane. Phys Rev Lett 60: 813-816

Smith, J. C. (1991) Protein dynamics: comparison of simulations with inelastic neutron scattering experiments. Q Rev Biophys 24: 227-291

Spetea, C. and Schoefs, B. (2010) Solute transporters in plant thylakoid membranes: Key players during photosynthesis and light stress. Commun Integr Biol 3: 122-129

Squires, G. L. (1978). Introduction to the Theory of Thermal Neutron Scattering. Cambridge, Cambridge University Press.

Stadler, A. M., Digel, I., Embs, J. P., Unruh, T., Tehei, M., Zaccai, G., Büldt, G. and Artmann, G. M. (2009) From powder to solution: hydration dependence of human hemoglobin dynamics correlated to body temperature. Biophys J 96: 5073-5081

Standfuss, J., Terwisscha van Scheltinga, A. C., Lamborghini, M. and Kuhlbrandt, W. (2005) Mechanisms of photoprotection and nonphotochemical quenching in pea light-harvesting complex at 2.5 A resolution. EMBO J. 24: 919-28

Stock, D., Leslie, A. G. and Walker, J. E. (1999) Molecular architecture of the rotary motor in ATP synthase. Science 286: 1700-5

Szabó, M., Lepetit, B., Goss, R., Wilhelm, C., Mustárdy, L. and Garab, G. (2008) Structurally flexible macro-organization of the pigment-protein complexes of the diatom *Phaeodactylum tricornutum*. Photosynth Res 95: 237-245

Tanaka-Kitatani, Y., Satoh, K. and Katoh, S. (1990) Interaction of benzoquinones with Q_A and Q_B in oxygen-evolving photosystem II particles from the thermophilic cyanobacterium *Synechococcus elongatus*. Plant Cell Physiol 31: 1039-1047

Thompson, L. K., Sturtevant, J. M. and Brudvig, G. W. (1986) Differential scanning calorimetric studies of photosystem II: Evidence for a structural role for cytochrome b559 in the oxygen-evolving complex. Biochemistry 25: 6161–6169

Thompson, L. K., Blaylock, R., Sturtevant, J. M. and Brudvig, G. W. (1989) Molecular basis of the heat denaturation of photosystem II. Biochemistry 28: 6686–6695

Tiedtke, K., Azima, A., von Bargen, N., Bittner, L., Bonfigt, S., Düsterer, S., Faatz, B., Frühling, U., Gensch, M., Gerth, C., Guerassimova, N., Hahn, U., Hans, T., Hesse, M., Honkavaar, K., Jastrow, U., Juranic, P., Kapitzki, S., Keitel, B., Kracht, T., Kuhlmann, M., Li, W. B., Martins, M., Núñez, T., Plönjes, E., Redlin, H., Saldin, E. L., Schneidmiller, E. A., Schneider, J. R., Schreiber, S., Stojanovic, N., Tavella, F., Toleikis, S., Treusch, R., Weigelt, H., Wellhöfer, M., Wabnitz, H., Yurkov, M. V. and Feldhaus, J. (2009) The soft x-ray free-electron laser FLASH at DESY: beamlines, diagnostics and end-stations New Journal of Physics 11: 023029

Ting, C. S. and Owens, T. G. (1994) The effects of excess irradiance on photosynthesis in the marine diatom *Phaeodactylum tricornutum*. Plant Physiol 106: 763-770

Tóth, S. Z., Puthur, J. T., Nagy, V. and Garab, G. (2009) Experimental evidence for ascorbate-dependent electron transport in leaves with inactive oxygen-evolving complexes. Plant Physiol 149: 1568-1578

Tóth, S. Z., Nagy, V., Puthur, J. T., Kovacs, L. and Garab, G. (2011) The physiological role of ascorbate as photosystem II electron donor: protection against photoinactivation in heat-stressed leaves. Plant Physiol 156: 382-392

Trapp, M., Gutberlet, T., Juranyi, F., Unruh, T., Demé, B., Tehei, M. and Peters, J. (2010) Hydration dependent studies of highly aligned multilayer lipid membranes by neutron scattering. J Chem Phys 133: 164505

Trissl, H. W. and Wilhelm, C. (1993) Why do thylakoid membranes from higher plants form grana stacks. Trends Biochem Sci 18: 415-419

Umena, Y., Kawakami, K., Shen, J. R. and Kamiya, N. (2011) Crystal structure of oxygen-evolving photosystem II at a resolution 1.9 Å. Nature 473: 55-60

van de Meene, A. M. L., Hohmann-Marriott, M. F., Vermaas, W. F. and Roberson, R. W. (2006) The three-dimensional structure of the cyanobacterium *Synechocystis* sp. PCC 6803. Arch Microbiol 184: 259-270

Van Hove, L. (1954) Correlations in space and time and Born approximation scattering in systems of interacting particles. Phys Rev 95: 14

Várkonyi, Z., Nagy, G., Lambrev, P., Kiss, A. Z., Székely, N., Rosta, L. and Garab, G. (2009) Effect of phosphorylation on the thermal and light stability of the thylakoid membranes. Photosynth Res 99: 161-171

Volker, M., Ono, T., Inoue, Y. and Renger, G. (1985) Effect of trypsin on PS-II particles. Correlation between Hill-activity, Mn-abundance and peptide pattern. Biochim Biophys Acta 806: 25-34

Vrettos, J. S., Limburg, J. and W., B. G. (2001) Mechanism of photosynthetic water oxidation: combining biophysical studies of photosystem II with inorganic model chemistry. Biochim Biophys Acta Bioenerg 1503: 229-245

Wagner, H., Jakob, T. and Wilhelm, C. (2006) Balancing the energy flow from captured light to biomass under fluctuating light conditions. New Phytol 169: 95-108

Wilhelm, C., Büchel, C., Fisahn, J., Goss, R., Jakob, T., Laroche, J., Lavaud, J., Lohr, M., Riebesell, U., Stehfest, K., Valentin, K. and Kroth, P. G. (2006) The regulation of carbon and nutrient assimilation in diatoms is significantly different from green algae. Protist 157: 91-124

Williams, W. P. and Quinn, P. J. (1987) The phase behavior of lipids in photosynthetic membranes. J Bioenerg Biomembr 19: 605-24

Williams, W. P. (1998). The Physical Properties of Thylakoid Membrane Lipids and Their Relation to Photosynthesis. Lipids in Photosynthesis: Structure, Function and Genetics. P. Siegenthaler and N. Murata. London, Kluwer Academic Publishers.

Wilson, A., Ajlani, G., Verbavatz, J. M., Vass, I., Kerfeld, C. A. and Kirilovsky, D. (2006) A soluble carotenoid protein involved in phycobilisome-related energy dissipation in cyanobacteria. Plant Cell 18: 992-1007

Yamane, Y., Kashino, Y., Koike, H. and Satoh, K. (1998) Effects of high temperatures on the photosynthetic systems in spinach: Oxygen-evolving activities, fluorescence characteristics and the denaturation process. Photosynth Res 57: 51–59

Yamashita, E., Zhang, H. and Cramer, W. A. (2007) Structure of the cytochrome b6f complex: quinone analogue inhibitors as ligands of heme cn. J Mol Biol. 370: 39-52

Yang, C., Boggasch, S., Haase, W. and Paulsen, H. (2006) Thermal stability of trimeric light-harvesting chlorophyll a/b complex 3 (LHCIIb) in liposomes of thylakoid lipids. Biochim Biophys Acta 1757: 1642-1648

Zaccai, G. (2000a) How soft is a protein? A protein dynamics force constant measured by neutron scattering. Science 288: 1604-1607

Zaccai, G. (2000b). Small-angle neutron scattering. Structure and Dynamics of Biomolecules: Neutron and Synchrotron Radiation for Condensed Matter Studies. E. Fanchon, E. Geissler, J. L. Hodeau, J. R. Regnard and P. A. Timmins. Oxford, Oxford University Press.

Zer, H., Vink, M., Keren, N., Dilly-Hartwig, H. G., Paulsen, H., Herrmann, R. G., Andersson, B. and Ohad, I. (1999) Regulation of thylakoid protein phosphorylation at the substrate level: reversible light-induced conformational changes expose the phosphorylation site of the light-harvesting complex II. Proc Natl Acad Sci USA 96: 8277-8282

Zimányi, L. and Garab, G. (1982) Configuration of the light induced electric field in thylakoid and its possible role in the kinetics of the 515 nm absorbance chance J Theor Biol 95: 811-821

Zimányi, L. and Garab, G. (1989) Configuration of the electric field and distribution of ions in energy transducing biological membranes: model calculations in a vesicle containing discrete charges. J Theor Biol 138: 59-76